國立臺灣大學電機資訊學院電信工程學研究所

碩士論文

Graduate Institute of Communication Engineering
College of Electrical Engineering and Computer Science
National Taiwan University

Master's Thesis

太赫茲頻段 4×4 側端陣列天線饋入之碟型天線設計

Design of Offset Reflector fed by a 4×4 End-Fire Antenna Array for Sub-THz Communications

Swetha Manupati

指導教授：周錫增博士

Advisor: Hsi-Tseng Chou, Ph.D.

中華民國 113 年 09 月

September, 2024

doi:10.6342/NTU202404478

doi:10.6342/NTU202404478

Acknowledgement

I wish to convey my deepest appreciation to everyone who offered their support during my research journey. I am profoundly grateful to my advisor, Prof. Hsi-Tseng Chou, whose invaluable guidance and constructive feedback have significantly shaped my research. Your hard work, expertise, and dedication have motivated me at every stage of this process.

I would especially like to extend my heartfelt appreciation to Prof. Yu-Hsiang Cheng and his fellow students, Mr. Sheng Chun Tsao, Mr. Chih-Han Lin, Mr. Yu-Hsiang Wang, and Miss Yi-Chi Li, for their assistance in completing the radiation measurements. Their expertise and assistance in configuring the measurement setup such as positioning of the antennas and calibration of the equipment for accurate radiation measurements ensuring smooth operation and reliable data acquisition, which was essential for the completion of my work. Your support has been precious.

I am also thankful to my fellow lab members, particularly Mr. Shi Kai, who assisted in fabricating the reflector antenna, along with Mr. Siddharth Panigrahi, Mr. Lee, Mr. Yi-Ting Chen, Mr. Chih-Ta Yen, Mr. David Wu, and the rest of the team for their collaboration, support, and friendship throughout this journey. Our discussions and shared experiences have greatly enriched my research. I also appreciate Mr. Yen-Ming Chen for providing the 1×4 antenna array used to feed the reflector.

Additionally, I wish to convey my sincere appreciation to Miss Hwa Lin, the laboratory assistant, for her kindness and support towards the students in Prof. Chou's lab.

I am profoundly thankful to my family and friends for their constant support and encouragement throughout this journey. Your belief in me has been a tremendous source of strength during this challenging time. I am grateful to all of you for your contributions, I could not have achieved this without your help.

doi:10.6342/NTU202404478

doi:10.6342/NTU202404478

摘要

本文提出了一種偏置反射器的設計，以增強用於亞太赫茲通信的 4×4 端射天線陣列的增益。工作頻率範圍約為 240 GHz 至 310 GHz，涵蓋了 Sub-THz 通信所需的頻率。雖然較高的頻率通常會導致陣列天線的增益增加，但設計的 4×4 線陣列尚未滿足所需的性能標準。在如此高的頻率下，拋物面反射面天線等高增益天線在增強天線增益方面發揮著關鍵作用，適用於長距離和衛星通信。本研究分析了偏置反射器的設計考慮因素和模擬機制，並通過反射器 天線與 4x4 H-pol 端射天線陣列的集成進一步增強。利用混合仿真方法，評估該覆合天 線系統的性能，並使用高頻結構模擬器 (HFSS) 軟件進行驗證。所設計的 偏置反射器在 260GHz 和 300GHz 頻率上將饋源天線的增益提高了 13dB（理論上）。隨後，分別使用數控加工和 3D 打印機制造偏置反射器及其機械支撐結構，並通過測量數據評估反射器的性能並與模擬結果進行比較，以驗證偏置反射器的特性。

所提出的偏置反射器有望在亞太赫茲頻率下實現高增益，並可廣泛用於 6G 應用和其他相關研究。

索引術語：偏置反射器、焦距、天線陣列、亞太赫茲頻率

doi:10.6342/NTU202404478

doi:10.6342/NTU202404478

Abstract

This paper presents the design of an Offset Reflector aimed at improving the gain of a 4×4 End-fire antenna configuration for Sub-THz communication systems. The frequency range of operation extends approximately from 240 GHz to 310 GHz, covering the necessary frequencies for Sub-THz communication. While higher frequencies generally lead to increased gain for array antennas, the designed 4×4 antenna array has not met the desired performance criteria. At such high frequencies, high-gain antennas like parabolic reflector antennas play a pivotal role in enhancing the gain of antennas, suitable for long-distance and satellite communications.

This study analyzes the design considerations and simulation mechanism of offset reflectors, further augmented by integrating the Reflector antenna with a 4x4 H-pol End-Fire Antenna array. Utilizing a hybrid simulation methodology, the performance of this composite antenna system is evaluated, and validation is carried out with the aid of HFSS (High-Frequency Structure Simulator) software. The designed offset reflector boosts the gain of the feed antenna by 13dB(theoretically) over the frequencies at 260GHz and 300GHz. Subsequently, the offset reflector and its mechanical support structure are fabricated using CNC machining and a 3D printer respectively, and the reflector's performance is assessed through measurement data and evaluated alongside simulation results to verify the characteristics of the offset reflector.

The proposed offset reflector holds promise for achieving high gain at Sub-THz frequency and can be widely used in 6G applications and other related research.

Index Terms: Offset reflector, Focal length, Antenna array, Sub-THz frequency

doi:10.6342/NTU202404478

CONTENTS

doi:10.6342/NTU202404478

doi:10.6342/NTU202404478

doi:10.6342/NTU202404478

doi:10.6342/NTU202404478

LIST OF FIGURES

doi:10.6342/NTU202404478

doi:10.6342/NTU202404478

doi:10.6342/NTU202404478

doi:10.6342/NTU202404478

LIST OF TABLES

doi:10.6342/NTU202404478

doi:10.6342/NTU202404478

Chapter 1 Introduction

1.1 Research Motivation

Considering the present advancements in technology, researchers are directing their focus toward exploring and harnessing the significance of Sub-THz frequency bands. The Sub-THz frequency band typically ranges from 100GHz to 300GHz. The representation of the sub-THz frequency band is shown in Figure. 1.1 [1]

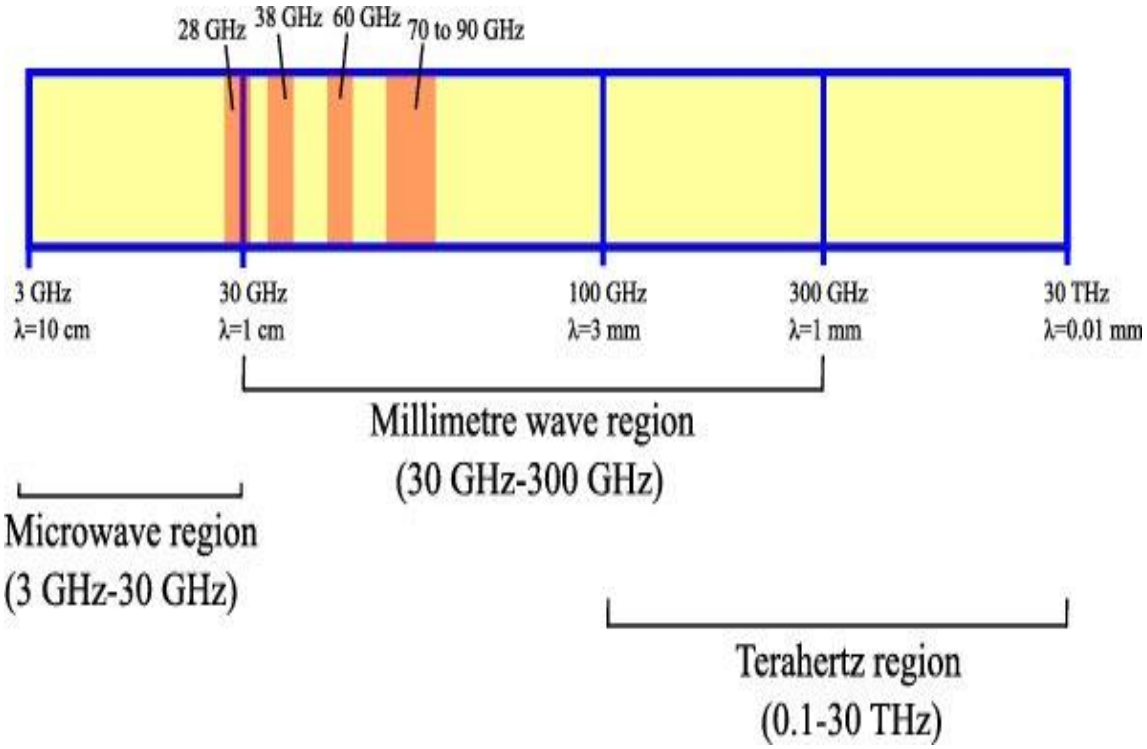

Fig. 1.1 Representation of electromagnetic spectrum of terahertz region [1].

While the mm-wave frequencies offer their advantages, Sub-THz frequencies stand out due to their ability to provide a wide range of bandwidths and support high data rates potentially reaching 100Mbps. This makes them perfectly suitable for next-generation communication systems such as 6G and for applications in Terahertz imaging and sensing, Satellite Communication, Nano scale applications, and beyond.

However, despite these advantages, there are some challenges to overcome particularly in antenna design. For reliable transmission of signals, the gain of the antenna plays a crucial role. As bandwidth increases in sub-millimeter waves and beyond, high-

doi:10.6342/NTU202404478

performance antennas become essential. However, arrays operating at Sub-THz frequencies often suffer limitations in terms of gain due to Substrate losses which are significant at higher frequencies, rendering them insufficient for certain applications. These deficiencies can lead to signal loss, particularly over extended transmission distances. To overcome these challenges, implementing high-gain antennas is necessary to improve the capabilities of antenna arrays at sub-TeraHertz frequencies. Indeed, in the realm of high-frequency applications, several High-gain antennas exist including reflector antennas, Yagi-Uda, and Phased arrays. As these bands are at higher frequencies, however, due to the shorter wavelengths other antennas are more complicated in terms of fabrication. Among those, reflector antennas are easy to fabricate and provide promising solutions for higher frequencies

1.2 Overview of Thesis

Based on the mentioned challenges, this thesis presents a comprehensive analysis of reflector antennas, especially focused on offset reflectors functioning within the sub-TeraHertz frequency spectrum. The structure of this thesis is designed to offer a structured method for design, analysis, simulation, and fabrication of a 300GHz offset Reflector System.

The structure of this thesis is outlined as: Chapter 2 introduces different types of parabolic reflector antennas and their operating principles. It discusses the suitability of offset reflector antennas compared to other types, based on their advantages, disadvantages, and applications. Additionally, it includes a review of various offset reflector antenna system architectures, along with an analysis of their simulation results.

Chapter 3 delves into developing a 4×4 horizontally polarized end-fire antenna array tailored for sub-THz frequencies. This chapter covers the detailed design methodology, including the choice of materials, dimensions, and the interleaved arrangement of the array elements. It presents simulation results that demonstrate the effectiveness of the

doi:10.6342/NTU202404478

antenna array as the feed component for the offset reflector, with a focus on its radiation patterns.

Chapter 4 focuses on the design of the offset reflector antenna at sub-THz frequencies, exploring various parametric studies that significantly influence antenna performance. Furthermore, it focuses on the design of the flexible support structure that holds the reflector antenna for accurate measurement.

Chapter 5 includes a thorough description of the measurement techniques and calibration procedures. It presents a comparative analysis of the simulation results versus measured data, highlighting the accuracy of the simulation model and discussing any deviations observed during testing. Finally, Chapter 6 brings the thesis to a conclusion, summarizing the findings and implications of the research.

doi:10.6342/NTU202404478

Chapter 2 Literature Review

This section offers a detailed examination of parabolic reflector antennas, focusing on offset reflectors. It aims to present a comprehensive exploration of various types of novel reflector antennas, along with their theoretical foundations, and provides insights into selecting the most suitable reflector antenna for specific applications. Furthermore, this chapter provides insights into existing research on offset reflector antennas, discussing the design parameters and methodologies, simulation techniques, that are necessary for creating efficient and effective reflector antennas.

2.1 Types of Parabolic Reflector Antennas

2.1.1 Axial or front feed reflector antenna

In the context of axial reflector antennas [2] [3], the source antenna (feed) is precisely positioned within the focal region of the parabolic reflector as demonstrated in Fig. 2.1 [2].

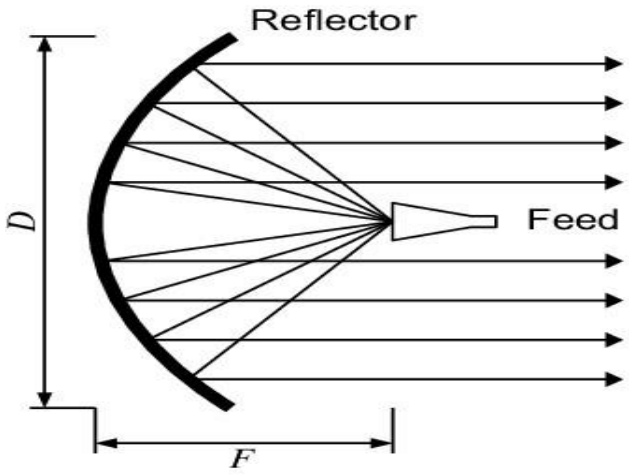

Fig. 2.1 Axial feed parabolic antenna profile [2].

The axial front feed reflector design places the feed antenna along the axis of the parabolic dish, causing the electromagnetic waves to be focused toward the reflector's surface. This arrangement, however, has some drawbacks. Because the feed is situated centrally, it can obstruct some of the reflected waves, which diminishes the antenna's

doi:10.6342/NTU202404478

overall gain and efficiency. Additionally, the feed's presence at the focal point can reduce the effective aperture of the reflector. This reduction impacts the antenna's performance by decreasing gain, lowering efficiency, and increasing side lobe levels.

2.1.2 Eccentric or offset feed reflector antenna

The off-Axis reflector antenna is a part of the primary parabolic dish which is carved out from a cylinder [10]. In the context of the off-axis, the feed is positioned off-centered by a precise angle concerning the reflector axis as shown in Fig. 2.2 [2]. In other words, the feed is placed off-center from the parabolic dish.

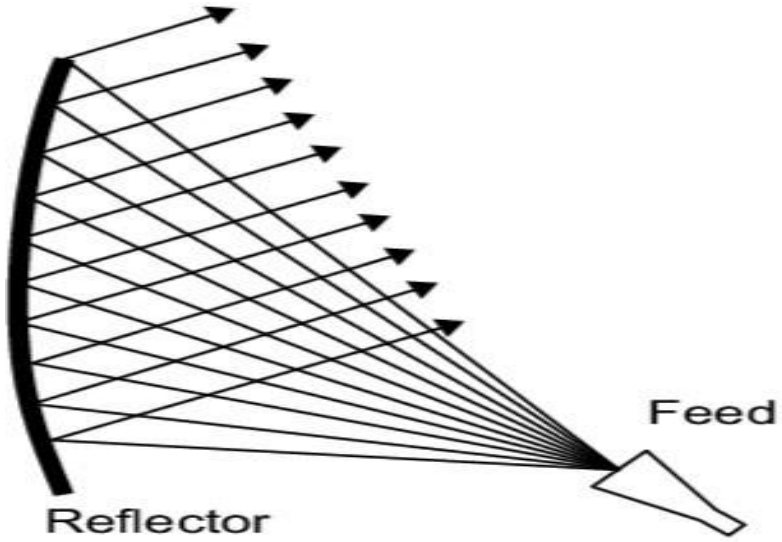

Fig. 2.2 Offset feed reflector antenna profile [2].

This orientation offers a significant advantage as it minimizes the feed blockage which is a challenge for common reflector antennas. Additionally, this configuration minimizes spillover losses, and reduces side lobe levels, leading to a more focused and efficient radiation pattern. Consequently, the offset reflector design offers improved performance compared to conventional reflector antennas. These advantages make offset reflector antennas particularly well-suited for applications such as satellite communications and long-distance electromagnetic signal transmission, where high gain and minimal interference are crucial.

doi:10.6342/NTU202404478

2.1.3 Cassegrain reflector antenna

Cassegrain reflector is a sophisticated design that incorporates a dual reflector system to achieve high performance in signal focusing and gain. This configuration consists of two reflectors, one is a parabolic reflector that serves as the primary reflector and the other one is the convex mirror/ Hyperboloid Sub-reflector that serves as the secondary reflector as depicted in Fig. 2.3.[3]

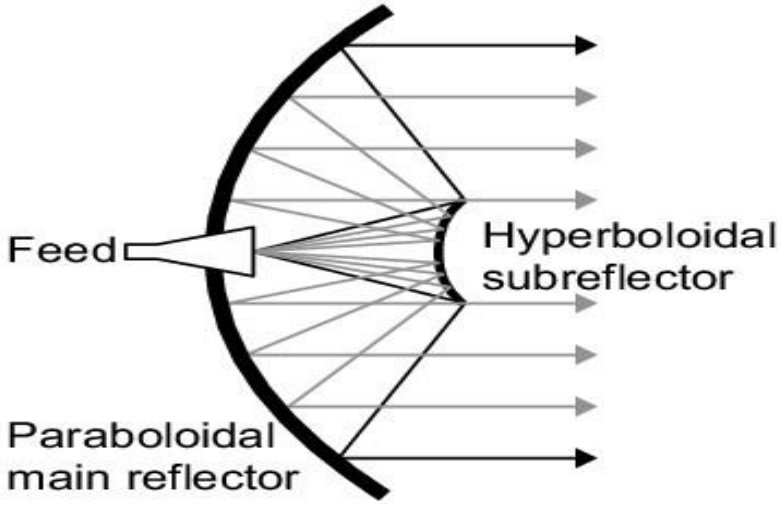

Fig. 2.3 Cassegrain reflector antenna profile [3].

Generally, both the secondary reflector and the feed antenna are situated along the central axis of the primary dish, such that EM waves are directed towards the sub-reflector and reflected towards the primary reflector. This arrangement allows for a compact design with the feed positioned behind the primary reflector, which helps to minimize blockage and maintain high gain. It is widely used in applications requiring precise signal reception and transmission, such as in radio telescopes, satellite communication systems, and high-frequency radar systems. The dual-reflector setup enhances the antenna's performance by improving the focus of the reflected waves, reducing side lobe levels, and increasing the effective aperture.

doi:10.6342/NTU202404478

2.2 Paper Survey on Offset Reflector Antennas

2.2.1 A 220-300GHz offset dual-reflector antenna for point-to-point radio

The reflector antenna proposed in [4] focuses on developing a sub-THz offset dual-reflector antenna with a feed element as a horn tailored for direct radio communication systems designed with a diameter of 115mm for operating at a frequency range of 220GHz- 300GHz. This large reflector is shown in Fig.2.4 [4], achieves a commendable gain of 48dBi, and wide bandwidth which is more suitable for long-distance communications.

Fig. 2.4 Dual offset cassegrain reflector [4].

However, the choice of fabricating brass material with gold plating poses a drawback due to its higher cost and several challenges, especially when dealing with high-frequency applications [4]. Given these extremely small skin depths, it is important to minimize surface roughness on the current-conducting surfaces. To mitigate surface roughness careful attention is necessary to enhance the antenna's conductivity and to improve the antenna's functionality, a gold plating thickness of 3 μm is considered [4]. This thicker gold plating layer provides a smoother and more uniform surface finish, which helps to reduce resistive losses and enhance signal transmission efficiency. Additionally, the lack of measured results in the paper [4] diminishes the ability to validate its performance. The

doi:10.6342/NTU202404478

normalized simulated results of the Electric(E)-plane and Magnetic(H)-plane of the dual offset Cassegrain reflector Antenna [4], are depicted in Figures 2.5(a) and 2.5(b), correspondingly.

(a)

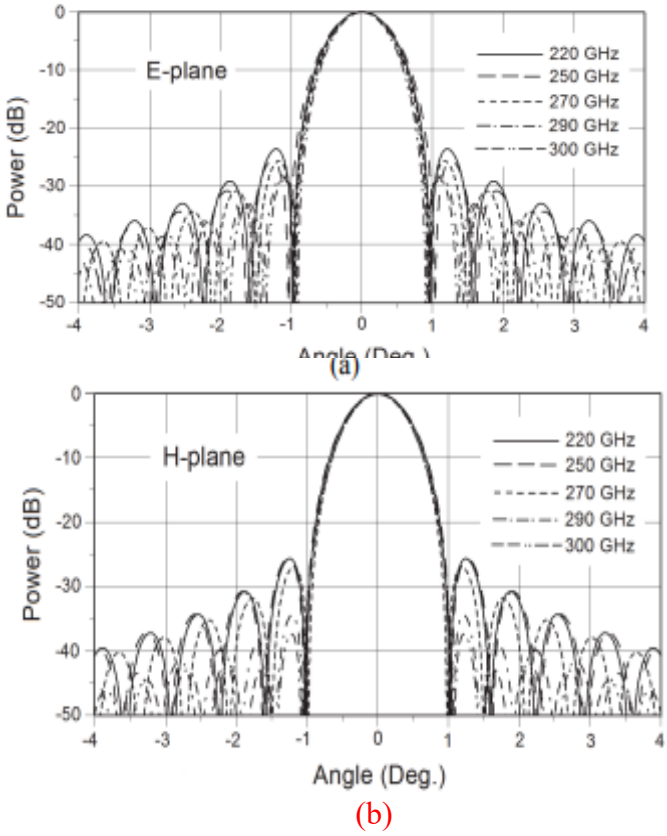

(b)

Fig. 2.5 Normalized gain patterns based on simulations (a) Electric(E)-plane (b) Magnetic(H)-plane [4].

2.2.2 A THz high-gain antenna with polarization-division multiplexing

The Reflector antenna architecture proposed in [5] seems to be interesting, focused on a high-gain offset parabolic dish antenna with the ability to utilize Polarization Multiplexing for terahertz communication systems operating at 300 GHz by incorporating two reflectors with overlapped apertures for horizontal and vertical polarizations with a reflector diameter of 360mm. Despite, achieving a gain of 60dBi, the lack of manufacturing support poses a drawback as two reflector antennas are overlapped, which might introduce cross-polarization [5]. While the paper [5] offers simulation results, it

doi:10.6342/NTU202404478

lacks valuable insights and detailed design information regarding the reflector. Moreover, this paper doesn't report any measured data. Additionally, the described frequency response is limited to a narrow range (280 GHz to 320 GHz), limiting the generalizability of the findings. The designed dual-gridded reflector antenna [5], is depicted in Fig.2.6.

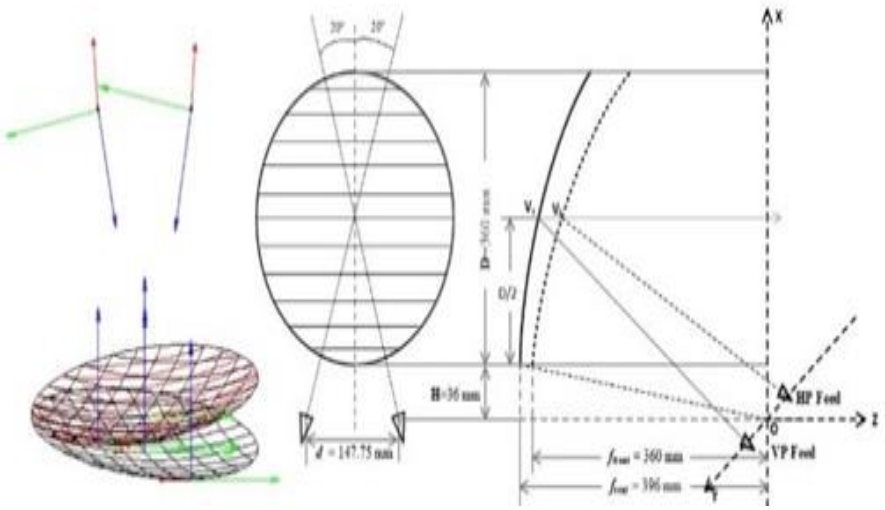

Fig. 2.6 Dual-gridded reflector antenna [5].

The simulated results of the Reflector antenna when HP and VP are employed as feeds [5], are depicted in Figures 2.7 and 2.8, correspondingly.

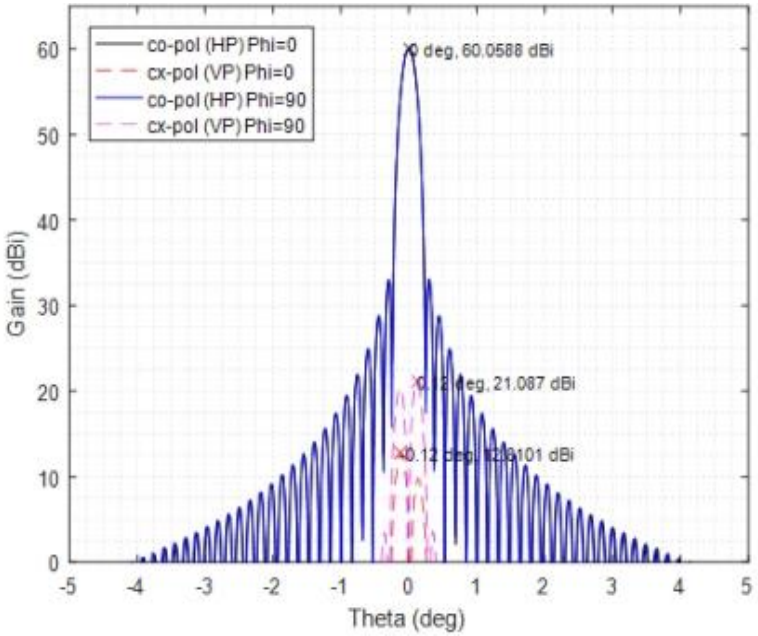

Fig. 2.7: Gain pattern of dual gridded reflector antenna with horizontal polarized (HP) feed [5].

doi:10.6342/NTU202404478

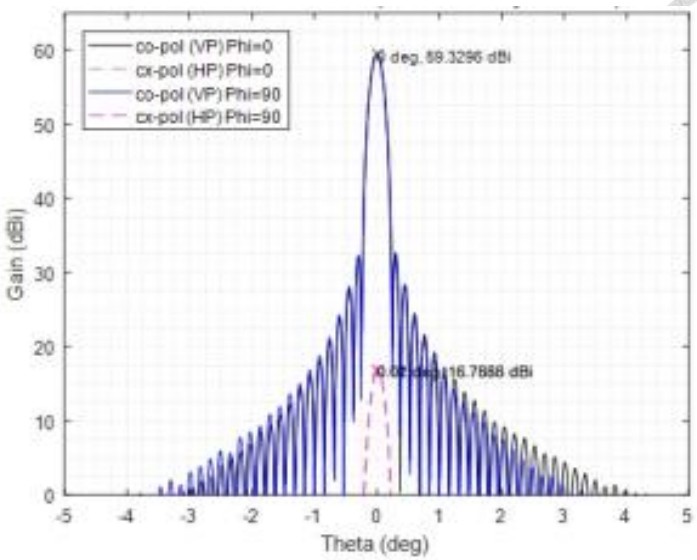

Fig.2.8: Gain pattern of dual gridded reflector antenna with vertically polarized (VP) feed [5].

2.2.3 High gain antenna for Sub-millimeter wave communications

One more offset reflector antenna proposed in [6] focuses on 330GHz tailored for sub-THz milli-meter wave communications designed with a maximum reflector diameter of 20cm, with a horn antenna as the feed element and a bandwidth of 70GHz. One gap in the research [6] is the lack of detailed information on the real-time results, even though the reflector gain was not measured the directivity of 50dBi was attained, and the reflector weight, which is approximately 2.5Kgs presents a notable drawback [6]. The fabricated offset reflector [6], is demonstrated in Fig.2.9.

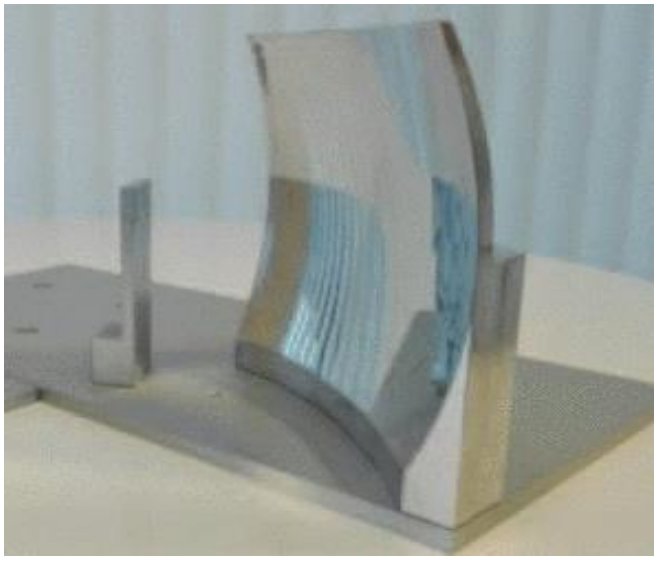

Fig. 2.9: Offset curved parabolic reflector antenna [6].

doi:10.6342/NTU202404478

Fig. 2.10(a) and Fig.2.10(b) illustrate the results of the offset reflector at 330GHz obtained through simulation and measurement, respectively [6].

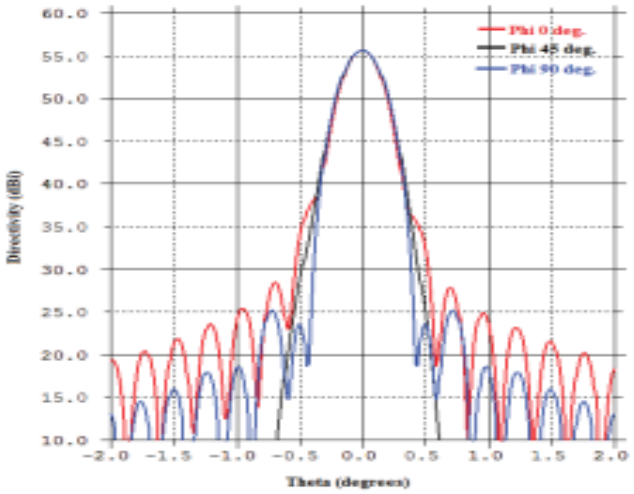

(a)

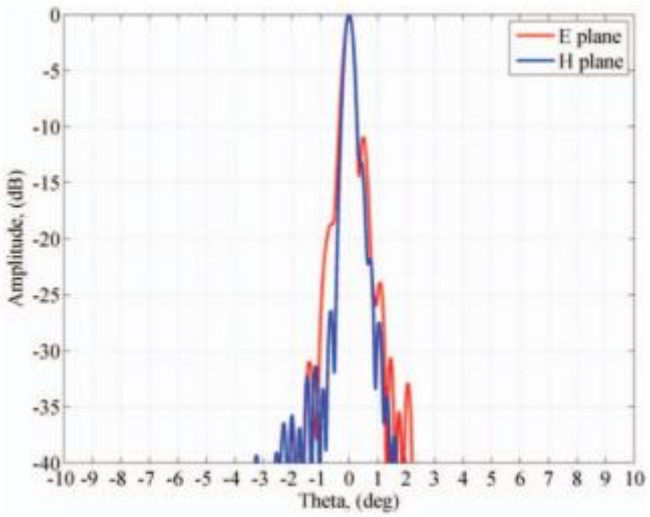

(b)

Fig.2.10 Reflector antenna gain characteristics at 330GHz (a) Simulated (b) Measured [6].

Based on the provided figures, it is evident that while the radiation characteristics plot in the simulation displays symmetry, the measured radiation pattern does not.

doi:10.6342/NTU202404478

Table. 2.1 provides a comparison of the above-discussed literature reviews on Reflector antennas.

Table. 2.1 Outlines the review of prior literature review on offset reflectors.

Parameters	[2]	[3]	[4]
Frequency	220GHz-300GHz	300GHz	330
Diameter	115	360	200
Weight	640	NA	2.5kgs
Feed type	Horn	Horn	Horn
Gain	48dBi	60.6dBi	50dBi
Material	Copper with gold plating	NA	NA

doi:10.6342/NTU202404478

Chapter 3 Design of Feed Antenna

Here, we present a concise review of the design procedure used to design a 4×4 dual-polarized antenna array with end-fire configuration operating at 300GHz [8]. This antenna design utilizes innovative AiP (Antenna in Package) technology architecture, serving as a feed element to the offset reflector. In our design, a 4×4 array of horizontally polarized elements serves as the feed component. Additionally, this chapter covers the fabrication process and provides a comprehensive evaluation based on numerical simulations of the antenna array. The detailed design of the end-fire array configuration is referred to [8], which is employed in this study.

3.1 Substrate Information

As the frequency increases, the antenna size typically decreases, so fabricating antenna arrays at Sub-THz frequencies poses significant challenges. Consequently, advanced fabrication technologies are often required to fabricate these kinds of miniaturized antennas due to their precise design requirements. The process needed to fabricate the array is shown in Fig. 3.1

Fig. 3.1 Stack-up representation of the substrate.

The design consists of four metal layers (M1~M4) made of copper material with a solder mask on top and bottom, each having a thickness of 20μm. The core layer in the

doi:10.6342/NTU202404478

substrate serves as the dielectric material and provides essential mechanical support while fabricating the antenna.

Furthermore, information on the substrate is given in Table 3.1. Based on the below process parameters Sub-THz antenna array operating at 300GHz is designed with relative thickness provided by the company and encompasses over the frequency range of 240GHz-310GHz.

Table. 3.1 Summary of substrate information.

	Thickness	Material	ε_r	$\tan\delta$
Prepreg	20 μm	HL972LF (LD)	3.6	0.005
Core	60 μm	HL972LF (LD)	3.6	0.005
Solder Mask	20 μm	AUS AR1Z	3.5	0.014

3.2 Antenna Design

The AiP design presented in [8] is an end-fire antenna with a 1×4 element array that supports dual-polarization. However, since this thesis concentrates on the design of the reflector to analyze its radiation characteristics, only the H-polarized elements are considered.

Although V-polarized elements are part of the antenna prototype, they are not included in this study due to the difficulty of configuring the output port alongside the H-pol elements for future measurement validation.

Figure 3.2 provides an overview of the H-pol antenna element architecture, highlighting its radiation characteristics. These characteristics serve as a reference to verify performance when the elements are used to feed the reflector for directional beam applications

.

doi:10.6342/NTU202404478

3.2.1 Design of horizontally-polarized antenna unit

Fig 3.2 illustrates the design for the horizontally polarized antenna unit in the 1×4 end-fire dual-polarized antenna array.

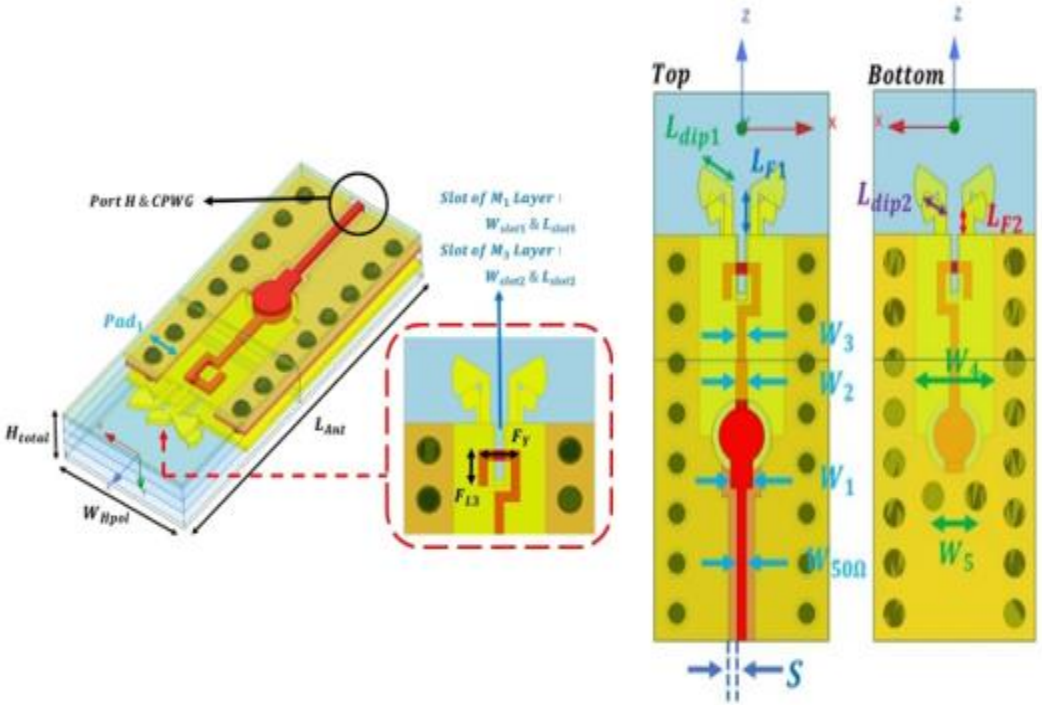

Fig. 3.2 Proposed horizontally polarized component side view.

The horizontally polarized component consists of slots of two bow tie dipole antennas one is on the M1 layer and the other is on the M3 layer, which is coupled through a feeding line on the M2 layer. The feeding line is a Microstrip balun that transforms the current port to a differential port for excitation of dipole. The size of the dipole on M1 is larger when compared to the dipole on the M3 layer to meet the broadband requirements. Bowtie dipole antennas are known for their wider bandwidth. Hence, Bowtie structures are indeed more advantageous when compared to triangular and square dipoles.

The feeding layer on the M2 layer is connected to a circularly polarized waveguide (CPWG) feed port located on the M1 layer through via. This surface routing facilitates a convenient connection with the chip. The spacing between these via walls on both sides related to the Horizontally polarized antenna component is 140um. These via walls help

doi:10.6342/NTU202404478

minimize spacing and isolate the field Pattern. The overall dimensions for Horizontally polarized elements are 1536×606×224 μm^3.

3.2.2 Design of 1×4 horizontally polarized end-fire antenna configuration

The designed Horizontally Polarized antenna elements are organized in an interleaved manner (V-pol antenna elements) to form a 1×4 antenna array as depicted in Fig. 3.3. The V-pol element structure is referred to [8].

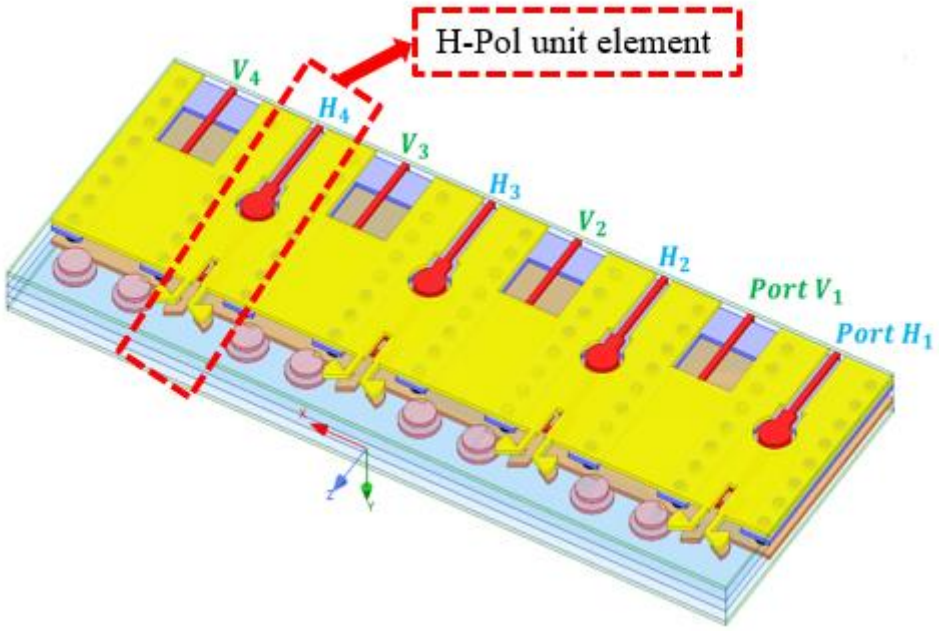

Fig. 3.3 Arrangement of a horizontally oriented 1×4 antenna array with end-fire configuration.

Figures 3.4 and 3.5 represent the modeled Gain patterns for the Horizontally-oriented 1×4 Antenna array, with the array achieving gains of 11.5 decibels at 260 Gigahertz and 9.5 decibels at 300 Gigahertz, respectively

doi:10.6342/NTU202404478

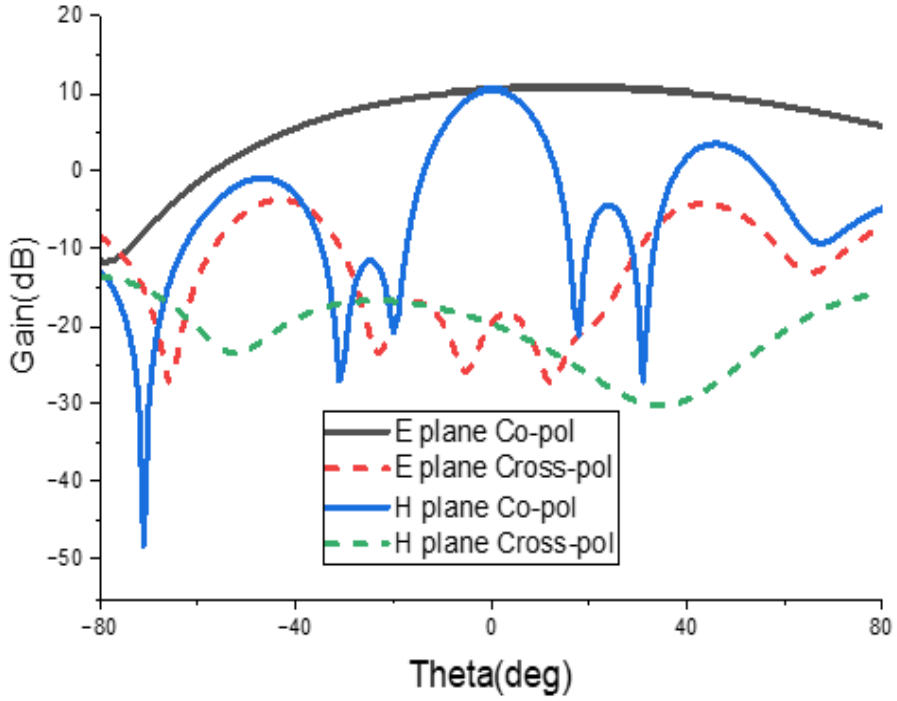

Fig. 3.4 Radiation pattern of the horizontally oriented 1×4 antenna array with an end-fire configuration at 260 GHz.

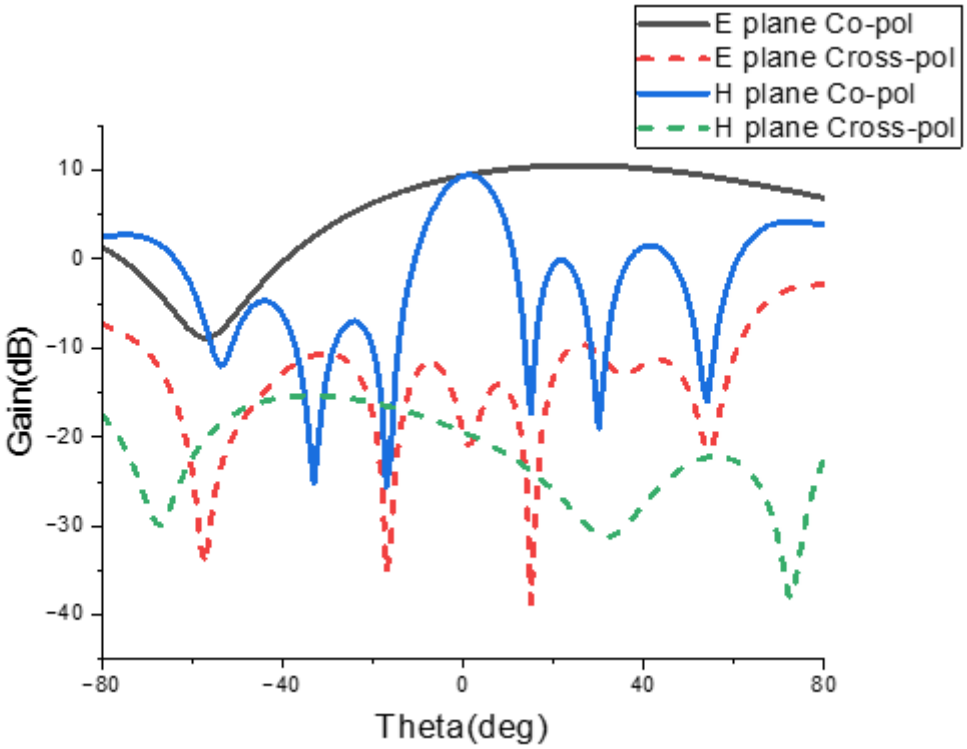

Fig.3.5 Radiation pattern of horizontally oriented 1×4 antenna array with an end-fire configuration at 300 GHz.

doi:10.6342/NTU202404478

3.2.3 Design of 4×4 H-pol Antenna array with End-fire configuration

The designed unit element is arranged in an interleaved manner to form a 4×4 array as shown in Fig. 3.6.

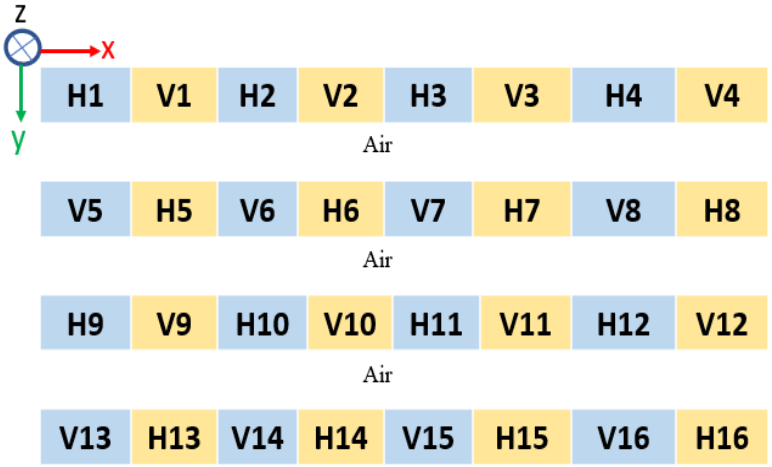

Fig. 3.6 Arrangement of 4×4 end-fire antenna array.

Each antenna element is individually fed by separate ports. Each port is supplied with a specific power level and phase to achieve desired radiation patterns, phase correction, and beam steering. To reduce cross-polarization level (XPL), the front-end of the H-pol feeding lines is configured with a hook-like structure placed in a mirrored arrangement, and they are given nearly 180° out-of-phase. To reduce the spacing between antennas, the arrangement order of the second row in the array will be opposite to the first row. Following this pattern, the array order can be expanded to 4x4. The port distribution diagram of the 4x4 end-fire array with HV interleaved arrangement as shown in Fig. 3.7. Fig. 3.7 presents the 3-D structure of the proposed Sub-THz dual-polarized 4x4 end-fire array with interleaved arrangement.

The vertical separation between each antenna array is $300\mu m$. This air gap will be created using solder balls in AiP (Antenna-in-Package) technology in the future implementation. The overall dimensions of the 4x4 array antenna are given by $1536 \times 3876 \times 1796$ (μm^3). The final values for the geometric parameters after fine-tuning are provided in Table. 3.2.

doi:10.6342/NTU202404478

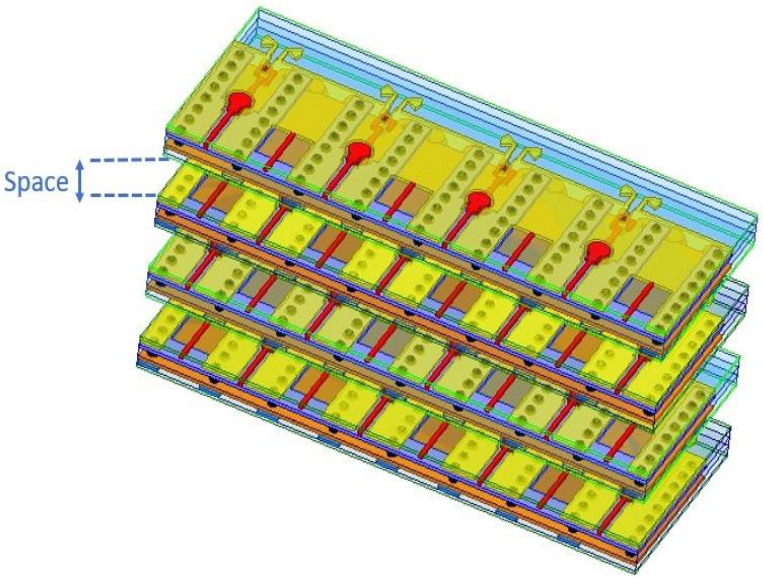

Fig. 3.7 Proposed 4×4 antenna array with end-fire configuration.

The final optimized geometric values of the 4×4 Antenna Array with End-fire Configuration are summarized in Table. 3.2

Table. 3.2 Final geometric values of the 4×4 H-pol antenna array.

Parameters	Value(um)
L_{dip1}	120
L_{dip2}	135
L_{F1}	90
L_{F2}	75
W_1	74
W_2	30
W_3	40
W_4	294

The proposed 4×4 array is completely simulated to verify its radiation characteristics. Figures 3.8 and 3.9 illustrate the modeled gain plots of the 4×4 horizontally polarized antenna array at 260 GHz and 300 GHz, respectively.

doi:10.6342/NTU202404478

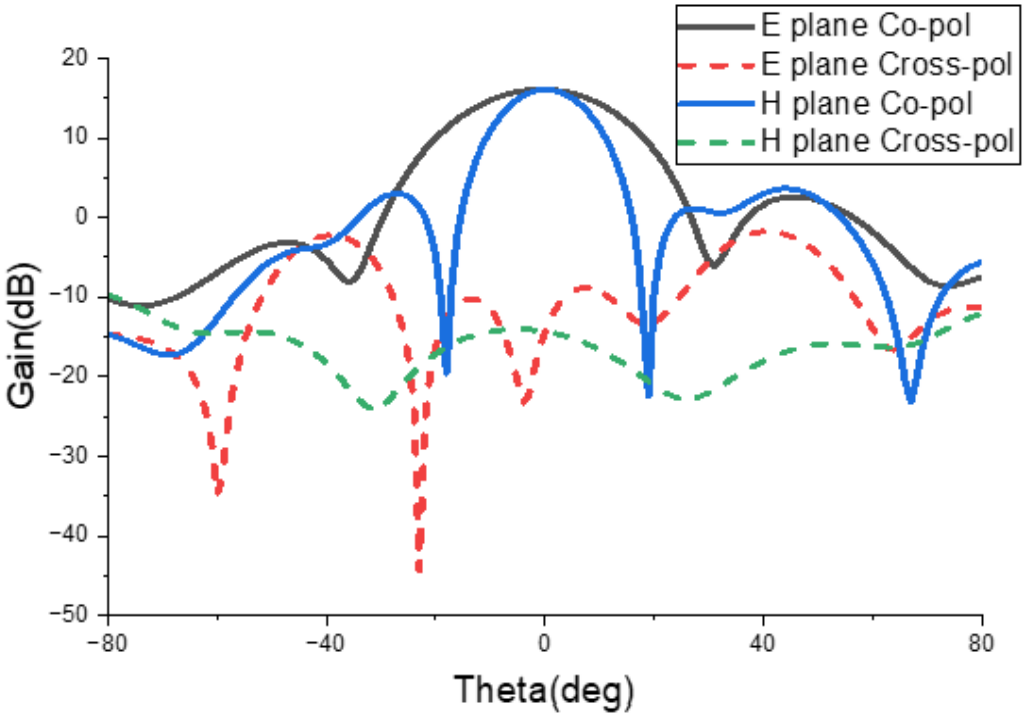

Fig. 3.8 Gain plot of 4×4 H-pol antenna array with end-fire configuration at 260GHz.

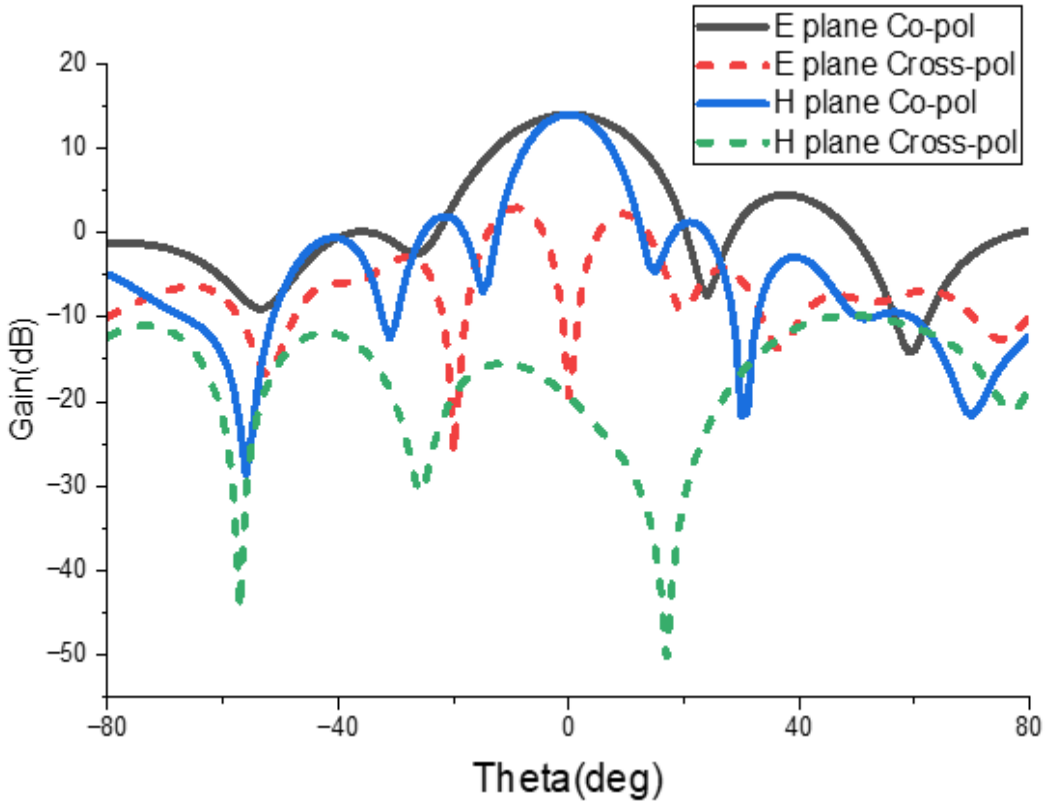

Fig. 3.9 Gain plot of 4×4 H-pol end-fire antenna configuration at 300GHz.

doi:10.6342/NTU202404478

Gain patterns for the 4 × 4 end-fire configuration of the horizontally polarized antenna, including 260GHz, and 300GHz are shown in Fig. 3.8 and Fig 3.9, the corresponding gains are 16.2, and 13.9 decibels, correspondingly. The sidelobes are suppressed by at least 12 dB compared to the main lobe, and the XPL (cross polarization level) is maintained below -15 decibels in the central beam region, exceptional for E plane cross-pol at 300GHz because the losses are of 4×4 antenna array are more pronounced at higher frequencies.

The rationale behind these gain performances is explained as follows. An array of N elements increases the antenna gain by $3\,log_2(N)$, resulting in a 12dB gain. Accordingly, the element gains at 260 GHz and 300 GHz are observed to be 4.2 dBi and 1.9 dBi, respectively

doi:10.6342/NTU202404478

Chapter 4 Design and Simulation of Offset Reflector Antenna

In this chapter, we explore the essential design considerations pivotal for crafting offset reflectors, laying the groundwork for an in-depth design process.

Designing an offset reflector necessitates careful attention to key parameters to ensure optimal performance. These parameters encompass geometrical considerations such as focal length, offset angle, offset height, material selection, structural design, and optimization techniques. Through meticulous consideration of these aspects, our goal is to craft an offset reflector design optimized for high gain and minimal sidelobe levels.

Moreover, we will underscore the significance of these design considerations in achieving desired antenna characteristics, including narrow beamwidth, enhanced gain, and low cross-polarization levels. By elucidating these considerations, we aim to provide a practical understanding of the offset reflector design process, which will be further detailed in section 4.2. This reflector will be fed by the proposed end-fire antenna array to investigate the radiation characteristics at sub-THz frequencies.

4.1 Design Considerations of Offset Reflector

4.1.1 Geometry & size of reflector

The geometry of the reflector is crucial in defining its functional characteristics. Typically, antennas are designed with specific sizes to attain the desired radiation Pattern. The dish antenna diameter is often expressed relative to the operating wavelength. According to guidelines, the reflector diameter should be approximately 30 times the wavelength to achieve optimal gain and minimal sidelobe levels. The larger the “dish” in terms of wavelength, the gain of the reflector increases proportionally higher directivity levels can be achieved increased with cost and should be manufactured with care, and vice versa [10]. Conversely, as the effective aperture of the reflector is smaller than its

doi:10.6342/NTU202404478

wavelength then the spillover efficiency of the reflector increases. In the context of Reflector antennas, spillover efficiency measures the amount of power radiated by the reflector. Due to finite size, some amount of power is radiated outside of the aperture which is not reflected is known as spillover efficiency. Therefore, optimizing reflector size requires balancing the gain against spillover efficiency.

4.1.2 Derivation of the offset angle

The angular offset represents the angle formed between the main feed axis and the central axis of the reflector. The primary importance of the offset angle lies in its ability to minimize blockage effects. In traditional parabolic reflector antennas, where the source antenna is conventionally placed at the center of focus, significant portions of the reflective surface can be blocked, leading to reduced efficiency and degraded performance. By offsetting the feed, the reflector's aperture remains unobstructed, maximizing the capture and reflection of electromagnetic waves. An inappropriate offset angle can lead to under-illumination or over-illumination resulting in decreased gain and increased sidelobe levels. Based on the parameters, the offset angle of the reflector can be calculated by using formulas as mentioned in [9].

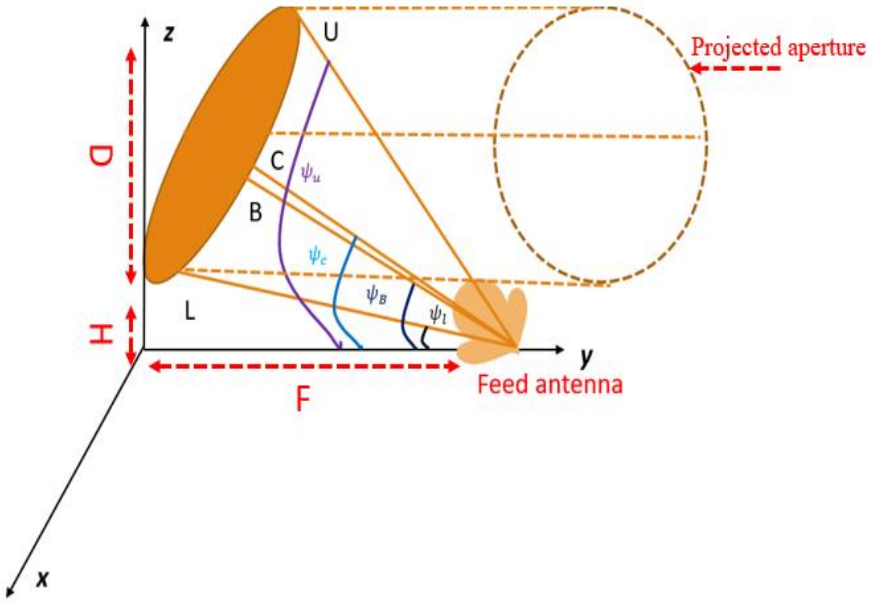

Fig. 4.1 Representation of offset angle.

doi:10.6342/NTU202404478

Based on the parameters depicted in Fig 4.1, the calculation of the offset angle for the reflector can be conducted to ensure effective illumination of the antenna surface. The equations to calculate the Offset angle of the reflector antenna are expressed in [9]. The equations are as follows:

$$\psi_u = 2\tan^{-1}\frac{(D+H)}{(2\times F)}, \tag{4.1}$$

$$\psi_L = 2\tan^{-1}\frac{(H)}{(2\times F)}, \tag{4.2}$$

$$\psi_c = 2\tan^{-1}\frac{(\frac{D}{2}+H)}{(2\times F)}, \tag{4.3}$$

$$\psi_B = \frac{\psi_u + \psi_L}{2}, \tag{4.4}$$

where F is the focal length, H is the offset height, D is the diameter of the offset reflector and ψ_c is the center angle towards which the feed antenna is rotated. Hence, the calculated offset angle is determined to be ψ_B, suggesting that initially the feed antenna should be placed at an angle of ψ_B concerning the feed axis. However, it is important to note that this might not be the fixed offset angle, as further adjustments or optimization of the offset angle may be necessary based on the illumination of the feed along with the performance of the reflector which can be discussed in detail in chapter 4.

4.1.3 Offset height

The offset height, defined as the separation from the feed to the vertex of the paraboloid along the axis perpendicular to the reflector surface, is crucial for determining the performance of offset reflector antennas.

It is essential tuning the offset height of the reflector to minimize blockage of EM waves helps in reducing cross-polarization levels compared to traditional on-axis feed antennas. Properly optimizing the offset height and the feed position can help in reducing spillover. By placing the feed antenna in a position where it can effectively illuminate the

doi:10.6342/NTU202404478

reflector without spilling over the edges. Fig. 4.2 illustrates the representation of offset height.

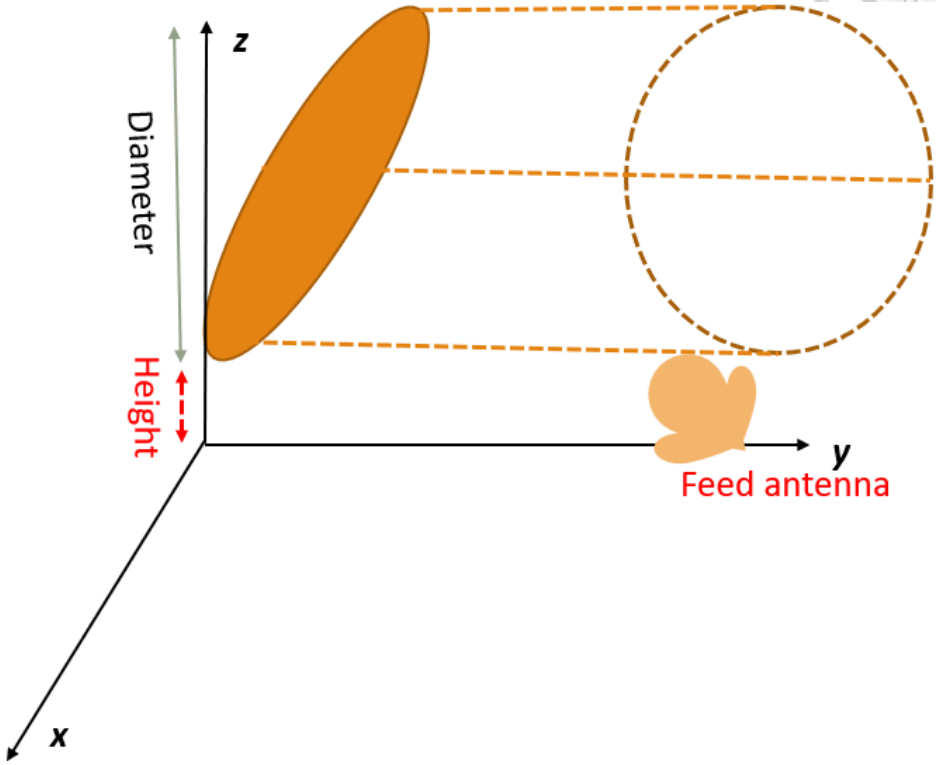

Fig. 4.2 Representation of offset height.

4.1.4 Focal length optimization

Focal length is a crucial parameter in the design of parabolic antenna dishes as it determines the distance between the feed and the dish antenna surface. Proper focal length selection is essential to ensure the effective convergence of reflected electromagnetic waves, thereby maximizing the signal strength of the antenna system. The relation between gain and Focal length can be represented as shown in 4.5. By eq (4.5), it can be stated that a longer focal length generally results in a shorter beam width and higher gain, while a shorter focal length leads to a wider beam width and lesser gain. This behavior can be explained by aperture efficiency, where a longer focal length results in a smaller surface curvature for the reflector, leading to a more uniform aperture field. However, when the focal length is longer the spillover increases because the span angle from the

doi:10.6342/NTU202404478

focal point (from the feed's position) becomes smaller. Thus, the Focal length should be chosen accordingly to satisfy the particular criteria of the antenna design.

$$G = \left(\frac{\pi D}{\lambda}\right)^2 \eta \tag{4.5}$$

The representation of focal length is presented in Fig. 4.3.

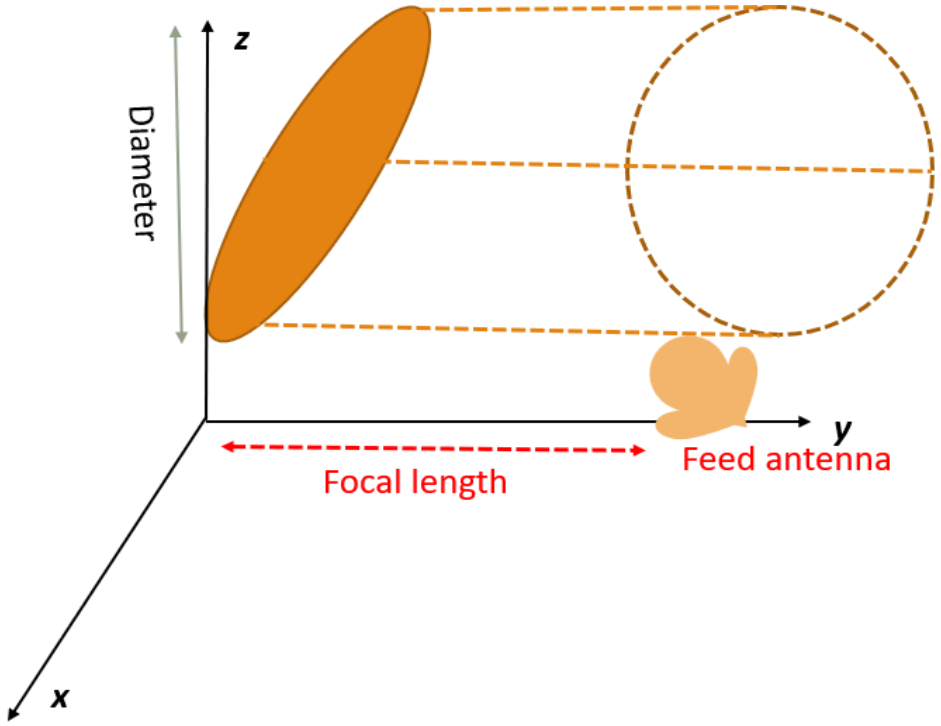

Fig. 4.3 Representation of focal length.

4.1.5 Material selection

As the antenna operates at such high frequencies, electromagnetic waves behave differently when compared to lower bands and the choice of materials becomes more limited due to increased losses. High electrical conductivity materials are chosen to minimize surface losses. Metals such as aluminum, copper, and gold are commonly used for reflector antennas at sub-THz frequencies due to their high conductivity, and to reduce the skin depth. However, it's essential to consider the skin depth effect at these frequencies, which may limit the choice of materials based on thickness.

Apart from the above requirements, cost is also a significant factor, as the chosen material not only meets the performance requirements but also be compatible with cost-

doi:10.6342/NTU202404478

effective fabrication technologies. For example, aluminum is a widely used material for reflector antenna due to its excellent conductivity and relatively low cost, whereas copper and gold offer superior conductivity and are more expensive, and it might be challenging to fabricate. There is another factor to consider while selecting the material, and that is penetration depth into the material (Skin-depth).

The skin depth (δ) represents the depth within a material where the electromagnetic field strength decreases to around 37% of its original value at the surface due to the skin effect. This phenomenon results in alternating current (AC) being confined mainly to the outer layers of the conductor, with the current density progressively reducing as it penetrates further inward. The formula for skin depth is expressed in [2] by using the following equation 4.6

$$\delta = \sqrt{\frac{2\rho}{\omega\mu}} \tag{4.6}$$

where is the ω angular frequency, μ is the magnetic permeability, and ρ is the electrical conductivity of the material.

4.1.6 Material thickness relative to skin depth

Thin Material (Thickness$< \delta$)

When the width of the material is less than the penetration depth, the electromagnetic wave penetrates through the entire thickness of the material. In this case, the material may not provide effective shielding or reflection because the wave can pass through or significantly penetrate the material.

Material Thickness Comparable to Skin Depth (Thickness$\approx \delta$)

When the thickness of the material is on the order of the skin depth, a significant portion of the electromagnetic wave is attenuated within the material, but some penetration still occurs. This scenario provides moderate shielding and is often used when

doi:10.6342/NTU202404478

some degree of penetration is acceptable or when designing specific components like certain types of antennas.

Thick Material (Thickness > δ)

When the material thickness is several times greater than the skin depth, electromagnetic waves are almost entirely attenuated near the surface, with negligible penetration. This ensures excellent shielding or reflection as the waves cannot penetrate deeply. For reflector antennas, the material thickness must be sufficient to prevent significant wave penetration, ensuring the majority of the wave's energy is reflected. Therefore, effective waves blocking or reflecting is achieved.

doi:10.6342/NTU202404478

4.2 Design Methodology for Offset Reflector

The detailed design flow of the offset reflector is depicted in Fig. 4.4. Following the design flow outlined offset reflector antenna is crafted.

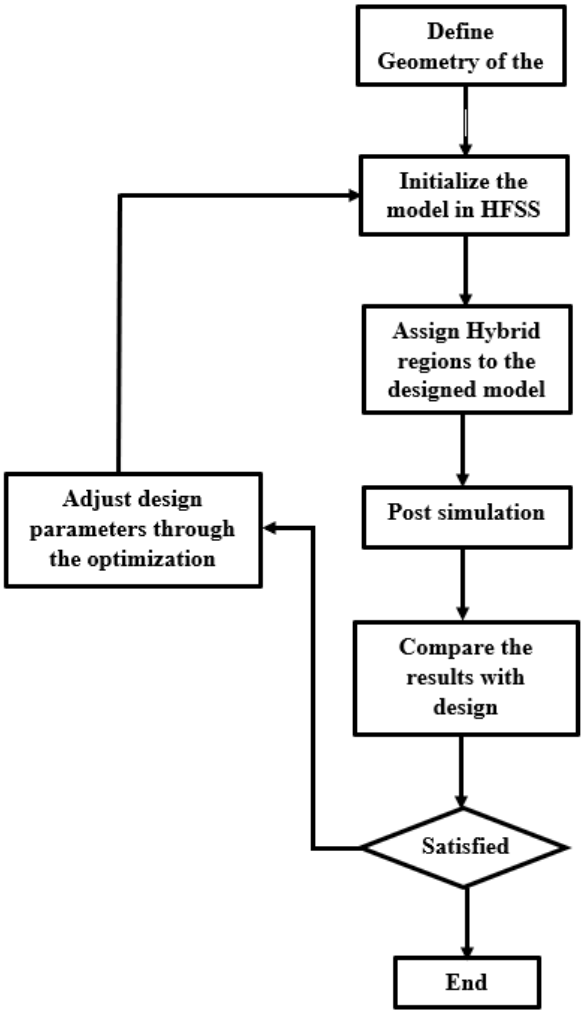

Fig. 4.4 Design flow for the simulation of offset reflector.

4.3 Design of Offset Reflector using HFSS

This sub-chapter discusses the design of an offset reflector antenna at 300GHz which relates to the design considerations mentioned in Sub-Chapter 4.1, and its simulation methodology and simulation results using a high-frequency structure simulator tool.

doi:10.6342/NTU202404478

4.3.1 Steps to design reflector antenna

An off-axis reflector antenna is a section of a symmetrical parabolic dish. The design of an offset reflector involves several steps discussed in detail. The general equation of an off-axis reflector antenna is expressed in by using the following equation 4.6.

$$z = \frac{x^2}{4F} \tag{4.6}$$

Step 1: Create an equation-based curve. In the equation-based dialog box input the mathematical equations that describe the Primary parabolic surface as shown in Fig. 4.5, where t varies from 0 to R.

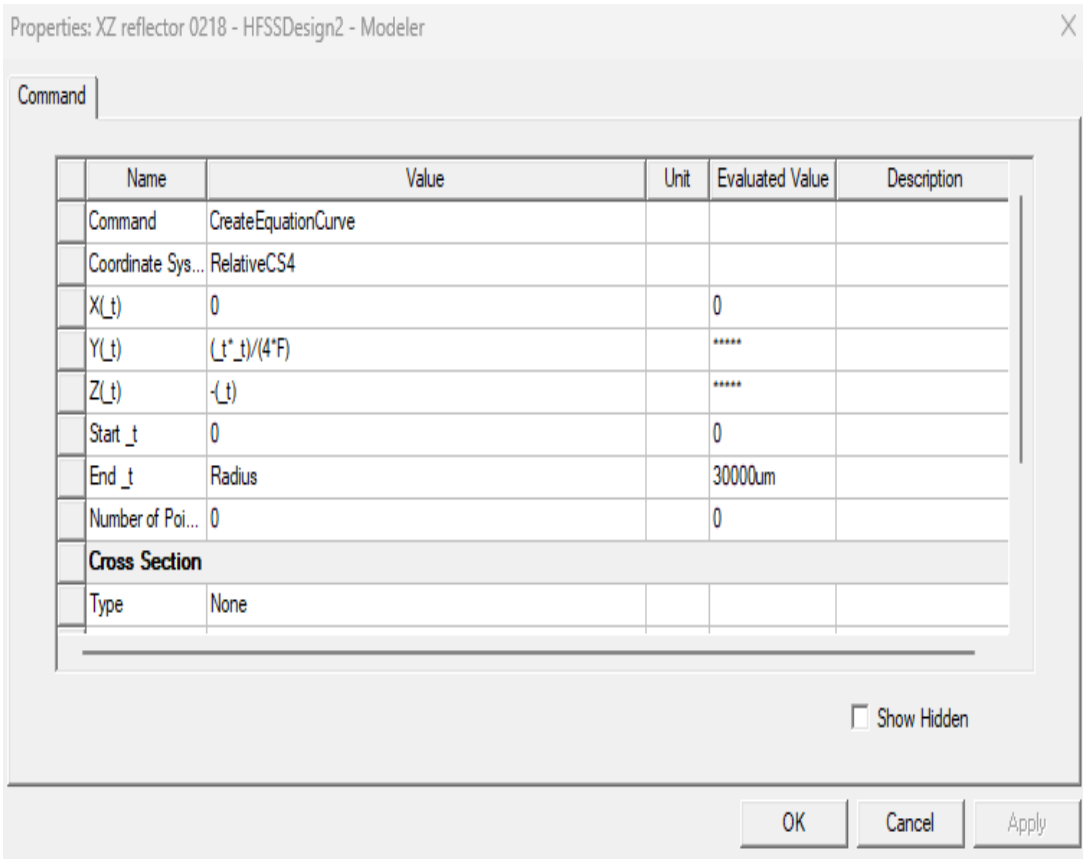

Fig. 4.5 Creation of equation-based curve.

doi:10.6342/NTU202404478

Step 2: As fabricating the curve-based model at sub-THz frequency is complicated, instead of directly assigning the thickness to the reflector we prefer to create a polyline with the required thickness of 10mm as it consists of a flat surface and connect the polyline to the curve illustrated in Fig. 4.6.

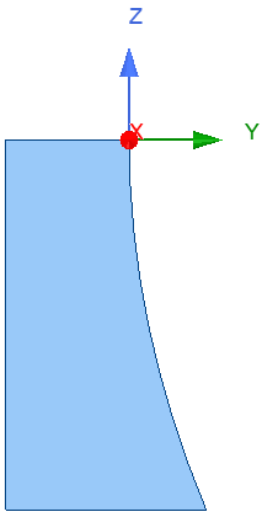

Fig. 4.6 Representation of equation-based curve.

Step 3: The created equation-based curve is swept using the sweep around axis command to create a loop that can be considered as a parabolic reflector or primary reflector with a diameter of 60mm as shown in Fig. 4.7.

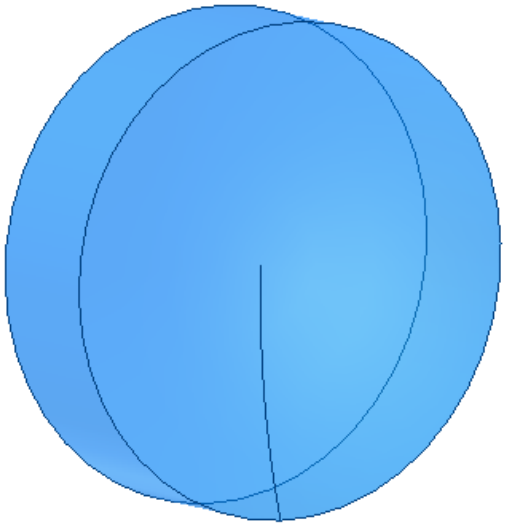

Fig. 4.7 Representation of parabolic reflector design.

doi:10.6342/NTU202404478

Step 4: The offset reflector surface is the intersection of a cylinder with a diameter of 30mm which is carved out from the primary parabola surface as shown in Fig. 4.8.

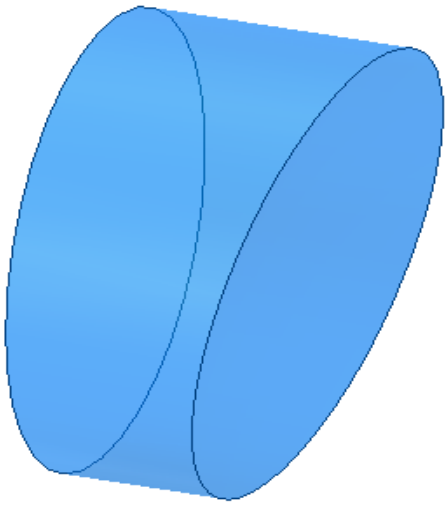

Fig. 4.8 Representation of offset parabolic reflector design.

The optimized dimensions of the above-designed off-axis paraboloid reflector antenna are shown in Table 4.1.

Table. 4.1 Geometry of offset Reflector.

Parameters	Value (mm)
Diameter of primary reflector(mm)	60
Diameter of offset reflector (mm)	30
Offset height (mm)	1
Offset angle (degrees)	36
Feed element	4×4 end-fire antenna array
Center Frequency (GHz)	300
Gain (dB)	>23dB
Bandwidth (GHz)	>60GHz
S11 (dB)	<-10

doi:10.6342/NTU202404478

After concluding the design, the reflector is fed by the 4×4 end-fire antenna array to assess the functionality of the offset reflector antenna. The reflector antenna setup including with is shown in Fig. 4.9.

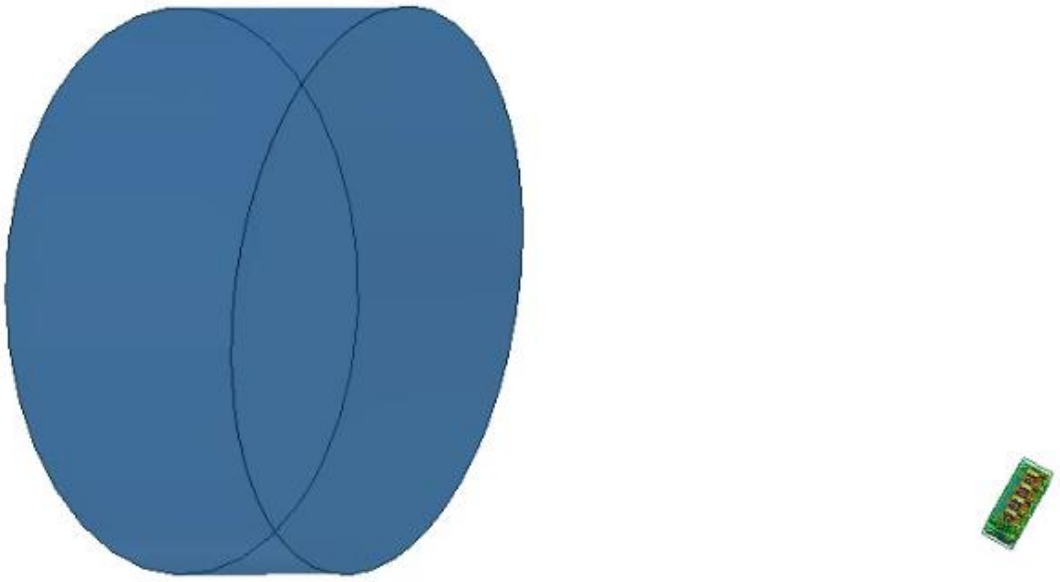

Fig. 4.9 Representation of offset reflector design set-up in HFSS.

Before delving into examining the parametric studies of the reflector few more crucial topics need to be discussed i.e., The methodology to simulate the reflector Antenna and Phase calibration of the antenna array.

4.4 Reflector Antenna Simulation Technologies in HFSS

HFSS provides various types of Simulation technologies tailored to the specific type of problem that you want to solve. They are:

- **Finite Element Method (FEM)**
- **Integral Equations**

Let's explore each simulation methodology to determine which one is most suitable for simulating a reflector antenna.

doi:10.6342/NTU202404478

4.4.1 FEM technique

The FEM method is well-suited for simulating 3D geometries with complex and arbitrary shapes. This approach involves discretizing the geometric model into numerous tetrahedral elements that align with the boundaries of the structure. These elements are particularly effective for creating irregular and varied meshes, as they can adapt to fit a wide range of shapes. The mesh represents the electromagnetic characteristics of the structure and is used in the simulation process. The simulation space is defined by the mesh and its surrounding boundary, which establishes the extent and boundary conditions for the FEM simulation. These boundaries and conditions are crucial for solving Maxwell's equations throughout the model using advanced mathematical techniques. FEM is proficient in managing intricate materials and geometries, generating a volume-based mesh to solve the model and derive field solutions, as depicted in Fig. 4.10 [13] [14]. However, FEM might not be the most effective method for modeling large aperture antennas due to its volume-based approach.

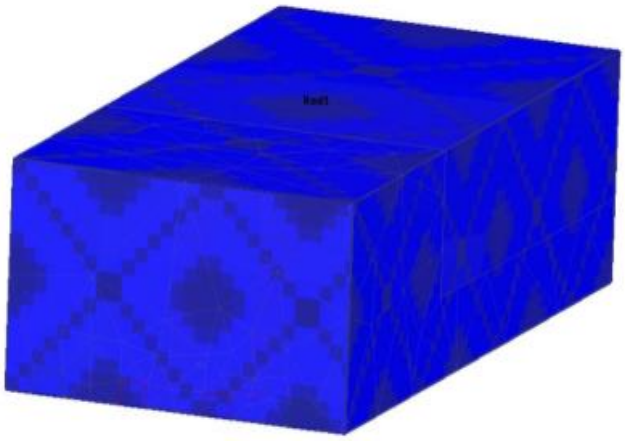

Fig. 4.10 FEM solution example [13].

4.4.2 Integral equations

HFSS-IE operates seamlessly within the HFSS desktop environment, sharing the same interface and analytical framework. This integration ensures that users already familiar with HFSS will find HFSS-IE straightforward to use, requiring minimal

doi:10.6342/NTU202404478

additional training. HFSS-IE employs the 3D Method of Moments (MoM) technique, which is highly effective for solving problems related to open radiation and scattering, making it particularly suitable for structures mainly composed of metal, although dielectrics can also be included. Practical applications of HFSS-IE include radar cross-section (RCS) analysis and the design of large aperture antennas. Unlike finite element methods, HFSS-IE works in an open environment, eliminating the need for radiation boundaries or air volumes. It is especially useful for evaluating electrically large metallic structures, such as vehicle-mounted antennas and reflector systems. Furthermore, HFSS-IE uses the adaptive cross approximation (ACA) technique, which significantly reduces computational resources for large-scale problems, complementing its automatic adaptive meshing algorithm. HFSS-IE includes two types of Integral Equation solvers. They are:

- **Hybrid FEM-IE**
- **Physical Optics Solver**

Hybrid FEM-IE

HFSS provides a hybrid approach that merges the finite element Technique (FEM) and the integral equations approach (IE) into a unified solution, offering several advantages. This combined method allows the IE technique to the transmission of fields through open space and around conductors external to the FEM region, which eliminates the need for a volumetric mesh throughout the FEM region typically required for detailed antenna geometry and dielectric modeling.

Additionally, the IE solution region can seamlessly integrate with the FEM region, enabling currents to flow between solution domains.

Fig.4.11[13], demonstrates the application as well as the use of this FEM and IE hybrid approach on two antenna designs.

doi:10.6342/NTU202404478

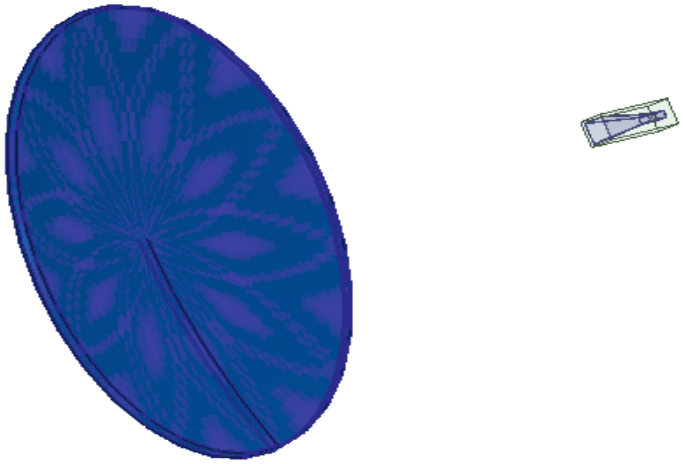

Fig. 4.11 Representation of hybrid simulation of parabolic reflector antenna [13].

HFSS solves by assigning FEM- BI technique to the source antenna (horn), the primary and secondary reflectors are evaluated using the IE method. Utilizing this HFSS FEM-IE solution type resulted in a 10-fold reduction in RAM usage compared to the FEM solution type.

Physical Optics Solution

Ansys High-Frequency Structure Simulator -Integral Equations also provides a Physical Optics (PO) method that can also be addressed for extensively large reflectors, where currents are estimated in lit regions and considered negligible in shadowed areas. This solver serves as an alternative in the Ansys HFSS-IE configuration and can use a linked HFSS simulation for input.

With the PO approach, Ansys High-Frequency Structure Simulator examines the antenna radiation patterns, considering reflections from surrounding objects. Common uses involve the analysis of large-scale reflector structures and determining antenna positioning. For instance, in Figure 7, a reflector antenna analysis is depicted, where the geometry comprises a large metallic reflector surface with a conical feed horn. The PO

doi:10.6342/NTU202404478

solver delivers results rapidly, making it well-suited for assessing electrically large structures and facilitating fast design evaluations.

4.5 Simulation of Offset Reflector using HFSS FEM-IE

As mentioned in section 4.4, to simulate an offset reflector antenna we prefer the HFSS-IE solver, as the current version of the HFSS PO solver available in the HFSS tool provides inaccurate results.

The representation of FE-BI and IE region assignment is shown in Fig. 4.12 and Fig. 4.13 respectively. To assign FE-BI region follow these steps go to the menu bar **HFSS> HYBRID> ASSIGN HYBRID> IE REGION**.

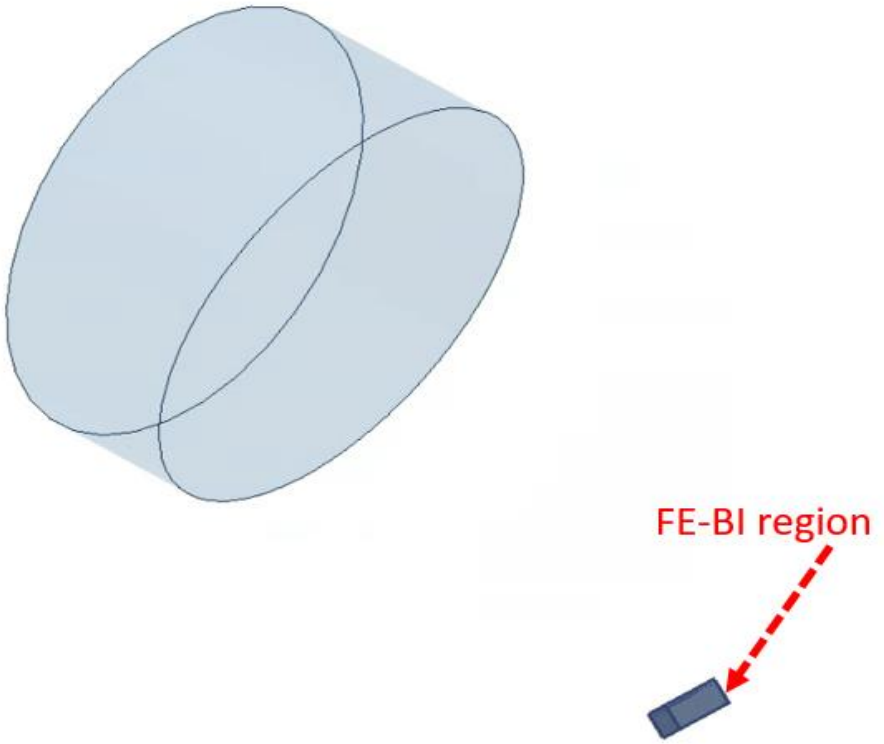

Fig. 4.12 Representation of HFSS FE-BI region.

In the same way, to assign the IE region for the reflector select the reflector structure and go to the menu bar **HFSS> HYBRID> ASSIGN HYBRID> IE REGION** as shown in Fig. 4.13.

doi:10.6342/NTU202404478

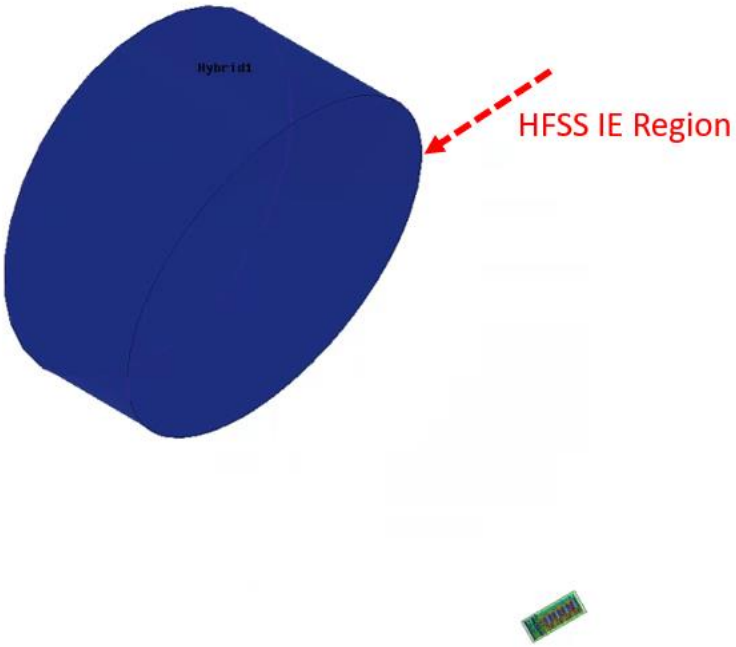

Fig. 4.13 Representation of HFSS-IE region.

The reflector antenna is now prepared for simulation and analysis to determine its characteristics. The total time and memory required to simulate the designed setup is approximately 3 hours and 130 GB of memory respectively.

4.6 Phase Calibration

The reflector is fed by the 4×4 end-fire antenna array as illustrated in Fig. 4.13. In this case, the location of the array should be properly determined. It is placed away from the focal point such that calibration can be performed to adjust the feed array's radiation pattern. This calibration intends to produce an equivalent phase center that can coincide with the reflector focal point to focus the radiation solely.

As the feed antenna is a 4×4 array, it is important to make the radiation pattern of individual elements in the presence of a reflector interfere constructively in a preferred direction for beam focussing. This can be controlled by exciting the Phase of individual antennas, also known as Phase calibration. For antenna arrays to work efficiently they must be calibrated both in amplitude and phase, where the calibration of phase is important. In the realm of an antenna array phase calibration is, exciting the array with

doi:10.6342/NTU202404478

the required phase to achieve the desired radiation pattern. Let's examine how this phase calibration affects the results with examples.

4.6.1 Procedure of phase calibration of reflector with Antenna array

In the context of reflector antennas, the phase of the antenna array is calibrated along with the reflector such that the radiation maximum radiation pattern can be focused on the reflector by which maximum gain can be achieved. Generally, calibrating the phase at an angle where the maximum gain occurs is common in antenna arrays and this requires following a specific procedure to determine the necessary phase adjustments.

Based on the orientation of the antenna's cut, in our case, the phase calibration is performed at theta=0 and phi=90 for each port. During calibration, the calibrating port amplitude is assigned to 1, the remaining ports are assigned to 0 and the same procedure is applied to calibrate the remaining ports. After calibration, the conjugate of the calibrated angle is assigned to the ports. Examples of phase calibration procedures are shown in Figures 4.14 and 4.15, correspondingly.

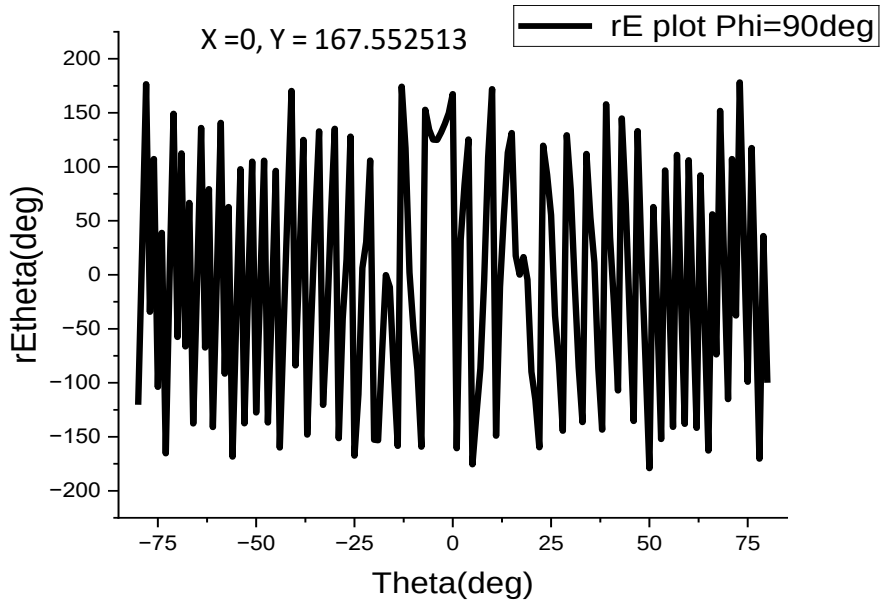

Fig. 4.14 Procedure of phase calibration.

As shown in Fig. 4.14, if the calibrated angle is 167.55 then -167.55(Conjugate) should be assigned to the ports as depicted in Fig. 4.15.

doi:10.6342/NTU202404478

Fig. 4.15 demonstrates the example calibrated phase of the antenna array of port 1 along with the reflector. The same procedure can be applied to all the ports and assign the desired phase value to obtain a uniform radiation pattern. In the scenario of the offset reflectors, phase calibration is necessary even if there is a minimal change in the displacement of the feed antenna. After calibrating, the calibrating phase values are assigned to their respective ports. By calibrating the phase in this manner, the antenna array is optimized to radiate maximum energy in the desired direction, enhancing its effectiveness regarding gain and radiation distribution characteristics.

Spectral Fields | Source Contexts

	Source	Type	Magnitude	Unit	Phase	Unit
1	H1:1	Port	1	W	-167.55	deg
2	H2:1	Port	0	W	0	deg
3	H3:1	Port	0	W	0	deg
4	H4:1	Port	0	W	0	deg
5	H5:1	Port	0	W	0	deg
6	H6:1	Port	0	W	0	deg
7	H7:1	Port	0	W	0	deg
8	H8:1	Port	0	W	0	deg
9	H9:1	Port	0	W	0	deg
10	H10:1	Port	0	W	0	deg
11	H11:1	Port	0	W	0	deg
12	H12:1	Port	0	W	0	deg
13	H13:1	Port	0	W	0	deg
14	H14:1	Port	0	W	0	deg

Fig. 4.15 Procedure for calibration.

4.6.2 Example without phase calibration of antenna system

Let's see how the antenna Pattern is affected if the Phase of the Antenna system is not calibrated accurately. In Fig. 4.16, the gain pattern of the reflector without phase calibration is depicted, revealing a noticeable reduction in antenna gain. Additionally, the peak gain is observed to shift to a different angle, indicating the impact if lacking phase

doi:10.6342/NTU202404478

calibration on the antenna's directional characteristics. Therefore, precise calibration of phase is crucial for optimizing reflector antenna performance.

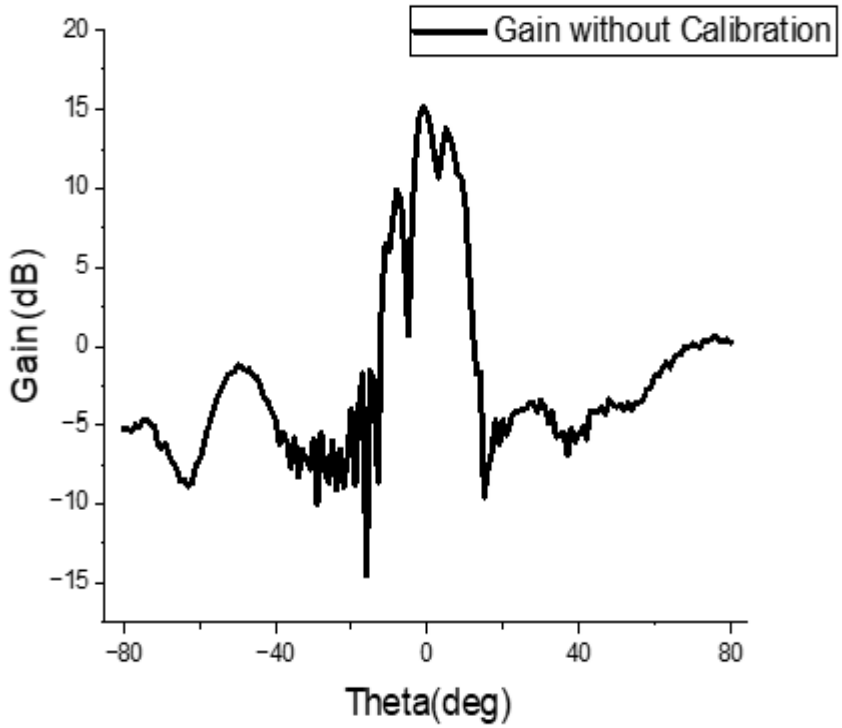

Fig. 4.16 Example of the gain plot without phase calibration.

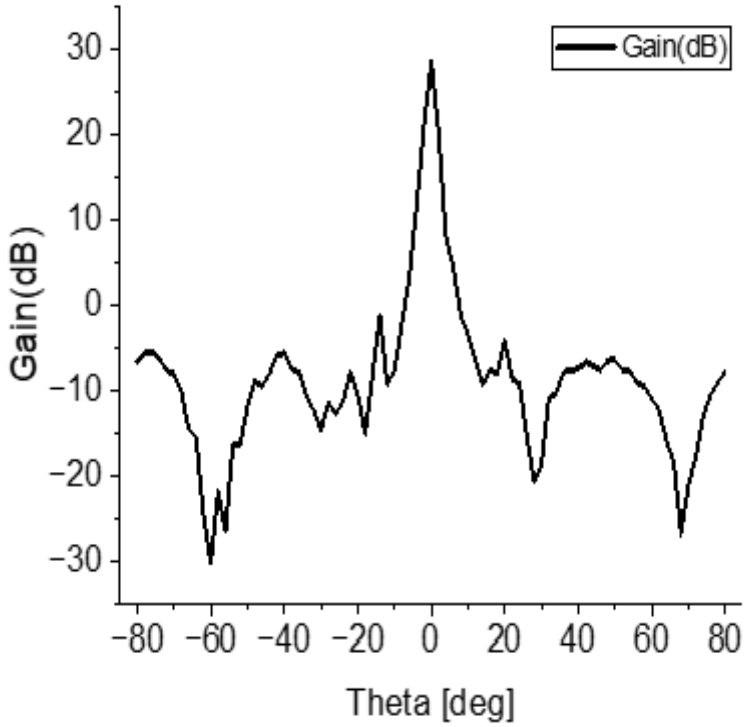

Fig. 4.17 Example of the gain plot with phase calibration.

doi:10.6342/NTU202404478

When examining the key differences between Figures 4.16 and 4.17, it becomes evident that phase calibration of the antenna array relative to the dish antenna plays a crucial role in enhancing the system's overall performance. Specifically, phase calibration helps to significantly improve the antenna gain. This improvement is achieved because phase calibration minimizes the phase differences between individual antenna elements, allowing the signals to combine coherently. When the signals from all antenna elements arrive in phase at the reflector, they constructively reinforce each other, which maximizes the radiated power in the desired direction. This is clearly illustrated in Figure 4.17, where proper phase calibration results in a substantial gain increase.

The 13 dB gain improvement observed directly results from optimizing the phase center alignment between the antenna array and the reflector’s focal point. This ensures that the reflected signals are effectively focused and directed, leading to a significant boost in the system's gain. The precise phase alignment of the antenna elements ensures that the radiated waves constructively interfere, rather than destructively canceling each other out, which would reduce the gain.

In addition to enhancing gain, phase calibration improves the symmetry of the radiation pattern. When the phase assignments of the antenna elements are correctly calibrated, the radiation pattern is more centered and focused around the reflector, reducing the dispersion of energy into unintended directions. Without proper calibration, the radiation pattern can become distorted and asymmetric, as seen in Figure 4.16, leading to the spreading of energy in undesirable directions. This asymmetry can cause destructive interference, where signals from different elements cancel out, lowering the overall gain and creating distortions in the radiation pattern.

By ensuring that the signals from the array are phase-aligned, calibration minimizes these detrimental effects and ensures that the energy is concentrated where it is most needed. This highlights the importance of precise phase calibration in optimizing both the gain and radiation pattern symmetry of the antenna system.

doi:10.6342/NTU202404478

4.7 Parametric Studies of Reflector

As seen in section 4.1, the major parameters affecting the reflector's radiation pattern are focal length, offset angle, and offset height.

Let's practically investigate these parameters and observe how they influence the reflector's characteristics. Certainly, through systematic analysis and optimization, we can fine-tune the reflector's geometry to achieve the desired radiation pattern, gain, and performance characteristics.

4.7.1 Simulation of offset reflector antenna at different focal lengths

An essential aspect of analyzing the reflector's performance involves examining its behavior across various focal lengths. By visualizing how changes in focal length influence simulation results, we can validate the reflector's radiation characteristics. Let's explore case studies involving varying focal lengths to gain insights into the reflector's performance.

Case 1

The feed antenna is positioned at a distance of 36mm from the reflector and see how the gain plot of the reflector would be impacted. Based on the antenna's orientation, to ensure that the array is well-calibrated, the rEtheta plot of the antenna should be zero, which signifies that the antenna phase is precisely calibrated as shown in Fig 4.18. This is applicable even when there is a minimal change in the position of the feed.

The gain characteristics of the reflector at 260GHz, 300GHz, and 320GHz are illustrated in Fig. 4.19, 4.20, and Fig. 4.21 correspondingly; the gains are 32.2dB, 27dB, and 23.3dB respectively. The maximum gain is achieved at 260GHz as compared to 300GHz and 320GHz.

doi:10.6342/NTU202404478

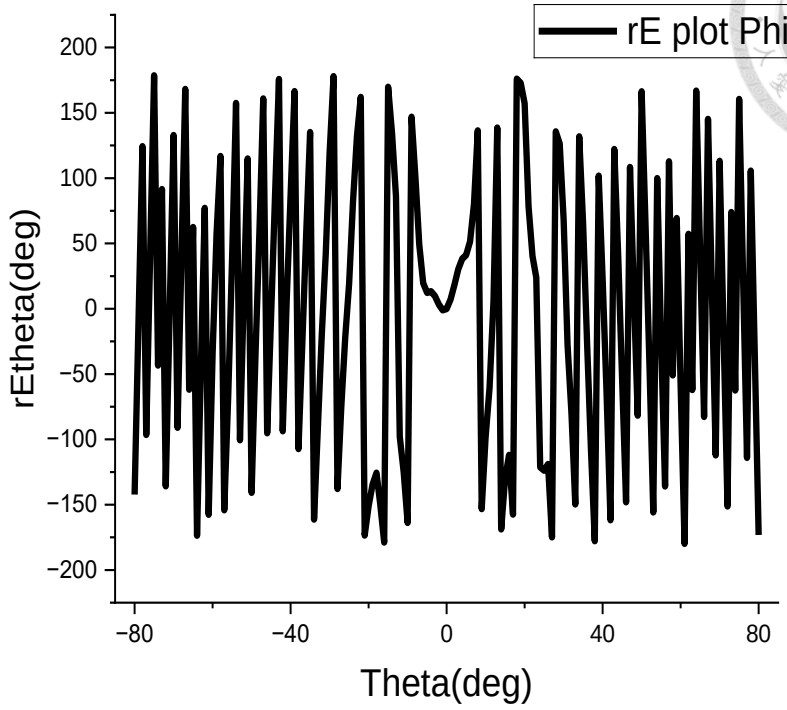

Fig 4.18 Representation of phase calibration of antenna array.

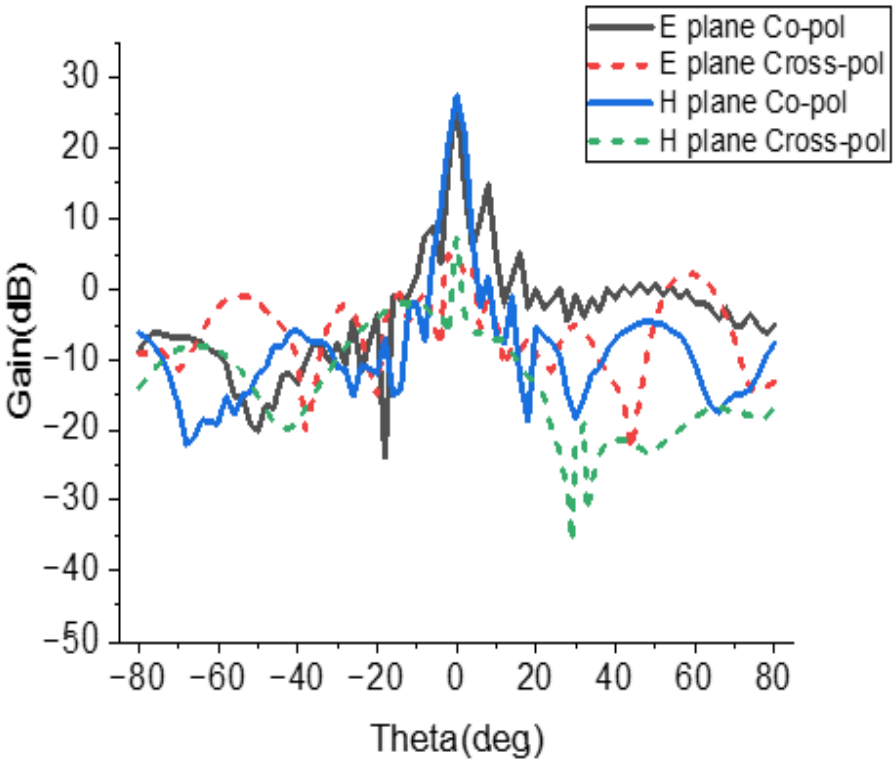

Fig. 4.19 Gain plot of electromagnetic field directions of the reflector at 260GHz

doi:10.6342/NTU202404478

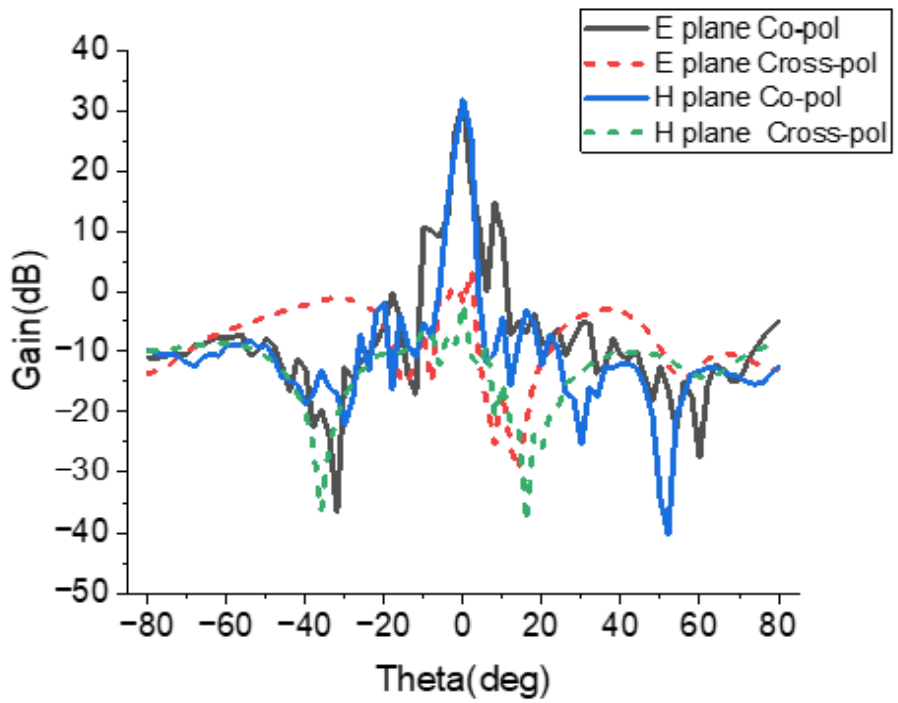

Fig. 4.20 Gain plot of electromagnetic field directions of the reflector at 300GHz.

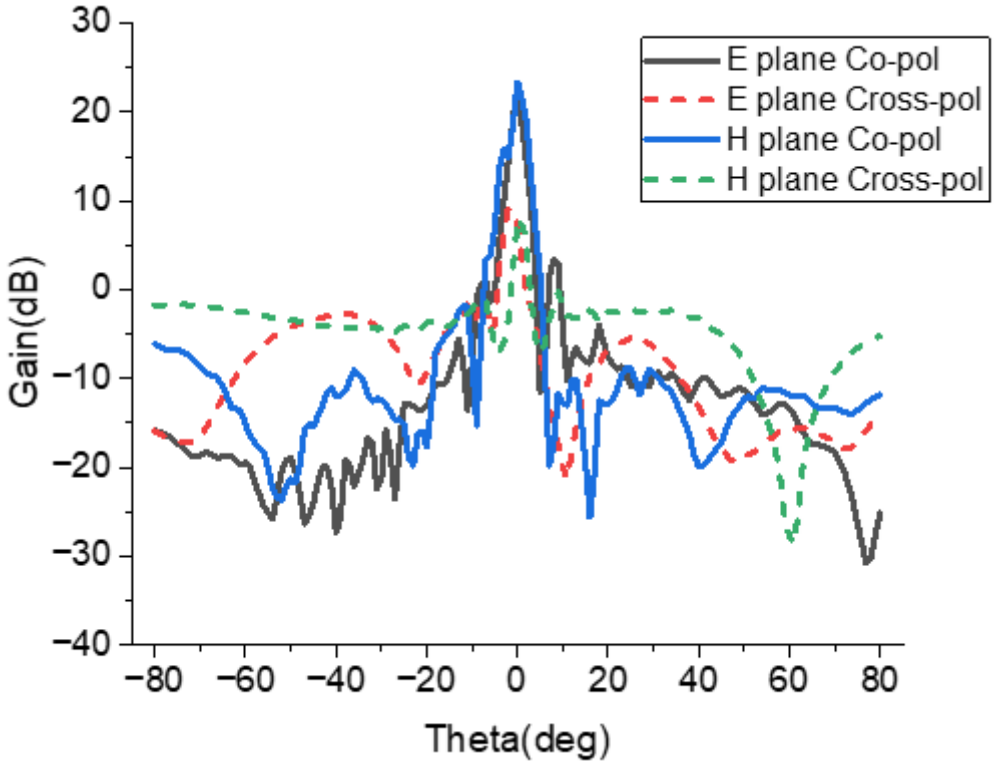

Fig. 4.21 Gain plot of electromagnetic field directions of the reflector at 320GHz.

doi:10.6342/NTU202404478

Case 2:

When the source antenna is located at 32mm from the reflector, the radiation plot of the reflector at 260GHz, 300GHZ, and 320GHz are illustrated in Fig. 4.22, Fig 4.23, and Fig. 4.24 respectively, and the gains are 29.7dB, 27.4dB, and 23.1dB respectively. As mentioned before, if the antenna position is displaced, the entire antenna system should be calibrated along with the reflector and assigned the desired phases to achieve maximum radiation.

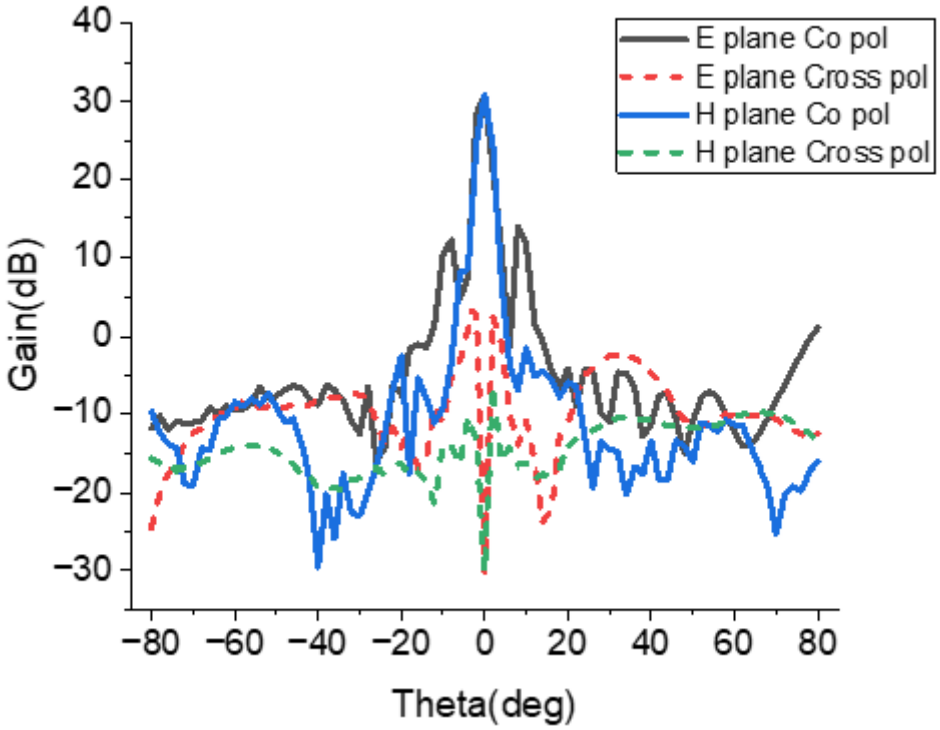

Fig. 4.22 Gain plot of electromagnetic field directions of the reflector at 260GHz.

As per the theory, if the antenna is displaced away from the convergence point of the dish, the focusing properties of the reflector will degrade, hence resulting in poor gain and an increase in sidelobe levels. Compared to case 1, the antenna gain is reduced as the feed is positioned further from its focal point.

doi:10.6342/NTU202404478

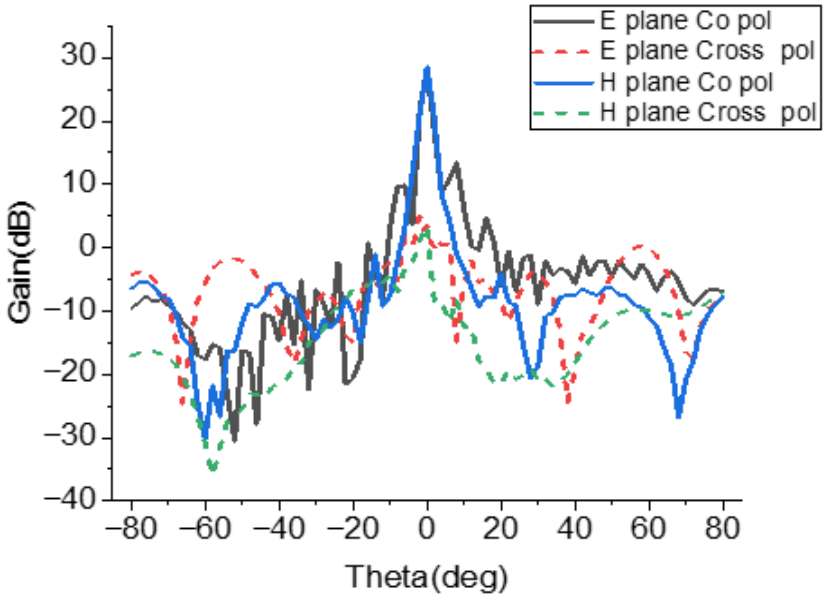

Fig. 4.23 Gain plot of electromagnetic field directions of the reflector at 300GHz.

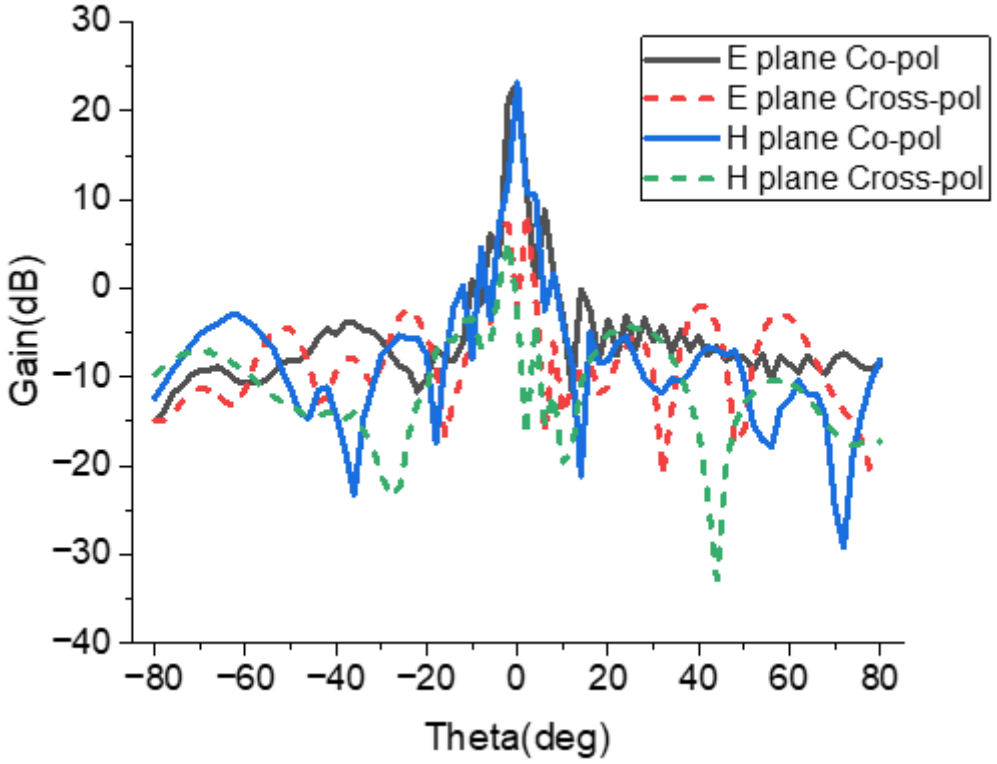

Fig. 4.24 Gain plot electromagnetic field directions of the reflector at 320GHz

doi:10.6342/NTU202404478

Case 3:

When the feed antenna is positioned at 24mm from the dish, the gain plot of the reflector at 260GHz, and 300GHz are depicted in Figure. 4.25, Fig. 4.26, and Fig 4.27 respectively, and the corresponding gains are 29.1dB, 26.85dB, and 24.5dB respectively.

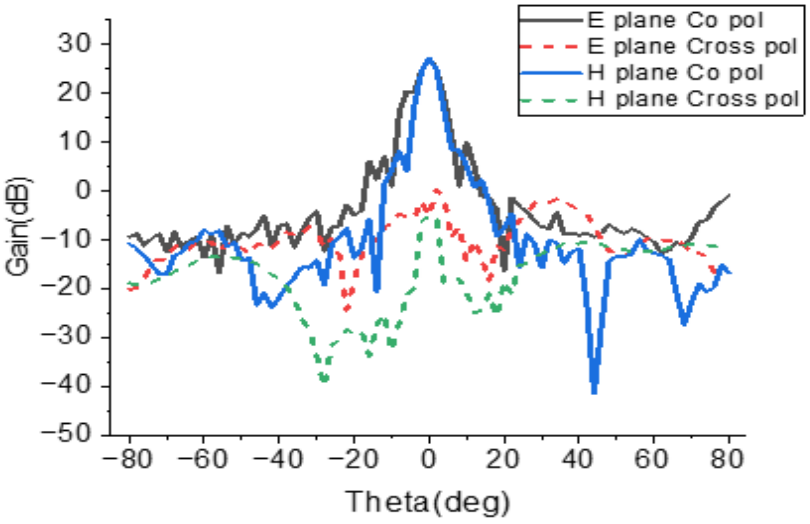

Fig. 4.25 Gain plot of electromagnetic field directions of the reflector at 260GHz.

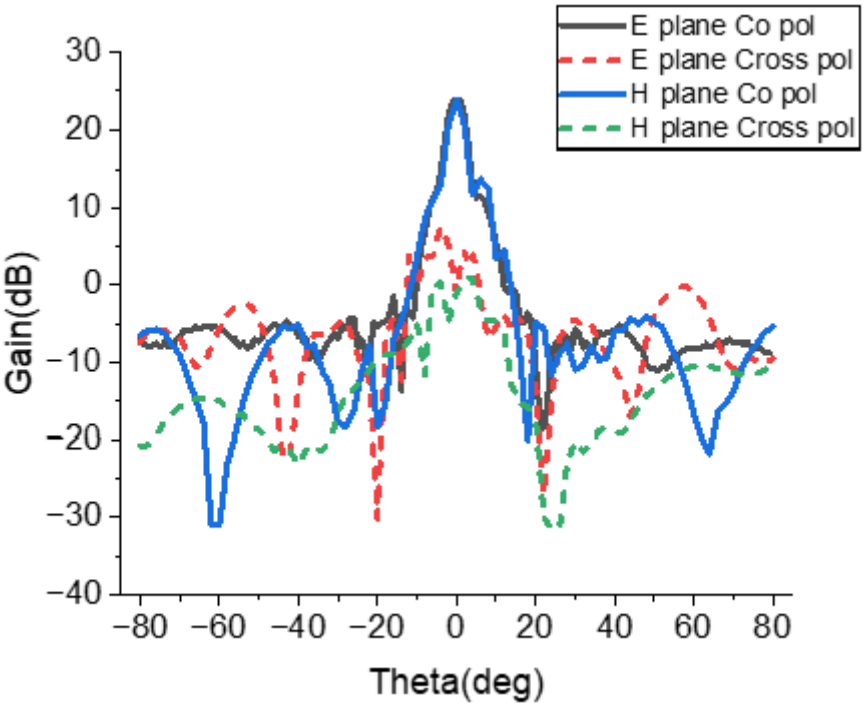

Fig. 4.26 Gain plot of electromagnetic field directions of the reflector at 300GHz.

doi:10.6342/NTU202404478

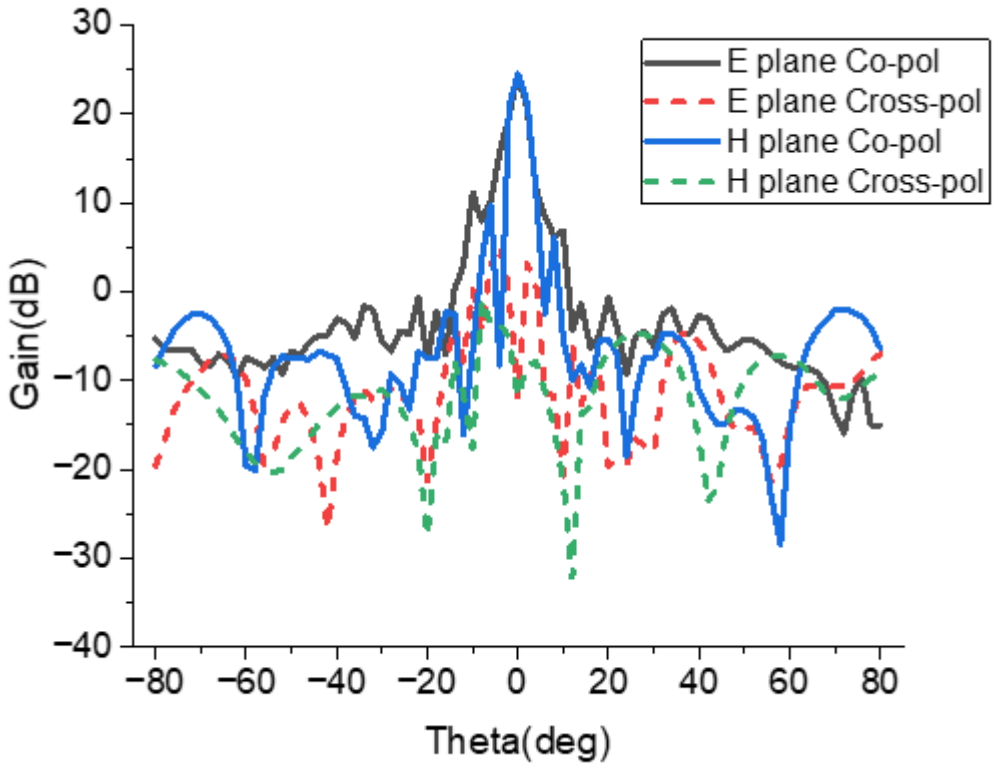

Fig. 4.27 Gain plot of electromagnetic field directions of the reflector at 320GHz

A comparison of gains at different focal lengths is tabulated in Table 4.2.

Table. 4.2: Evaluation of various focal lengths.

Focal length(mm)	Gain (dB)		
	260GHz	300GHz	320GHz
Case 1 (36mm)	32.2	27.9	23.3
Case 2 (32mm)	29.7	27.4	23.1
Case 3 (24mm)	28.1	26.5	24.5

Based on the comparison of different focal lengths, it can be inferred that as the focal length decreases there is a corresponding reduction in gain and rise in beamwidth. Conversely, as the focal length increases the gains tend to increase while the beamwidth becomes narrower with an increase in cross-pol levels of E-plane. The elevated cross-polarization levels are primarily attributed to the feed antenna, particularly its higher E-plane cross-polarization level, which significantly impacts the overall cross-polarization

doi:10.6342/NTU202404478

performance of the reflector antenna. Finally, after conducting multiple iterations and considering various factors, including the antenna's radiation pattern, minimization of sidelobe levels, wider beamwidth, and enhancing the overall performance, the final placement of the feed antenna is determined to be 24mm. This placement is chosen because it can broaden beamwidth while maintaining accountable gain.

4.7.2 Simulation of offset reflector antenna at different offset angles

As discussed in section 4.7.1, the focal length of the off-axis reflector was optimized to be 24mm through iterative design processes and simulations. Now, considering the focal length to be 24mm, we investigate how the offset angle affects the antenna's radiation pattern. In this section, we explore how varying the offset angle influences the radiation characteristics of an offset reflector antenna using simulation studies.

As outlined in section 4.1, formulas are provided for calculating the offset angle. To optimize the illumination of the offset reflector antenna's surface at 300 GHz with a wavelength of 1 mm, the relevant parameters are calculated. Given a fixed focal length and offset height, we utilize the equation from [7] to calculate the offset angle of the reflector antenna. The equation is given as follows:

where D=30mm, F=24mm, H=1mm

$$\psi_u = 2\tan^{-1}\frac{(D+H)}{(2\times F)} = 2tan^{-1}(0.65) = 66.04° \tag{4.7}$$

$$\psi_L = 2\tan^{-1}\frac{(H)}{(2\times F)} = 2tan^{-1}(1.2) = 2.4° \tag{4.8}$$

$$\psi_c = 2\tan^{-1}\frac{(\frac{D}{2}+H)}{(2\times F)} = 2tan^{-1}(0.33) = 36.4° \tag{4.9}$$

$$\psi_B = \frac{\psi_u + \psi_L}{2} = 34.22° \tag{4.10}$$

doi:10.6342/NTU202404478

As per the above calculations, the feed antenna must be positioned at an angle of 36.4° from the primary axis. Additionally, we examine the antenna's performance at different offset angles say 45° and 50°, assessing their impact on the radiation pattern through simulation results. Let's evaluate each case individually and analyze the outcomes. The calculated offset angle for the focal length of 24mm is depicted in Fig. 4.28.

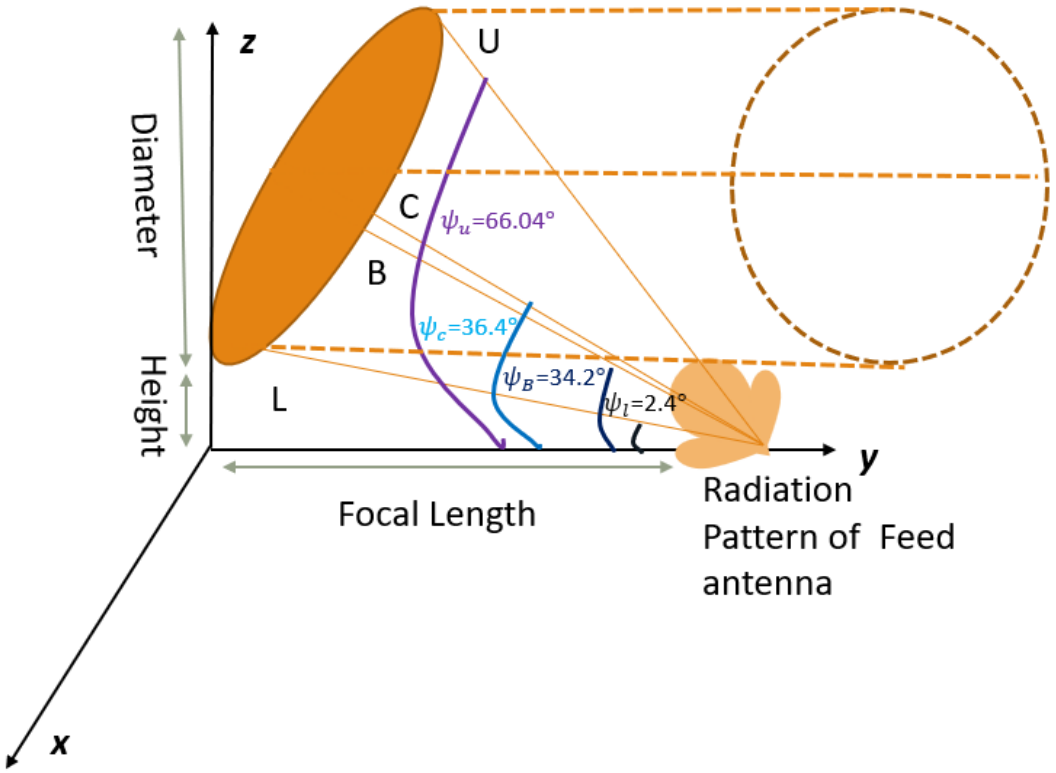

Fig. 4.28 Representation of offset angle analysis of reflector.

Case 1:

When the feed antenna is positioned at an angle of 36°, the Radiation Patterns of the reflector at 260GHz, 300GHz, and 320GHz are illustrated in Figure. 4.29, 4.30, and 4.31 correspondingly, and the gains are 28.2 dB, 26.5 dB, and 24.5 dB respectively.

doi:10.6342/NTU202404478

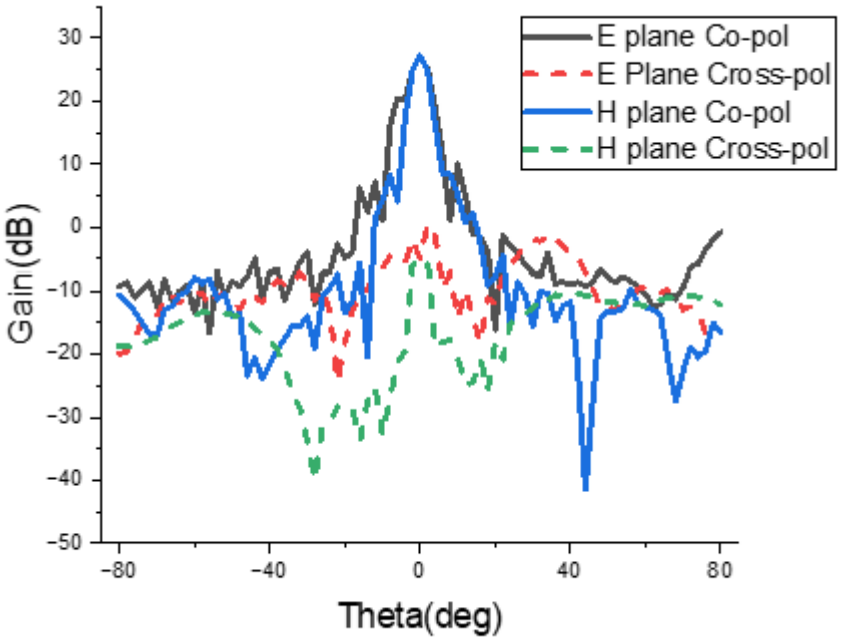

Fig. 4.29 Gain plot of electromagnetic field directions of the reflector at 260GHz.

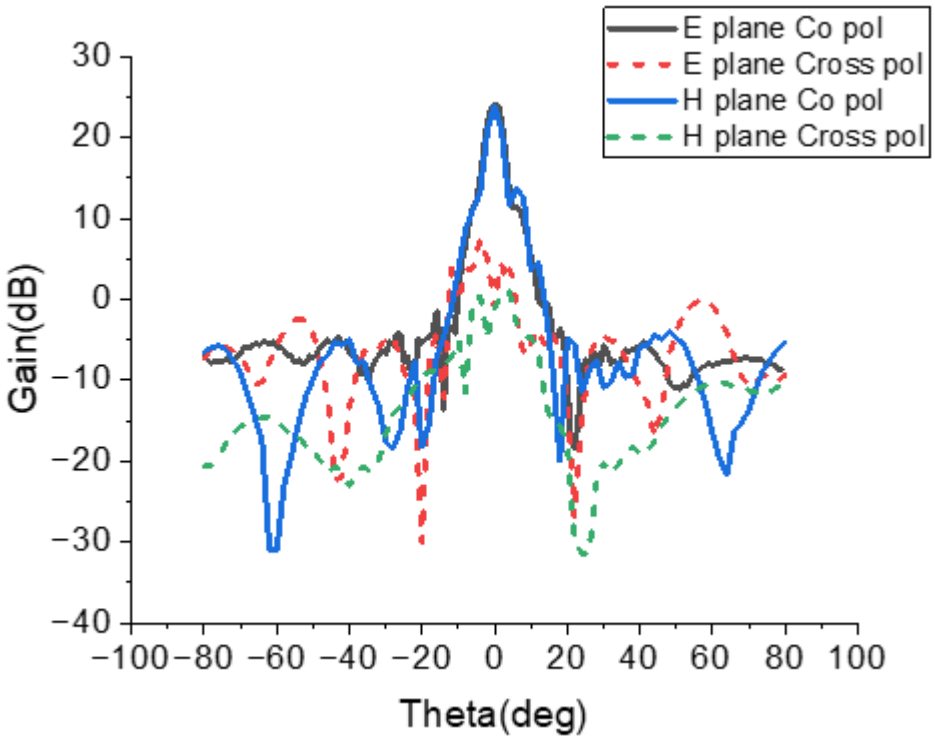

Fig. 4.30 Gain plot of electromagnetic field directions of the reflector at 300GHz.

doi:10.6342/NTU202404478

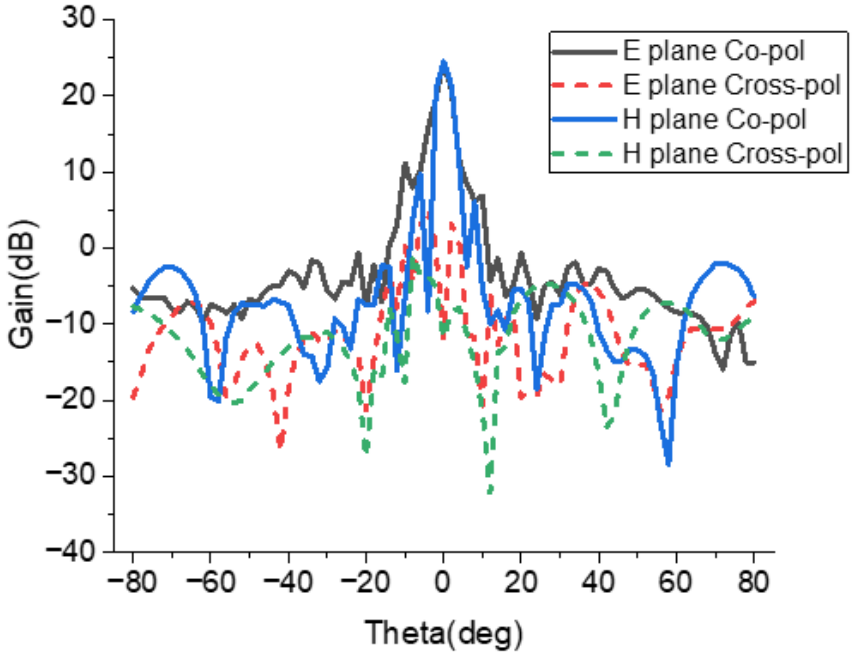

Fig. 4.31 Gain plot of electromagnetic field directions of the reflector at 320GHz.

Case 2:

When the feed antenna is placed at an angle of 45°, the Gain plots of the offset dish at 260GHz, and 300GHz are illustrated in Figures 4.32, 4.33, and 4.34 correspondingly, and the gains are 28 dB, 27.1 dB, and 22.1dB respectively

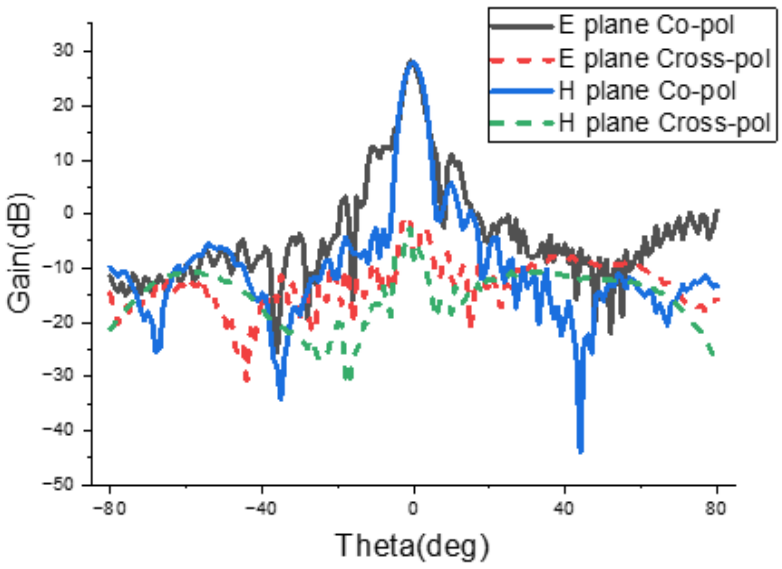

Fig. 4.32 Gain plot of electromagnetic field directions of the reflector at 260GHz

doi:10.6342/NTU202404478

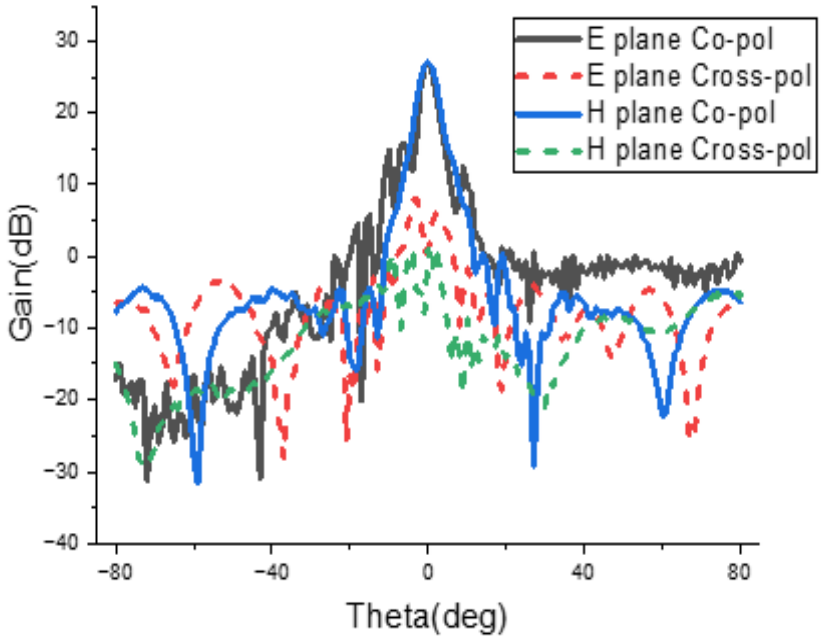

Fig. 4.33 Gain plot of electromagnetic field directions of the reflector at 300GHz.

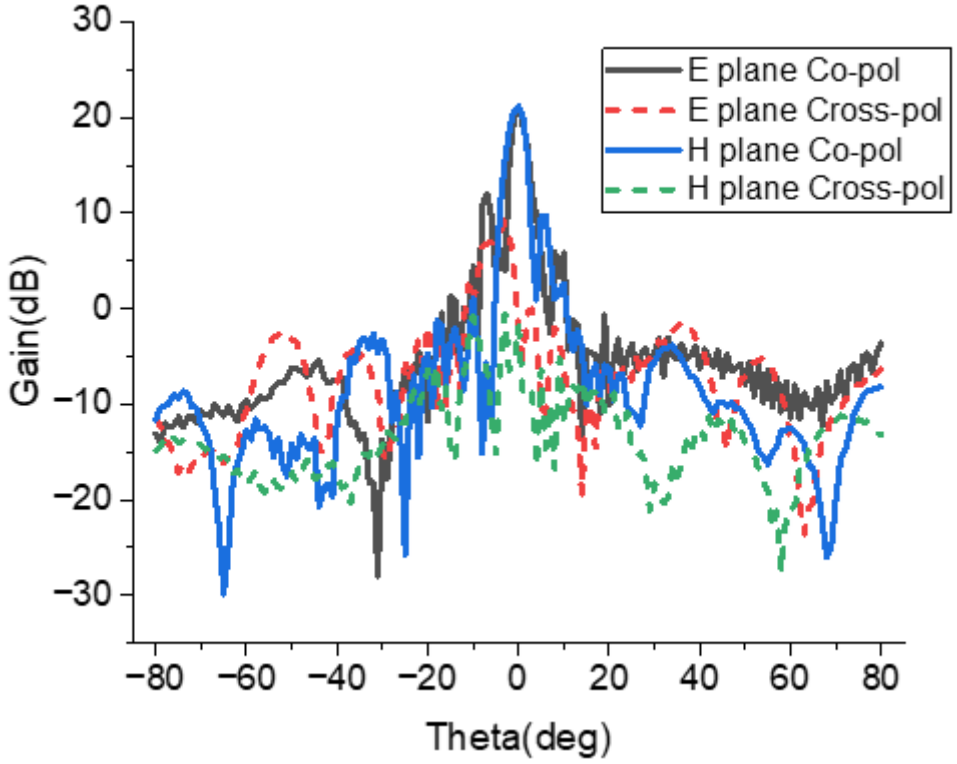

Fig. 4.34 Gain plot of electromagnetic field directions of the reflector at 320GHz.

doi:10.6342/NTU202404478

Case 3:

When the feed antenna is placed at an angle of 50°, the Radiation Patterns of the reflector at 260GHz, and 300GHz are illustrated in Figures 4.35, 4.36, and 4.37 correspondingly, and the gains are 27.9 decibels, 25.6 decibels, and 23.4dB respectively.

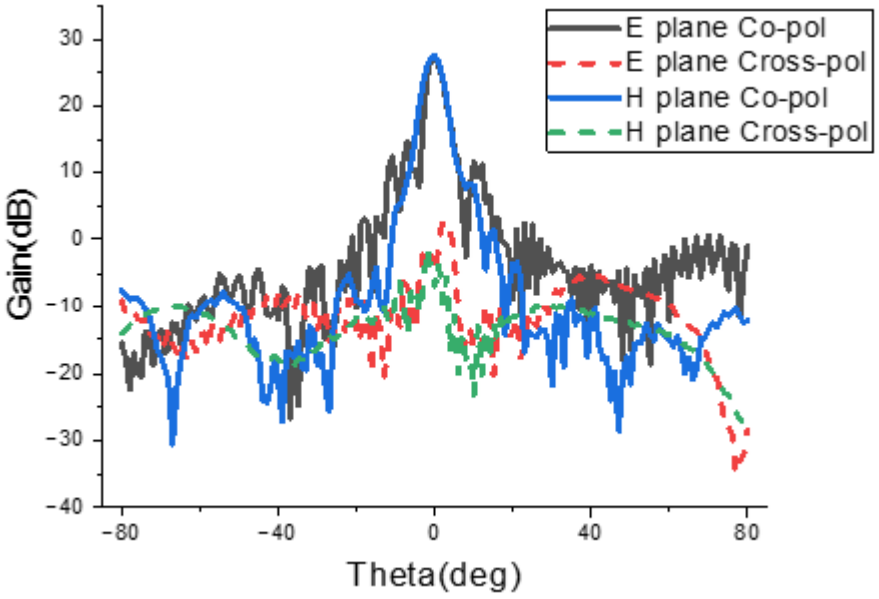

Fig. 4.35 Gain plot of electromagnetic field directions of the reflector at 260GHz.

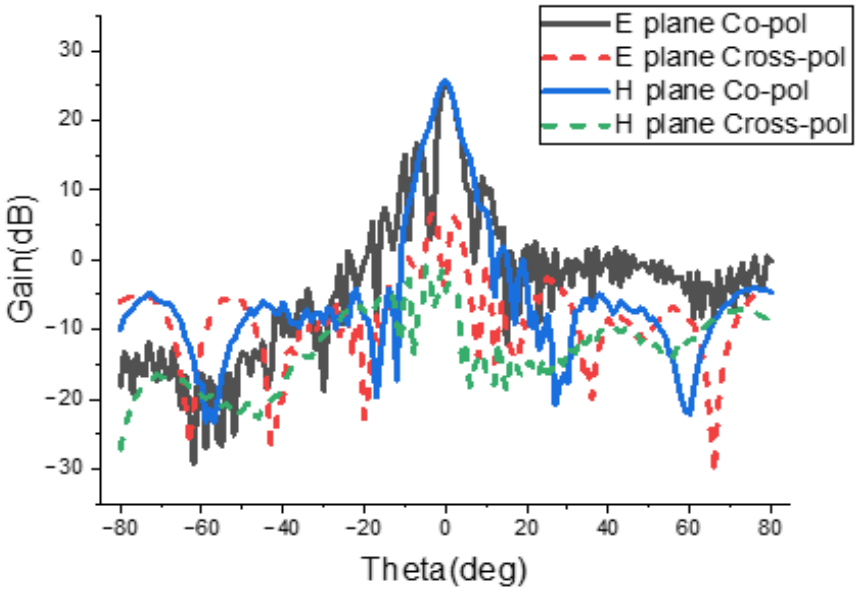

Fig. 4.36 Gain plot of electromagnetic field directions of the reflector at 300GHz.

doi:10.6342/NTU202404478

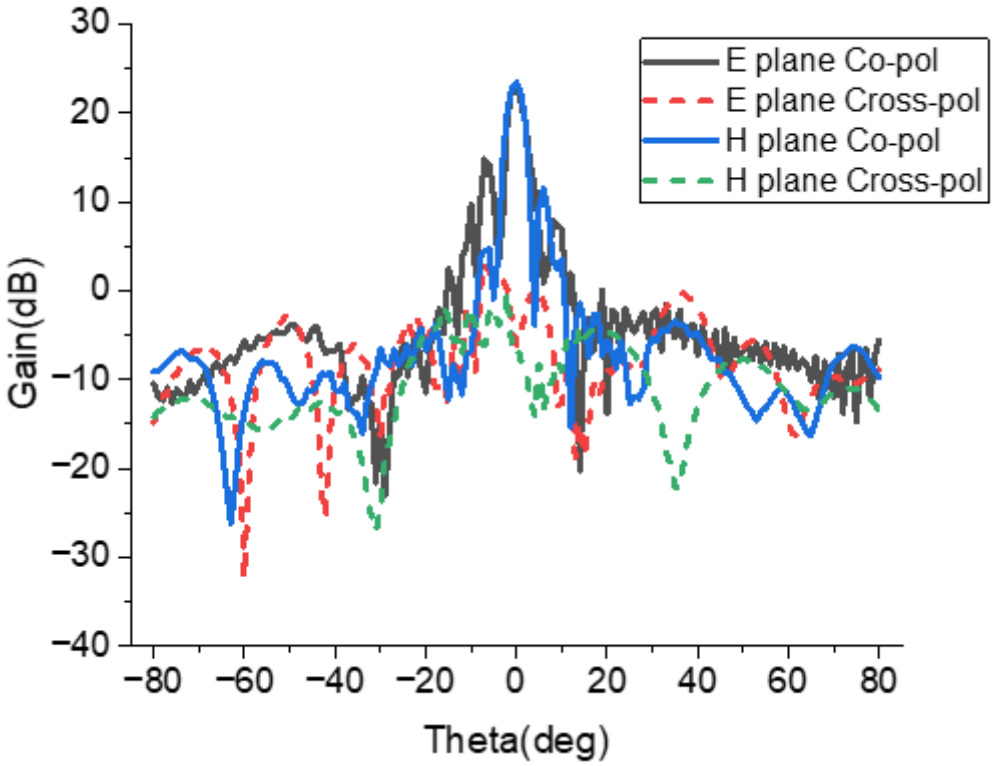

Fig. 4.37 Gain plot of electromagnetic field directions of the reflector at 320GHz.

Comparison of different angle gains are tabulated in Table 4.3.

Table. 4.3 Evaluation of various offset angles.

Offset Angle (deg)	Gain (dB)		
	260GHz	300GHz	320GHz
36	28.2	26.5	24.5
45	28	27.1	22.1
50	27.9	25.6	23.4

Experimental data show that the reflector antenna achieves greater gain across all calculated offset angles at 260 GHz. In contrast, the gain diminishes at 300 GHz. This change suggests that the reflector antenna's performance varies with frequency, reaching optimal levels at certain offset angles for different frequencies.

doi:10.6342/NTU202404478

To ensure consistent performance across both frequencies, optimization of the offset angle is necessary. The results show that an offset angle of 36° achieves a balance of improved gain and symmetry for both 260 GHz, 300GHz and 320 GHz. This angle provides a favorable compromise, enhancing gain while maintaining symmetrical properties in the radiation pattern. Although higher gains might be observed at offset angles such as 45° and 50°, these angles do not maintain the required symmetrical properties in the radiation pattern. The lack of symmetry at these angles suggests that the feed antenna's alignment can significantly impact the reflector antenna's overall radiation pattern and symmetry. Misalignment can lead to asymmetrical patterns and reduced performance, underscoring the importance of precise offset angle optimization.

Therefore, the reflector antenna is determined to perform optimally at the theoretically calculated offset angle, as specified in Equation (4.10). This angle provides a suitable balance between gain and symmetry, ensuring reliable performance across the considered frequency ranges.

4.7.3 Simulation of the offset reflector at different offset heights

With fixed offset angle and focal length let us examine when the reflector antenna is positioned at different offset heights and observe how the gain plot varies. This distance must be carefully designed to ensure that the feed antenna properly illuminates the reflector surface. In an offset reflector, the feed antenna is positioned at a certain angle and height to prevent blockage by the antenna structure, a common issue in conventional center-fed designs An improperly chosen offset height can lead to suboptimal illumination of the reflector, which results in reduced gain and increased side lobes or spillover. Spillover occurs when part of the radiation from the feed antenna misses the reflector and radiates into space, which reduces the efficiency of the system and can cause unwanted interference. Conversely, a well-chosen offset height minimizes these losses and ensures that most of the feed antenna's energy is directed toward the reflector surface.

doi:10.6342/NTU202404478

In all cases, we primarily focus on the gain plot because simulating the antenna efficiency takes significantly longer, particularly at higher frequencies. This is due to the increased complexity of the simulations required to account for both the antenna's gain and efficiency. Hybrid solvers, which combine different computational methods to provide accurate results, often struggle to balance the detailed modeling required at high frequencies. As a result, simulating the overall antenna efficiency, especially in large and complex antenna systems, can be highly time-consuming.

Case 1:

When the offset dish antenna is positioned at an offset height of 500mm, the Radiation patterns of the reflector at 260GHz, 300GHz, and 320GHz are illustrated in Figure. 4.38, 4.39, and 4.40 correspondingly, and the gains are 27.5 dB, 21.8 dB, and 20.6 dB respectively.

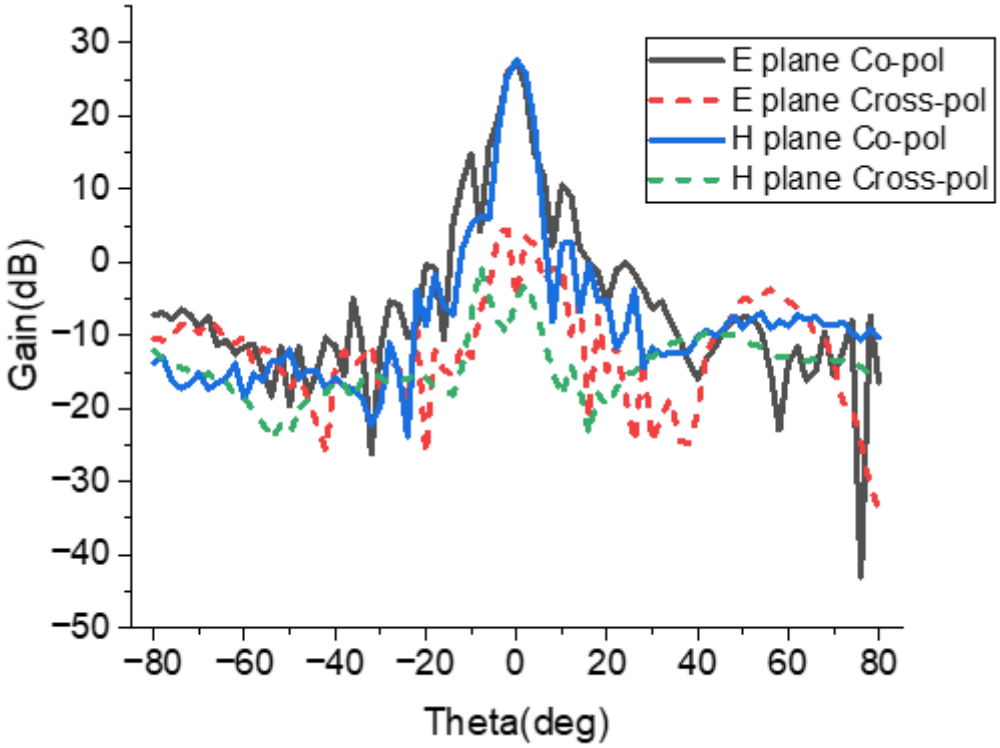

Fig. 4.38 Gain plot of electromagnetic field directions of the reflector at 260GHz

doi:10.6342/NTU202404478

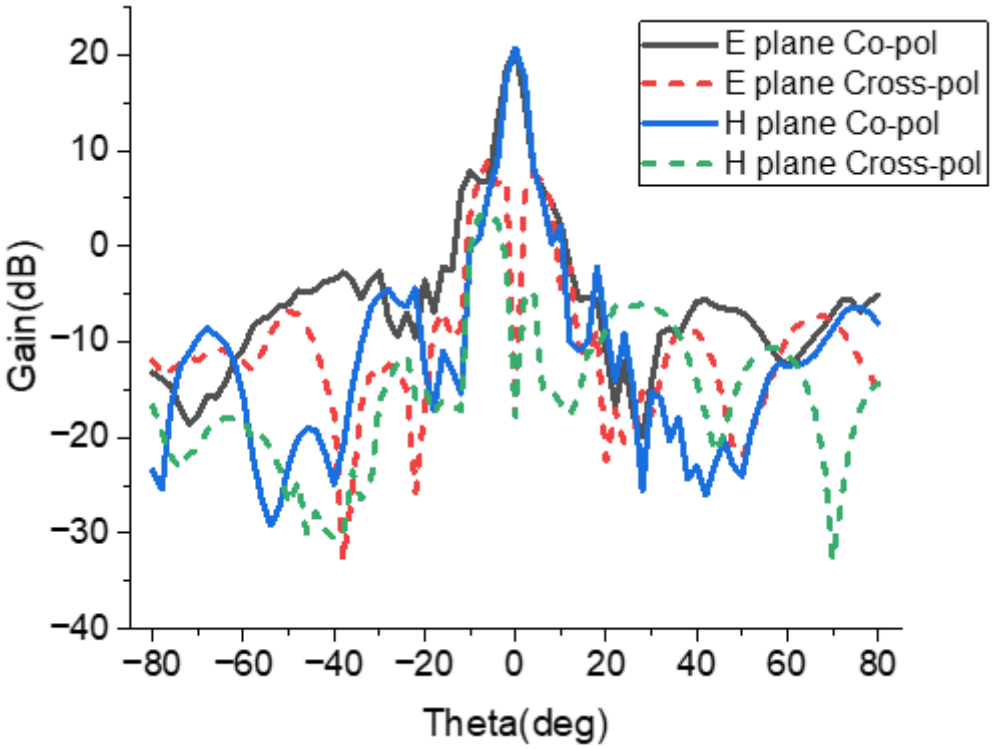

Fig. 4.39 Gain plot of electromagnetic field directions of the reflector at 300GHz.

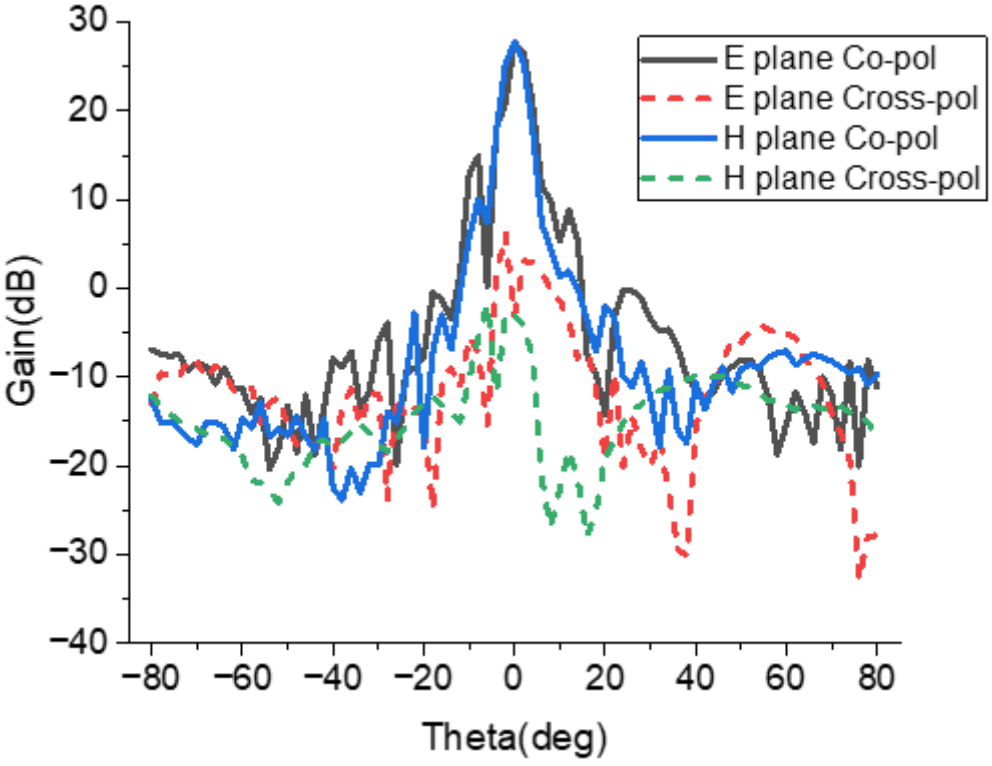

Fig. 4.40 Gain plot of electromagnetic field directions of the reflector at 320GHz.

doi:10.6342/NTU202404478

As the frequency increases to 300 GHz, a slight decrease in gain is observed, with the measured gain at this frequency being 26.5 dB.

This drop in gain can be attributed to the fact that higher frequencies often introduce greater sensitivity to design imperfections, such as misalignments or material losses. Additionally, the radiation pattern at 300 GHz shows a slight increase in side lobe levels, indicating some dispersion of energy into unintended directions, and at 300GHz the cross-pol level of the reflector antenna is more pronounced which might introduce interference.

Case 2:

When the offset dish antenna is positioned at an offset height of 1000mm, the Radiation patterns of the reflector at 260GHz, 300GHz, and 320GHz are illustrated in Figures. 4.41 4.42, and 4.43 correspondingly, and the gains are 28.2 dB, 26.5 dB, and 24.5dB respectively.

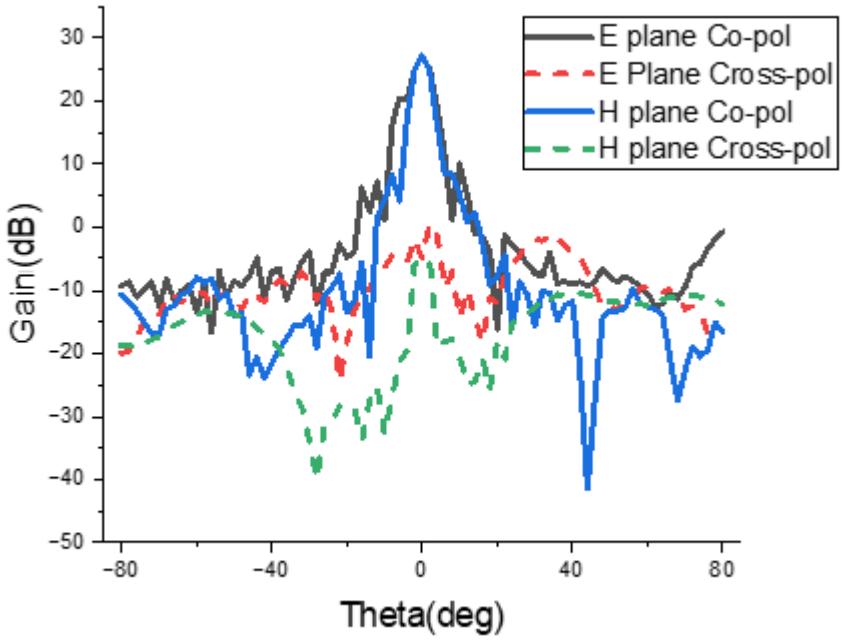

Fig. 4.41 Gain plot of electromagnetic field directions of the reflector at 260GHz.

doi:10.6342/NTU202404478

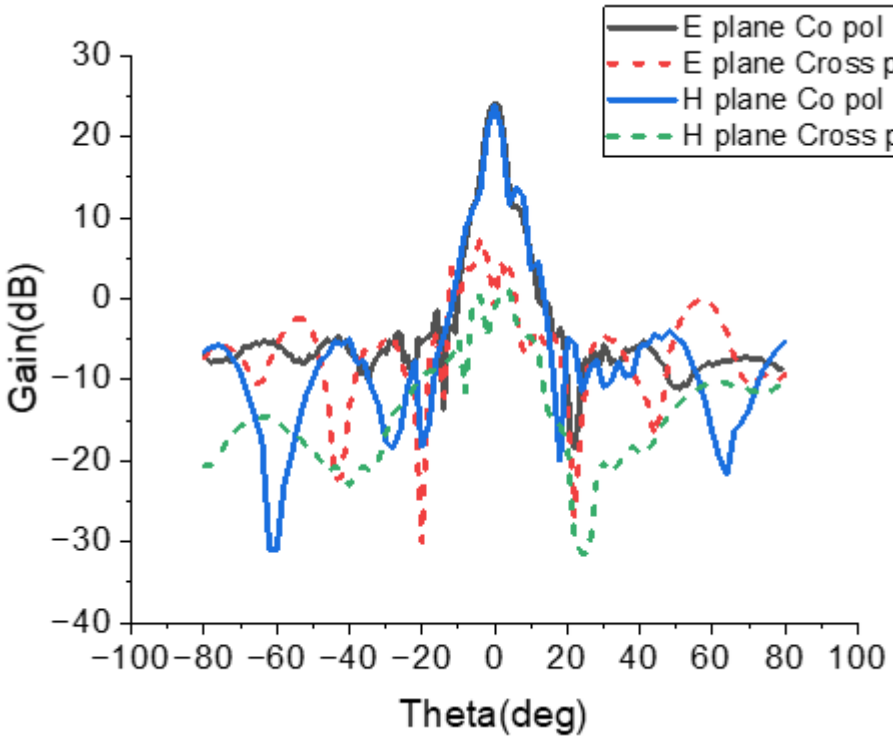

Fig. 4.42 Gain plot of electromagnetic field directions of the reflector at 300GHz.

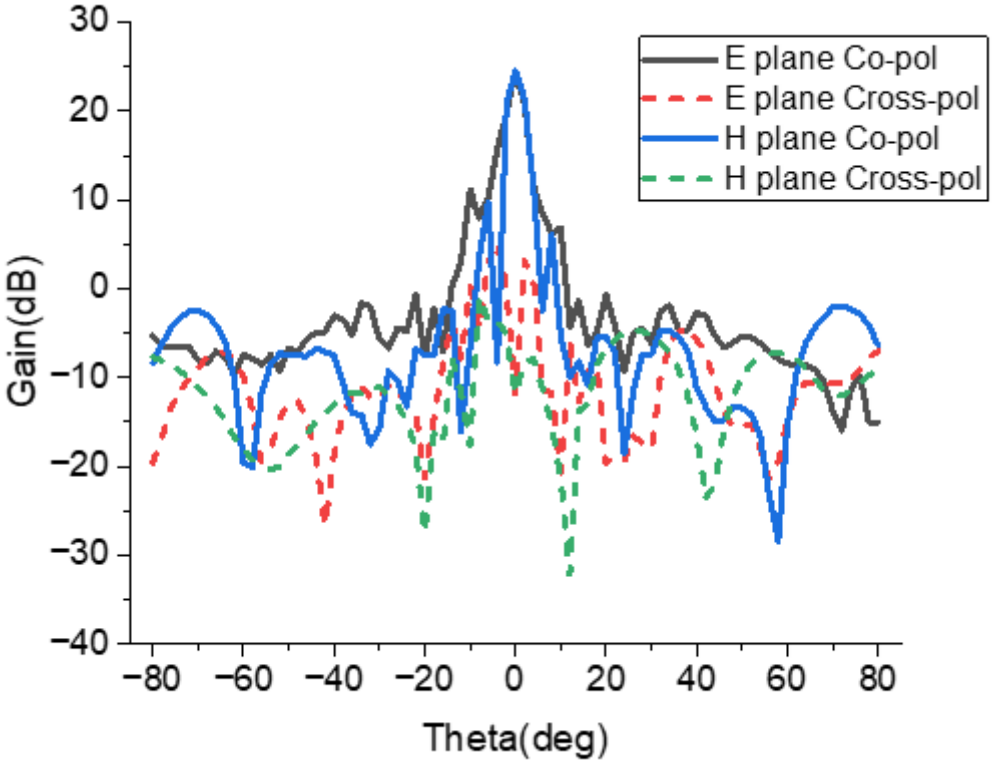

Fig. 4.43 Gain plot of electromagnetic field directions of the reflector at 320GHz.

doi:10.6342/NTU202404478

Case 3:

When the offset dish antenna is positioned at an offset height of 1500mm, the Radiation patterns of the reflector at 260GHz, 300GHz, and 320GHz are illustrated in Figure. 4.45, 4.46, and 4.47 correspondingly, and the gains are 27.7 dB, 22.4 dB, and 20.5dB respectively.

In all cases, we primarily focus on the gain plot because simulating the antenna efficiency takes significantly longer, particularly at higher frequencies. This is due to the increased complexity of the simulations required to account for both the antenna's gain and efficiency. Hybrid solvers, which combine different computational methods to provide accurate results, often struggle to balance the detailed modeling required at high frequencies with computational efficiency.

As a result, simulating the overall antenna efficiency, especially in large and complex antenna systems, can be highly time-consuming

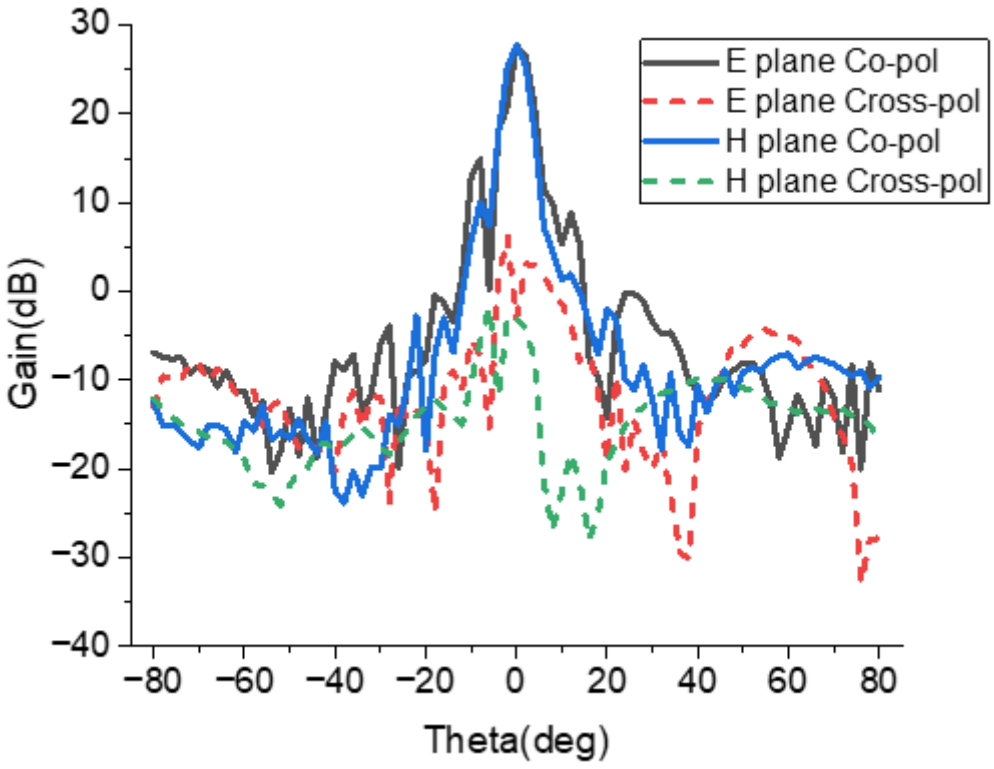

Fig. 4.44 Gain plot of electromagnetic field directions of the reflector at 260GHz.

doi:10.6342/NTU202404478

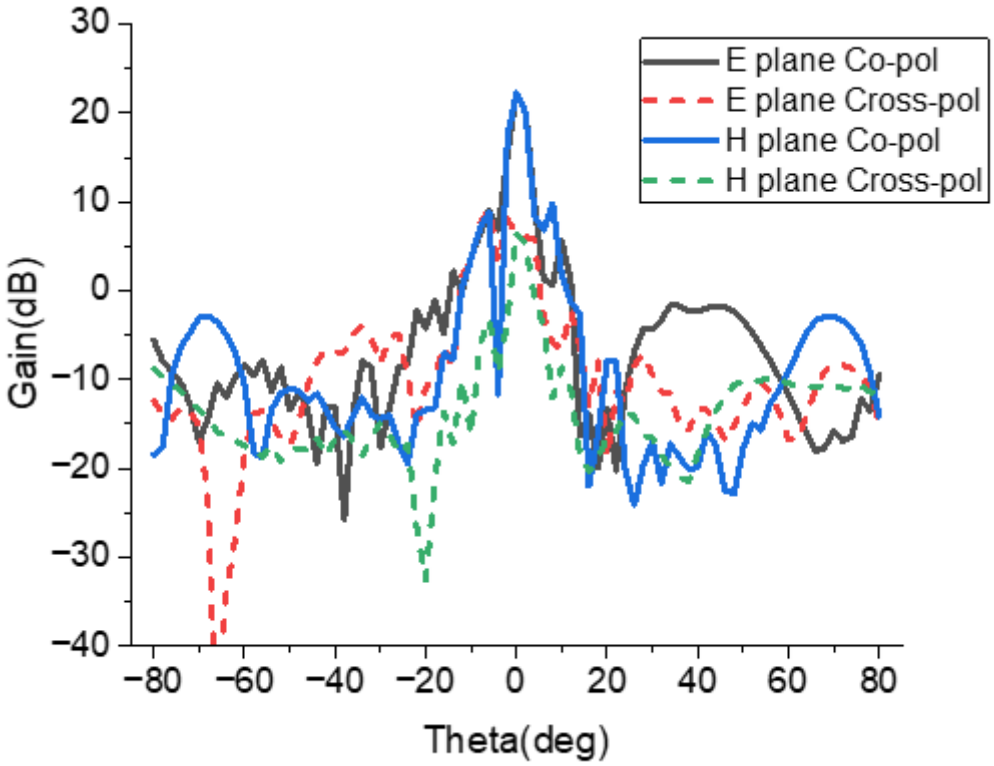

Fig. 4.45 Gain plot of electromagnetic field directions of the reflector at 300GHz

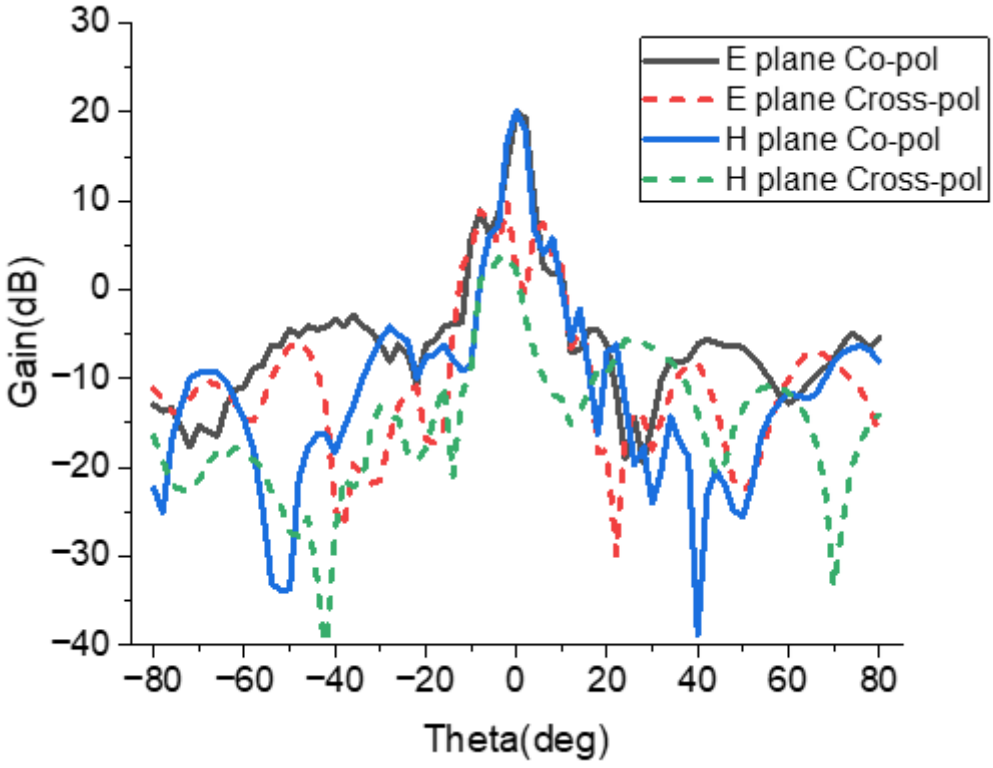

Fig. 4.46 Gain plot of electromagnetic field directions of the reflector at 320GHz.

A comparison of different offset heights is tabulated in Table 4.4

doi:10.6342/NTU202404478

Table. 4.4 Evaluation of various offset heights.

Offset Angle (mm)	Gain (dB)		
	260GHz	300GHz	320GHz
500	27.5	21.8	20.6
1000	28.2	26.5	24.5
1500	27.7	22.2	20.5

Out of all iterations, and based on the results, it is concluded that the feed antenna should be placed at a focal length of 24 mm, with an offset height of 1000 mm and an offset angle of 36°. At these specifications result in the gain variations of the dish antenna across different frequencies, as shown in Fig. 4.47.

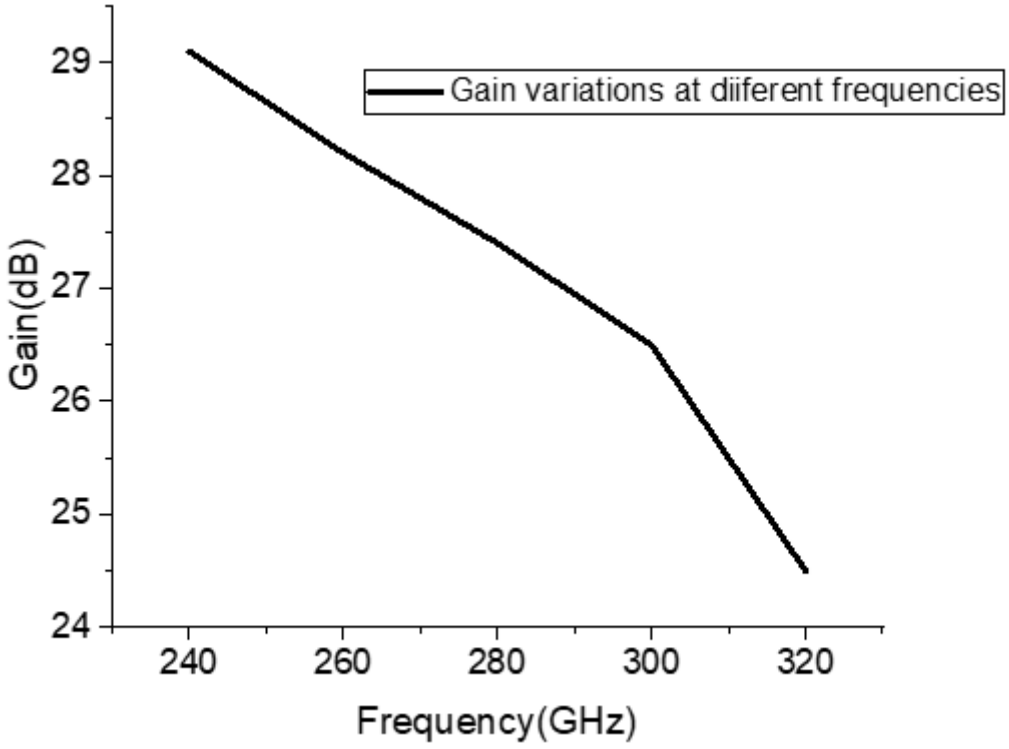

Fig 4.47 Gain Variations of reflector antenna at different frequencies

Fig. 4.47 represents that as the frequency increases the gain tends to decrease because the losses at high frequencies are more pronounced such as the material losses

doi:10.6342/NTU202404478

and the sensitivity of the antenna geometry to higher frequencies when compared to lower frequencies.

The changes in gain for the reflector antenna at various focal lengths and offset heights have been analyzed for the previously discussed case. The resulting gains are shown in Fig. 4.48 and Fig. 4.49, respectively.

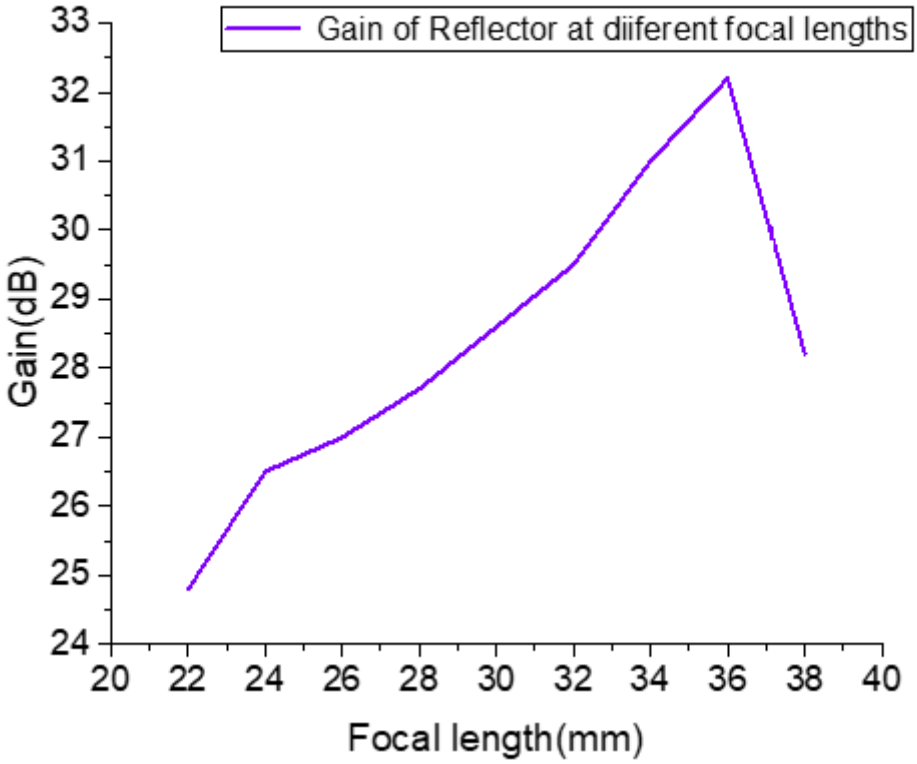

Fig 4.48 Gain variations at different focal lengths

Fig. 4.48 represents that when the feed is positioned away or closer to the focal point of the main reflector, the gain tends to decrease the feed no longer properly illuminates the reflector. Therefore, a longer focal length generally results in a shorter beam width and higher gain, while a shorter focal length leads to a wider beam width and lesser gain.

Fig. 4.49 represents the gain variations of the reflector antenna when the feed is positioned at different offset heights.

doi:10.6342/NTU202404478

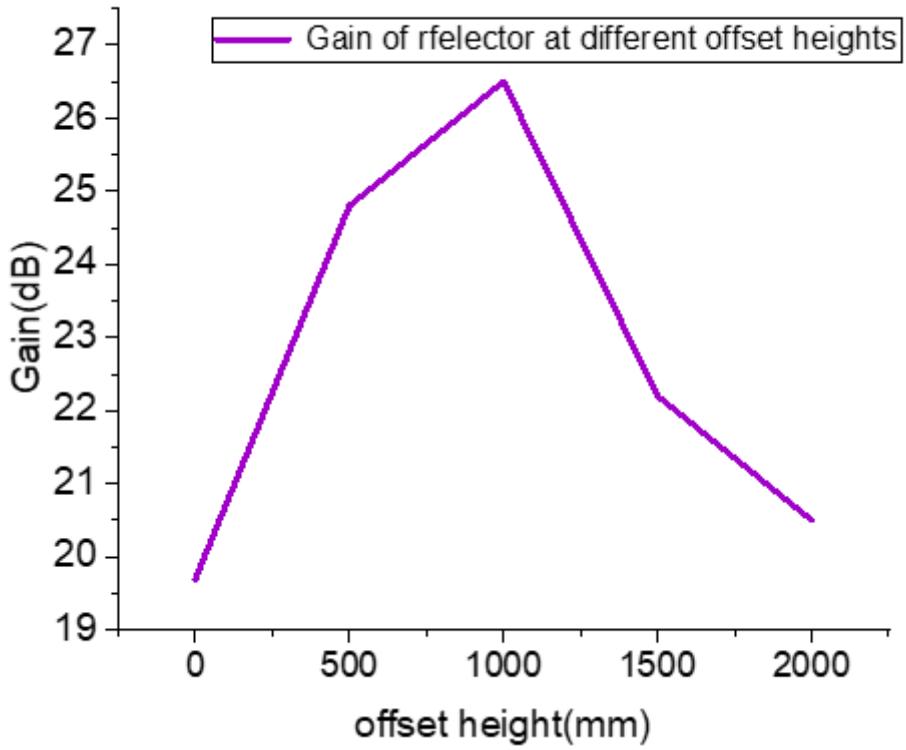

Fig.4.49 Gain variations at different offset heights.

From fig.4.49, a higher offset minimizes blockage from the feed, reducing interference and improving overall gain.

4.8 Design of Support Structure

Once the dish antenna design is completed, the next step involves the construction of a support structure to securely hold the reflector in place. For this reflector, an optical mount structure was selected for this purpose. The choice of an optical mount is due to its ability to seamlessly integrate with linear motion systems, which is essential for achieving precise adjustments of the reflector antenna with micrometer-level accuracy. This integration allows for fine-tuning the position of the reflector, ensuring optimal performance.

The support structure is designed with specific dimensions to ensure a proper fit and stability. The outer cylinder of the mount has a radius of 26 mm, while the inner cylinder has a radius of 15.3 millimeters. The dimensions of the outer cylinder are 10 millimeters,

doi:10.6342/NTU202404478

which matches the thickness of the reflector. This design allows the reflector to accommodate its size with the linear motion systems. It is crucial to select a material for fabricating the mechanical structure that does not adversely affect the performance of the reflector antenna. In this case, Polylactic Acid (PLA) was chosen for its suitability in high-frequency applications. PLA is known for its minimal impact on electromagnetic waves, making it an ideal material for constructing components that will not interfere with the antenna's performance.

Once the mechanical model of the support structure is designed, a .stl file is generated. This file format contains the necessary information to create the 3D model of the structure. The .stl file is then loaded into software that segments the model into multiple thin slices. These layers are translated into specific instructions for the 3D printer, guiding it through the printing process. The 3D printer then fabricates the physical model by depositing PLA material layer by layer. This additive manufacturing process ensures precision and accuracy in the final structure. The fabricated support structures are illustrated in Figures 4.50 and 4.51, showcasing the completed design and its integration with the reflector antenna.

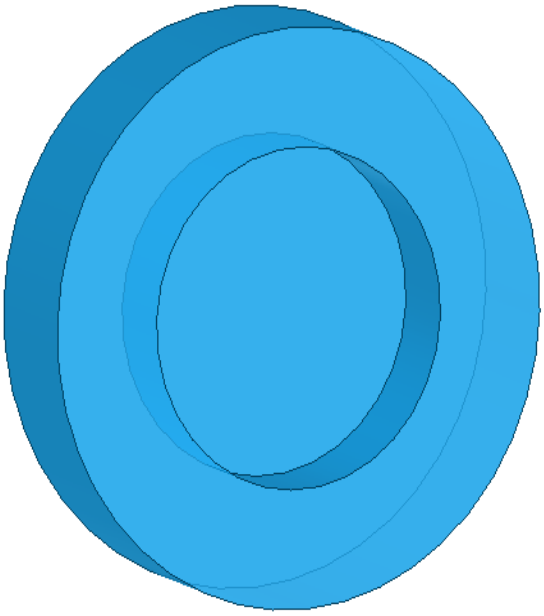

Fig. 4.50 Designed model of the support structure for the reflector antenna.

doi:10.6342/NTU202404478

Fig. 4.51 Representation of 3D printed structure.

The reflector is fabricated with the help of CNC machining because of the following reasons. CNC machines automate the fabrication process, which reduces the time required for fabrication compared to traditional manual methods. So this helps in the reduction in errors and surface roughness. As the reflector antenna operates at 300GHz, CNC machining provides high precision which is crucial for high-frequency reflector antennas. At high frequencies, even small deviations in the shape or alignment of the reflector can significantly impact performance. CNC machines ensure that the dimensions and contours of the reflector are fabricated with minimal deviation from the design specifications. CNC machining can produce a high-quality surface finish, which is crucial for high-frequency applications where surface roughness can affect signal reflection and dispersion.

The fabricated reflector antenna is shown in Fig 4.51 and is integrated into the printed support structure as depicted in Fig 4.50.

doi:10.6342/NTU202404478

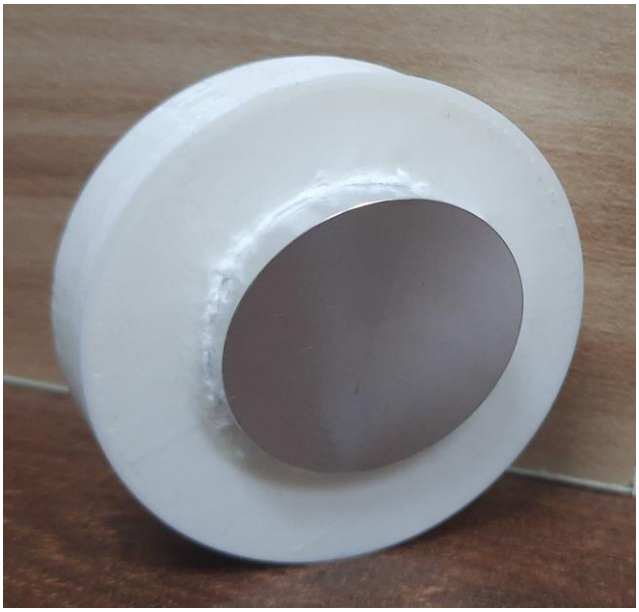

Fig.4.52 Integration of offset reflector with 3D printed structure.

The structure represented in Fig.4.52 is integrated with the linear motion system illustrated in Fig.4.53.

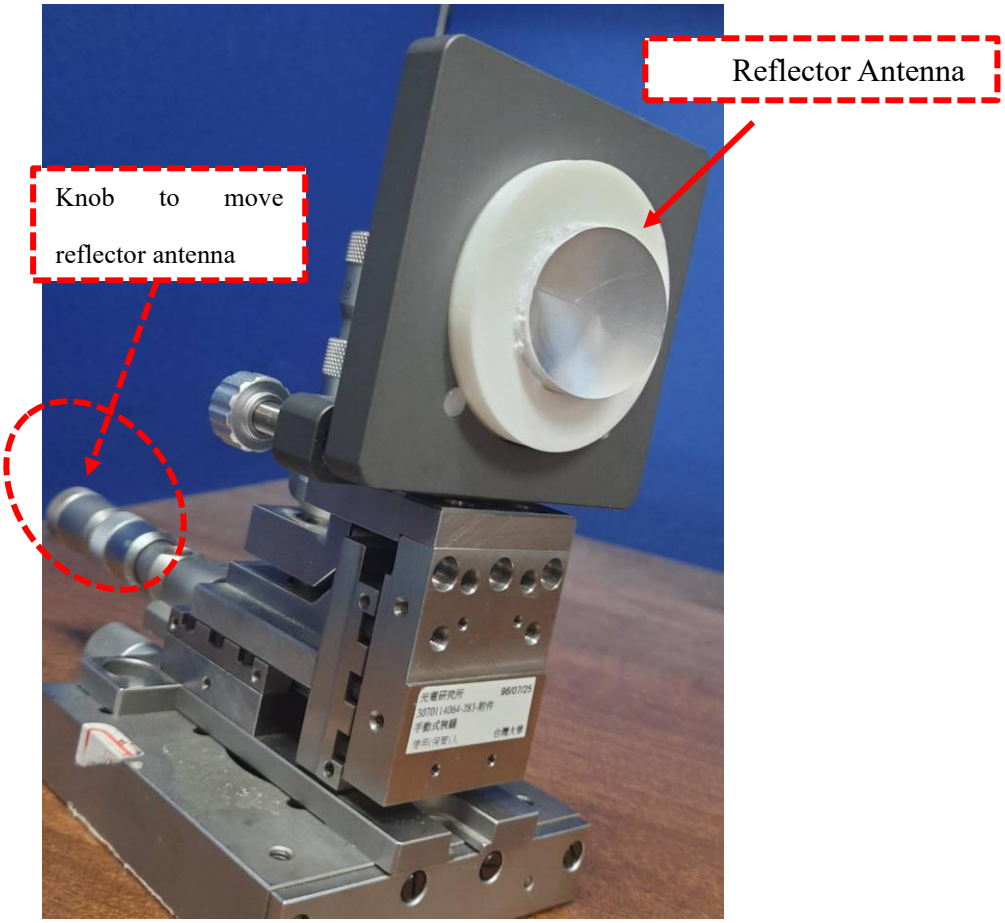

Fig. 4.50 Representation of reflector antenna with linear motion system.

doi:10.6342/NTU202404478

As the Reflector antenna needs to be displaced four times, the knob depicted in the figure is essential for fine-tuning the reflector antenna's position allowing for precise alignment of the antenna according to the specifications needed for the measurement or operational setup.

The design of the support structure for the reflector antenna must be flexible as it should be capable of accommodating both the feed antenna and the reflector itself, considering the high frequency of operation. At these high frequencies, extenders are required to transform the signals into the desired frequencies and integrate with waveguides, as detailed in the measurement setup of Chapter 5. Given the complexities involved in integrating the entire system, isolating the dish antenna from the source and positioning the feed at the convergence point of the dish is a recommended approach. This configuration simplifies the system integration and helps to achieve optimal performance by minimizing interference and ensuring that the feed antenna effectively directs signals to the reflector for accurate measurement and operation.

doi:10.6342/NTU202404478

Chapter 5 Measurement Results of the Offset Reflector

The objective of this chapter is to describe the measurement setup, alongside the results from the measurements are compared against the simulation, and an evaluation is made to determine how closely the simulation aligns with the experimental data.

5.1 Block Diagram of the Measurement Setup

The antenna is measured in the NTU sub-THz antenna measurement laboratory. The measurement setup of the system is detailed in the schematic illustrated in Fig.5.1, which has been employed to measure 2-D radiation patterns of various antennas.

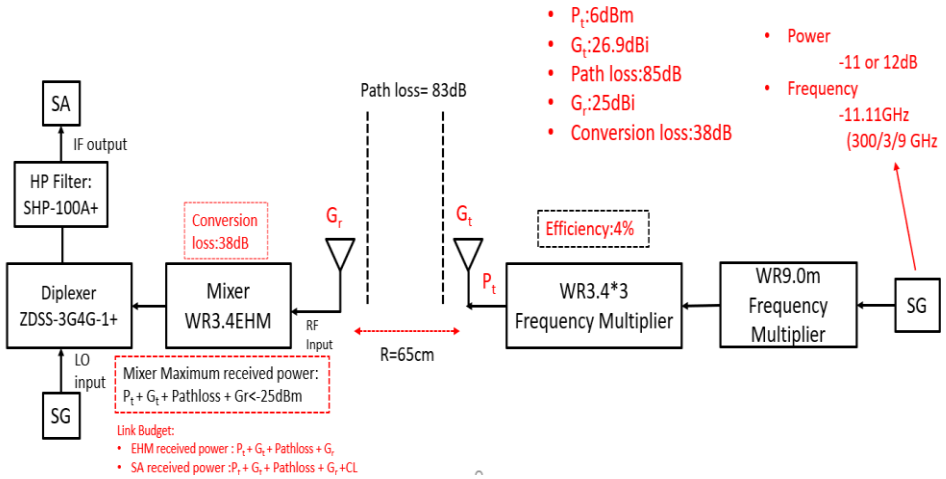

Fig.5.1 Block diagram of the measurement setup in NTU sub-THz antenna measurement laboratory.

The probe antenna is a horn antenna connected via a WR3.4 waveguide, whose frequency band covers the desired range of 220 to 325 GHz. The mixer, model 3.4EHM, is utilized to down-convert these high-frequency signals to a frequency that is compatible with the spectrum analyzer (SA) for output analysis. The mixer has a conversion loss of 38 dB, meaning that the signal strength is reduced by this amount during the down-conversion process which might affect the measurement range due to the system noise level. Given the mixer's sensitivity, it is crucial to ensure that the power received by the mixer does not exceed -25 dBm to avoid potential damage, which is another constraint.

doi:10.6342/NTU202404478

To achieve this, the Device Under Test (DUT) antenna must be positioned carefully to minimize the power incident on the mixer, ensuring that it remains within the safe operating range.

5.2 Measurement Setup of Reflector with Feed as Horn

Based on the setup depicted in the above figure, the reflector antenna is arranged for measurement as described. Before using the actual feed, we first utilized a horn antenna as the feed element to evaluate the functionality of the reflector antenna. The horn antenna, which operates within the sub-THz frequency range, was employed to evaluate how effectively the reflector antenna enhances the gain of the feed. This preliminary measurement helps to ensure the reflector's performance before deploying the intended feed. The configuration of the dish antenna with the horn antenna as the source element is shown in Fig. 5.2 in the sub-THz antenna measurement system.

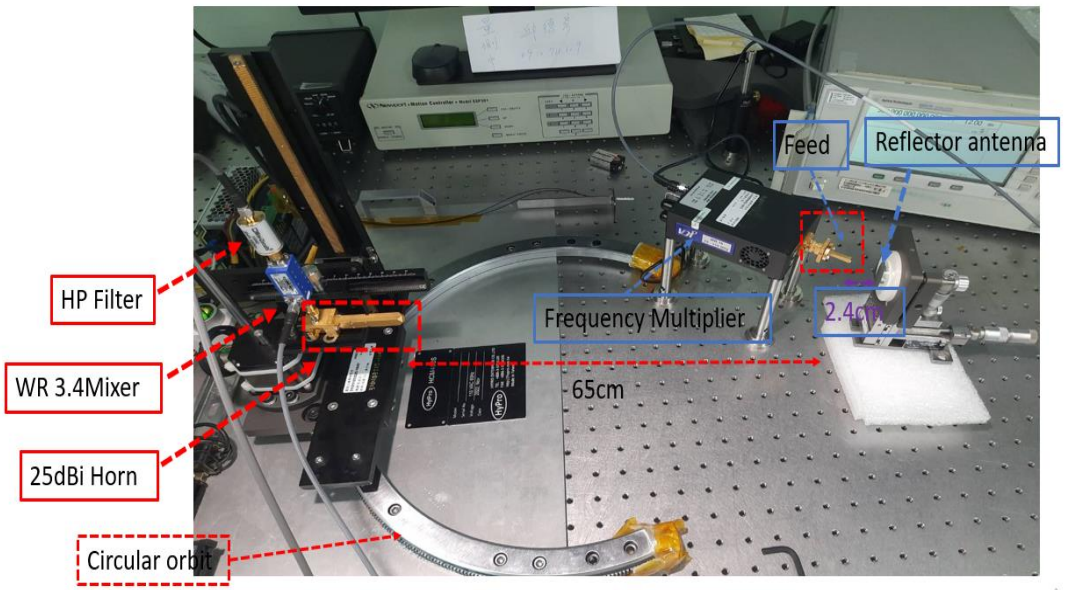

Fig.5.2 Measurement setup of reflector with the horn as feed element.

The focal distance between the Reflector and feed antenna is considered set at 2.4cm and the distance between the Tx Antenna (DUT) is 65cm. these distances are determined based on link budget calculation.

doi:10.6342/NTU202404478

5.2.1 Measured results of the reflector antenna with horn as feed element

The measured gains of the horn antenna with and without a reflector are evaluated for the Electric field plane and the Magnetic field plane are illustrated in Figures 5.3 and 5.4 correspondingly. For both cases, the gray curve and the red curve represent the magnitude of the horn antenna and the magnitude of the horn with reflector respectively.

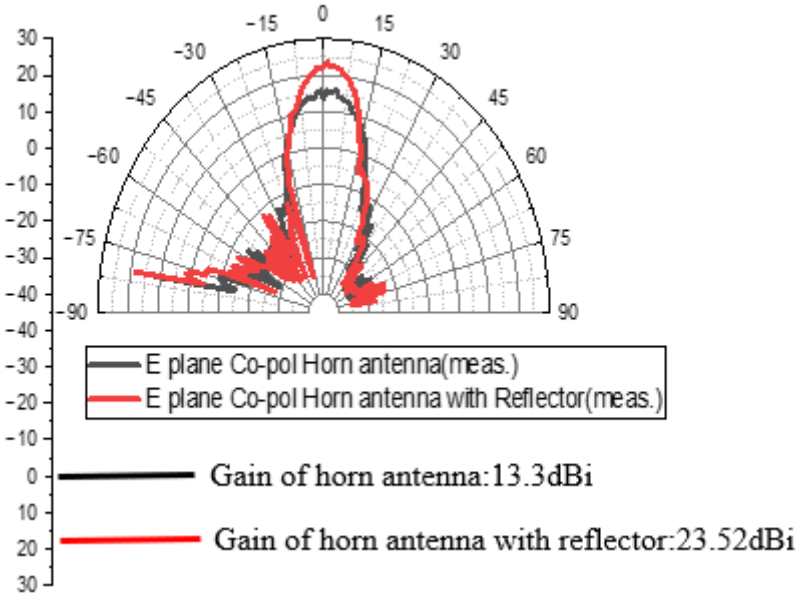

Fig.5.3 E-plane gain pattern measurement plot.

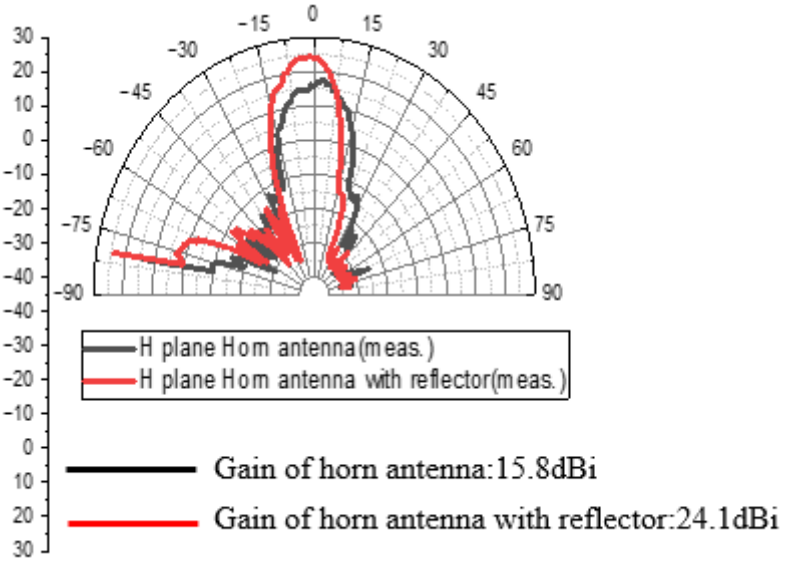

Fig.5.4 H-plane gain pattern measurement plot.

doi:10.6342/NTU202404478

The gain pattern of the reflector depicts that the reflector similarly boosts the gain of the feed antenna by 10dB in the measurement, approximately matching the observed simulation results. Based on the measured results, it can be confirmed that the reflector antenna effectively enhances the gain. It is noted that at this frequency band, it is difficult to align the position of the feed antenna to ensure the maximum gain of radiation from the reflector antenna. To address this, the phase center of the horn antenna should be determined and positioned at the reflector's focal point, though this is particularly difficult in a 2-D measurement setup. In this paper's validation process, the simulation was carried out under conditions identical to those of the prototype during measurement.

5.3 Measurement setup of the reflector Antenna with 4×4 H-pol End-Fire Antenna Array as feed element

The simulation's antenna array is replaced instead of the horn as the actual source element. Figure 5.5 shows the measurement setup of the reflector antenna with the antenna array as the feed in the measurement system.

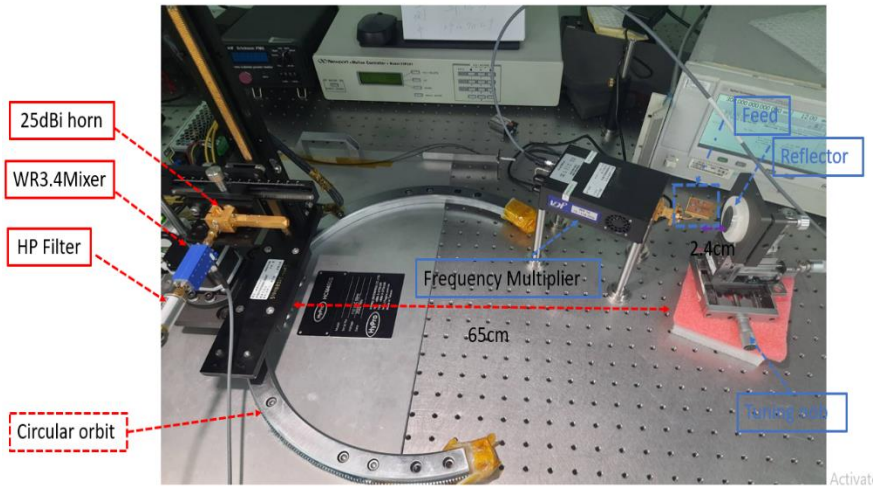

Fig.5.5 Measurement setup of reflector antenna with array as feed element.

Before discussing the measurement results, it is crucial to address several key factors that contribute to differences between the measurement and simulation environments.

Firstly, in the simulation, the reflector antenna incorporates a 4×4 antenna array as the feed element. However, in the measurement setup, a 1×4 antenna array is used due to

doi:10.6342/NTU202404478

practical constraints. Note that, the separation between the components in the 4×4 array with end-fire configuration is 300 μm, which makes it infeasible to stack the array elements within the thickness constraints of the waveguide used because one needs to build feed ports for excitations by the signal sources. Consequently, to validate the simulation outcomes of the 4×4 antenna configuration, the measurement approach involves using a 1×4 antenna array and moving the reflector four times to build the relative positions corresponding to a feed offset for the array elements, each displacement equal to the spacing between array elements in the adjacent rows. The resulting radiation pattern should be evaluated against the simulated results of the 4×4 horizontally polarized antenna array with end-fire configuration by summing the measured data from these four positions.

It is also noted that the current measurement system lacks the capability to capture phase information, making it impossible to perform the superposition of all 1×4 array radiations to to form the overall radiation pattern of the intended 4×4 antenna array. This difficulty is resolved by a hybrid approach from the simulation because accurate comparison requires both the phase and magnitude of the results obtained from measurements, as the electric field is a vector quantity. These measurements are added using basic vector equations to obtain a composite radiation pattern.

Secondly, it is crucial to consider that the simulation does not account for array losses such as waveguide losses, stripline losses, and power divider losses. The Hybrid Solver in HFSS does not support the simultaneous simulation of these additional loss mechanisms. Therefore, the simulations focused solely on the ideal antenna array without incorporating these practical loss factors. Additionally, the phase of the antenna array in the experimental configuration is fixed, whereas in the simulation, the feed is inclined at a specific offset angle. In contrast, in the measurement, the feed is positioned perpendicular (90°) to the dish antenna, as illustrated in Fig. 5.5, due to the fixed angle of the waveguide. These discrepancies in alignment and additional losses can significantly

doi:10.6342/NTU202404478

impact and degrade the performance of the measured results, potentially leading to variations between the measured and simulated outcomes.

The designed and fabricated 1×4 H-pol end-fire antenna Array along with waveguide and power divider employed for measurement are represented in Figures 5.6(a) and 5.6(b) correspondingly. This setup was used to measure the 1×4 antenna arrays radiation pattern in [8]. This setup is directly adopted here to measure the radiation from the reflector antenna.

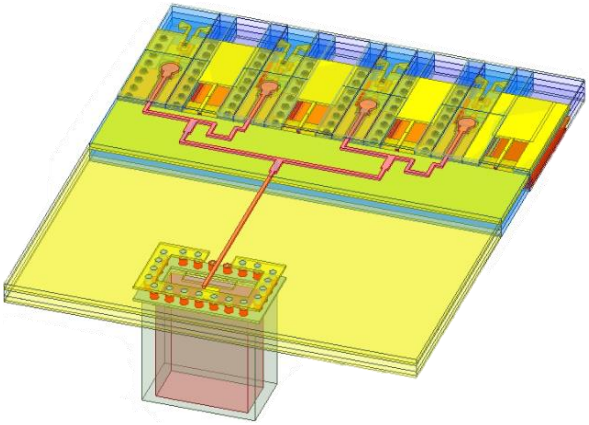

(a)

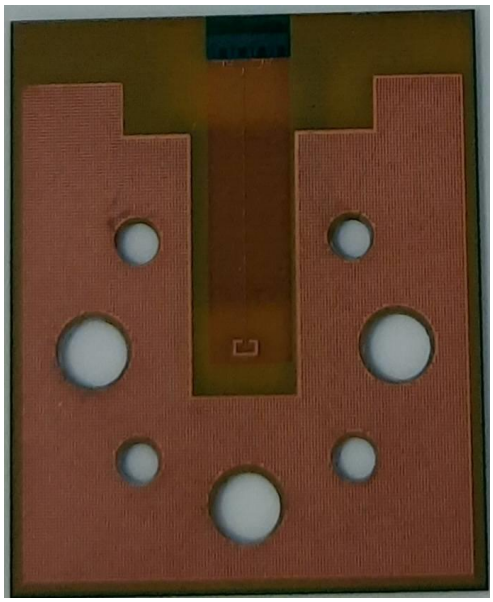

(b)

Fig 5.6 (a) Designed horizontally oriented 1×4 antenna array with end-fire configuration for measurement (b) Fabricated horizontally oriented 1×4antenna array with end-fire configuration for measurement [8].

doi:10.6342/NTU202404478

As discussed before, the antenna array includes losses, which are not incorporated in the simulation. Hence, the waveguide loss, strip line loss, and power divider loss at 300GHz are illustrated in Figures 5.7 (a), 5.7(b), and 5.7(c) correspondingly.

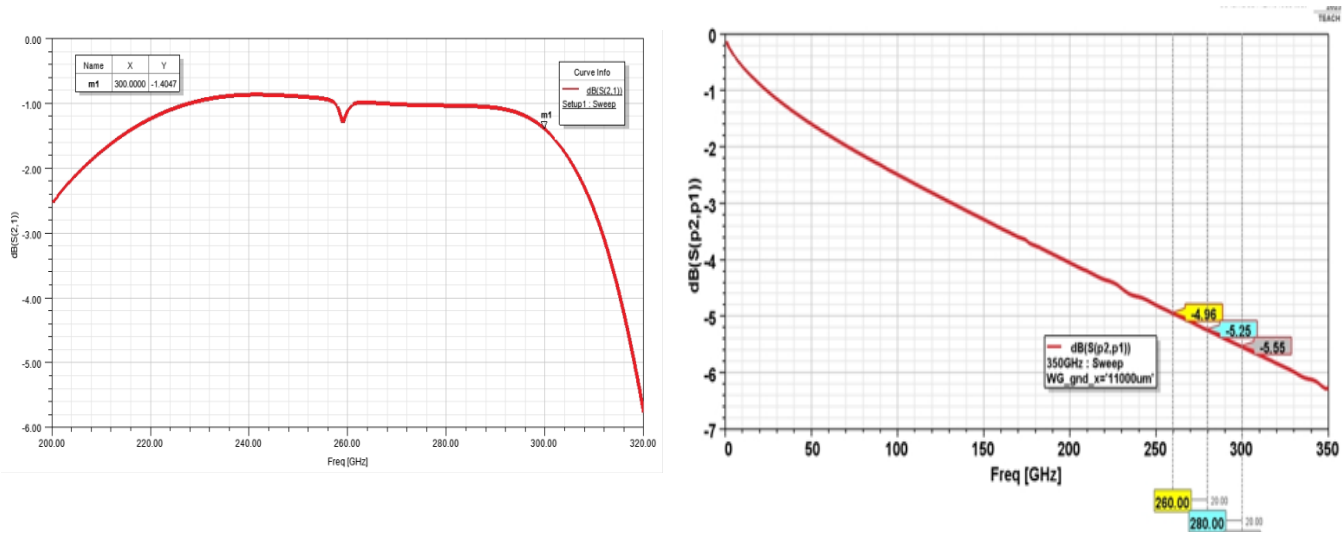

(a) (b)

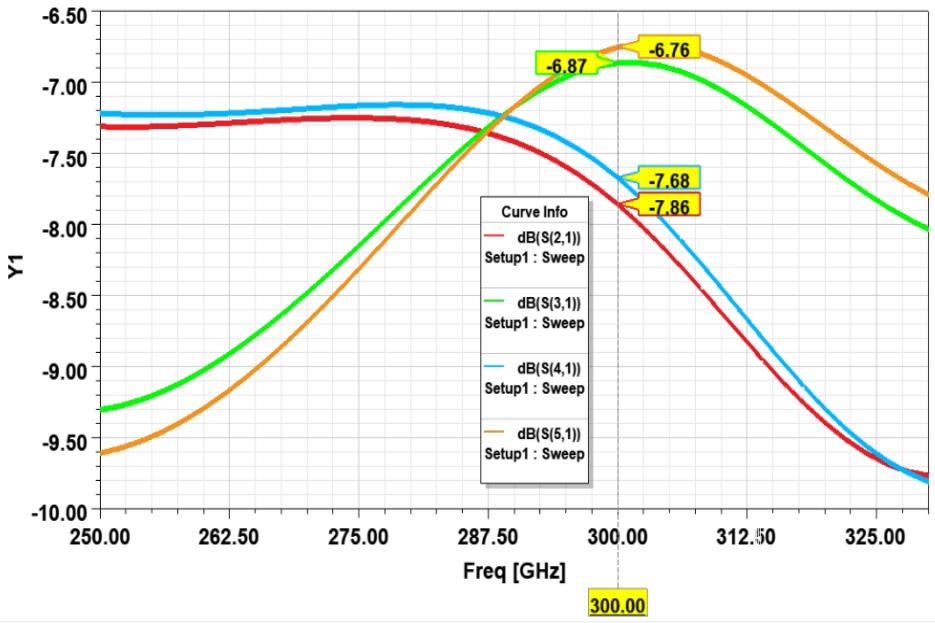

(c)

Fig.5.7 Simulated losses of 1×4 antenna array with end-fire configuration (a) Waveguide loss (b) Strip line loss (c) Power divider loss.

doi:10.6342/NTU202404478

When evaluating the performance of the antenna array, it's crucial to account for the various losses introduced by different components within the system. Based on the simulation results, the waveguide contributes a loss of approximately -1.4 dB, while the microstrip line introduces a more substantial loss of around -5.55 dB. Additionally, the power divider, responsible for distributing the signal across multiple paths, incurs a loss of approximately -0.6 dB. These individual losses cumulatively result in a total attenuation of approximately -7.66 dB for the 1×4 antenna array, encompassing the waveguide, microstrip line, and power divider losses.

Given that the measured results will be numerically combined to validate the performance of the 4×4 antenna array, it is important to recognize that the overall losses will scale proportionally with the increased number of elements. Consequently, the attenuation in a 4×4 array configuration is anticipated to be notably higher, which could substantially affect the overall system performance.

These losses are significant in determining the antenna array's effectivensess and must be carefully considered when comparing measured data to simulation outcomes. It's important to highlight that simulation results typically assume ideal conditions. However, when the antenna array is fabricated on a PCB board, additional losses may emerge. These could stem from material imperfections, variations in manufacturing processes, and parasitic effects, all of which are not captured in the simulations.

As a result, the measured performance of the antenna array may exhibit significant deviations from the simulated results, reflecting the impact of these additional losses. Such discrepancies underscore the importance of considering these real-world factors when validating simulation data against actual measurements. The degradation in performance due to these factors must be acknowledged and accounted for to ensure an accurate comparison between the measured and simulated results.

doi:10.6342/NTU202404478

5.3.1 Procedure to numerically add the E-field patterns

The estimation of antenna radiation from the reflector antennas fed by a 4×4 end-fire antenna array is presented. As mentioned earlier, the measurement is insufficient to provide detailed information on field magnitudes and phases to satisfy the superposition principle. Thus, it is necessary to extract the phases from the simulation. This may not accurately show the measurement patterns, but it provides a good trend estimation when the simulation results are used for comparison.

This Phase incorporation is more accurate to estimate the radiation pattern when phaseless data is synthesized to extract phases. To validate the simulated results, the measured radiation pattern must be compared by obtaining both the amplitude and phase of the electric field. Once these values are acquired, they can be combined to facilitate an accurate comparison between the measured and simulated radiation patterns.

Since the measured E-field magnitude is expressed in power units in dBm, it must first be converted to linear values (mW or Watts) before any addition can be performed. This is because dBm represents a logarithmic scale, and the direct addition of logarithmic values is not valid. Converting these values to their linear equivalents allows for accurate numerical addition and proper combination of the radiation patterns for comparison. If the measured Phase is in degrees, it should be converted to radians. The formulas to convert dBm to mW and degrees to radians are expressed by using below eqn(5.1) and eqn(5.2) respectively.

$$P_{mw} = 10\frac{P_{dBm}}{10} \tag{5.1}$$

$$\phi = Phase_{radians} = Radians(deg)\ or\ degrees \times \frac{\pi}{180} \tag{5.2}$$

After the phase is converted from degrees to radians, transform the complex exponential phase representation ($e^{j\theta}$) to rectangular form of complex number which can be represented by using below formula.

doi:10.6342/NTU202404478

$$E_i = \sqrt{P_{mw}} e^{j\emptyset_i} \tag{5.3}$$

where the constraint rate of free space impedance is not considered as it doesn't affect the final computation. This computation is applied to all the measured data.

As we know that, to validate the simulation results of the 4×4 antenna configuration, the reflector antenna should be displaced four times when it is fed by a 1×4 antenna array to produce the relative positions for 4×4 antenna arrays. These above steps should be applied for all the four cases. Now add the obtained patterns of all the four cases (E_{total}) and normalize it according to the form given in eqn(5.4).

$$E_{total} = \sum_{i=1}^{4} E_i \tag{5.4}$$

Where E_i is computed in (5.3) for all four cases.

Calculate the amplitude(E_{total}) of the electric field, denoted as |E|, is a measure of the signal's strength and is computed using the applied to the above-mentioned complex components of the field. The below formula represented in eqn(5.5) helps us to calculate the magnitude of the electric field vector.

$$|E_{total}| = \sqrt{a^2 + b^2} \tag{5.5}$$

where a and b are the real and imaginary parts of E_{total} in (5.4)

Field strength alone does not give full understanding of the signal's energy. Power represents the energy transmitted by the electromagnetic wave, which is crucial for understanding signal strength and performance in practical scenarios. So, the $|E_{total}|$ should be converted into $|P_{total}|$ by using the formula illustrated in eqn(5.6)

$$|P_{total}| = \frac{|E_{total}|^2}{2 \times Z_0} \tag{5.6}$$

where Z_0 is the intrinsic impedance of free space which is approximately equal to 377 ohms. However, it is noted that in (5.3), the influence of Z_0 was not accounted for, so one can simply one can simply make $Z_0 = \frac{1}{2}$ in (5.6) for consistency.

doi:10.6342/NTU202404478

Generally, the gain pattern is plotted in decibels, so we need to convert the calculated $|P_{total}|$ which is in mW to $|P_{total}|$ in dBm by using the below eqn(5.7)

$$P_{total(dBm)} = 10\,log(P_{total}\ in\ mW) \tag{5.7}$$

After completing the numerical addition of the radiation patterns, the final step is to calibrate the electric field magnitude using the receiver horn antenna. This process is used to extract the accurate data of the DUT antenna.

$$Gain_{DUT} = Gain_{(reciever\ horn)} - Power_{(reciever\ horn)} + Amp_{(DUT)} \tag{5.8}$$

After the calibration, the ultimate step is to plot the Electric field magnitude and compare it with the simulated 4×4 Ed-fire Antenna Array patterns to check whether the measured data aligns with the simulation.

5.3.2 Measurement results of reflector antenna with 4×4 horizontally polarized antenna array with end-fire configuration as feed

This chapter presents the measurement results, beginning with the radiation patterns for a 1×4 antenna array. The results are illustrated in Figures 5.8 and 5.9, where the observed patterns are analyzed with the corresponding simulation results. These radiation patterns provide a foundational basis for formatting the feed of a 4×4 antenna array.

As previously mentioned, the measurement system at NTU does not provide phase information, necessitating a reliable method for phase extraction. In this study, the phase information is derived from full-wave simulations and integrated with the amplitude data obtained from measurements. It is important to note that once this phase information is incorporated, the measured gain patterns of all 1×4 antenna arrays can be effectively optimized to determine the overall gain patterns of the 4×4 antenna array feed.

The fabricated reflector antenna was evaluated at a frequency of 300 GHz. Figures 5.8 and 5.9 illustrate the measured results for co-polarized and cross-polarized fields in E-plane, as well as co-polarized and cross-polarized fields in H-plane at different

doi:10.6342/NTU202404478

positions. These results provide insights into the functionality characteristics of the antenna across various configurations, highlighting the effectiveness of the measurement and simulation process in achieving accurate radiation pattern assessments. In the figures, cases 1-4 correspond to the gain pattern of the reflector antenna fed by the 1×4 antenna array fed when the reflector is located at four different positions

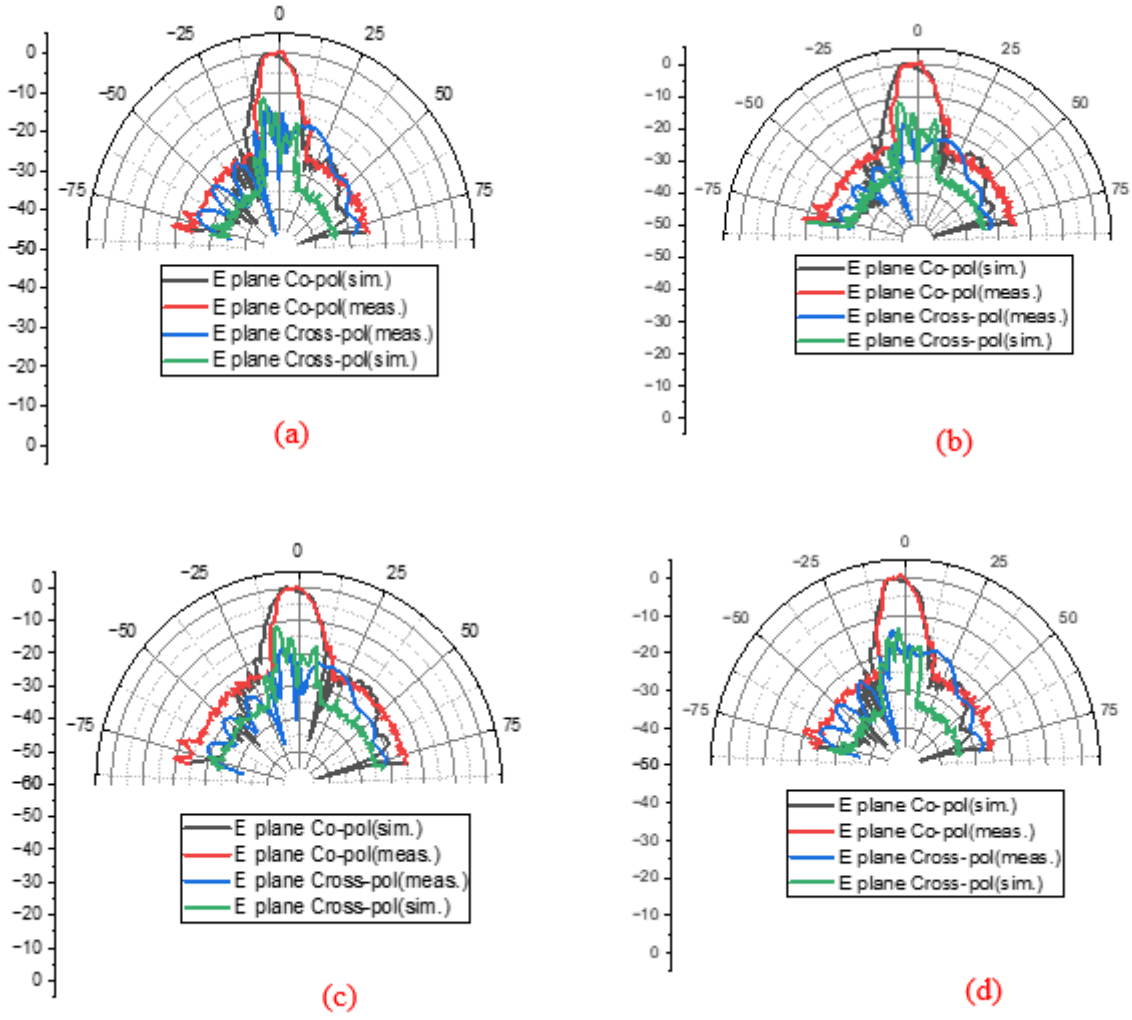

Fig. 5.8 Radiation pattern measurements for the electric field plane of reflector antenna fed by 1×4 antenna array feed, including both co-polarized and cross-polarized components at four different positions (a) Case1 (b) Case2 (c) Case3 (d) Case4.

doi:10.6342/NTU202404478

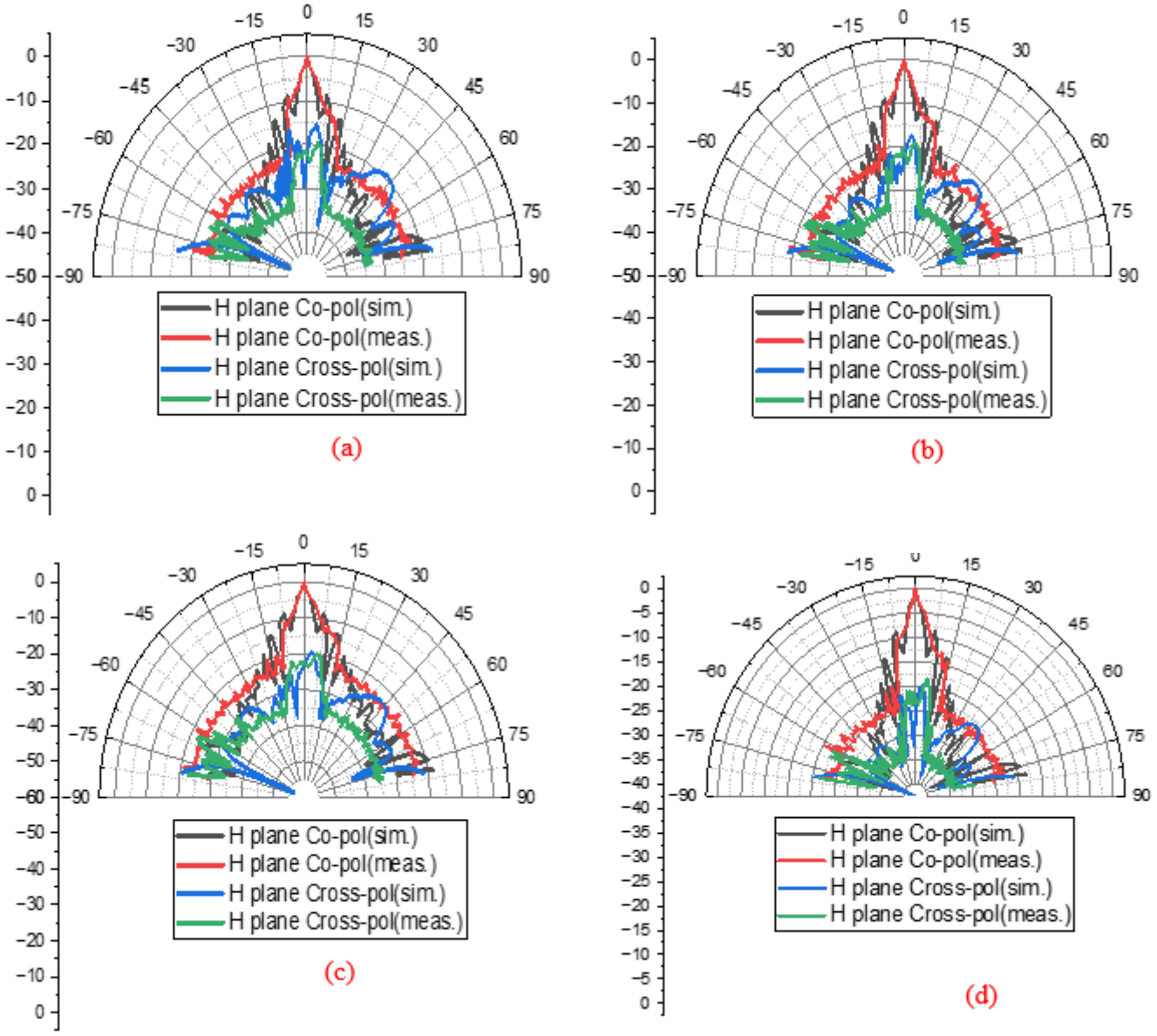

Fig. 5.9 Radiation pattern measurements for the magnetic field plane, including both co-polarized and cross-polarized components at four different positions at four different positions (a) Case1 (b) Case2 (c) Case3 (d) Case4.

The simulated gain of the reflector antenna with a 1×4 antenna array feed shows a 7 dB improvement. The measured radiation pattern exhibits symmetry, with the main lobe aligning well with the simulated results. However, in practice, the reflector enhances the antenna's gain by 5 dB, due to the practical losses which already illustrated before. The discrepancy in the sidelobes could be attributed to inaccuracies in the spectrum analyzer.

doi:10.6342/NTU202404478

As mentioned earlier, we could only measure the magnitude of the E-field, as the Spectrum Analyzer is not designed to measure phase. To measure both magnitude and phase, we needed a Vector Network Analyzer (VNA), which is the only instrument that provides this capability. However, the VNA's limitation is its incompatibility with the NTU circular orbit setup used for scanning. Although the circular orbit was easily integrated with the SA and the associated mixer, this mixer could not be used with the VNA because it does not pass phase information. Consequently, we chose to use frequency extenders instead of mixers in the NTU sub-THz antenna measurement system. Unfortunately, the size of the frequency extenders made it impractical to incorporate them into the circular orbit setup.

To address this problem, we switched to an alternative approach using a linear rail. The linear rail allowed us to move the VNA and the measurement setup along a linear path, thus avoiding the size constraints imposed by the frequency extenders. Despite this adjustment, we faced additional difficulties related to the software used for operating the linear rail. The software was not compatible with the VNA, which meant that we had to manually record the measurement values at each point along the rail. This manual recording process was not only labor-intensive but also introduced the potential for human error, further complicating our data collection. Moreover, the high noise floor of the VNA added another layer of complexity to our measurements. The VNA's high noise floor, combined with the relatively weak signal strength of the measurements, made it challenging to accurately distinguish the actual signal from the background noise. This issue led to fluctuations in both the measured phase and magnitude, impacting the reliability of our data.

As detailed in Section 5.3.1, the simulated phase is now merged with the measured magnitude, and the procedure outlined in Section 5.3.1 is followed to combine the simulation data to derive the results for the 4×4 antenna array.

doi:10.6342/NTU202404478

The added-up normalized measured results of Electric-plane co-polarized and cross-polarized fields as well as the magnetic-plane co-polarized and cross-polarized fields of Reflector antenna with 4×4 Horizontally polarized antenna array End-fire configuration as feed is depicted in Figures.5.10 and 5.11 correspondingly.

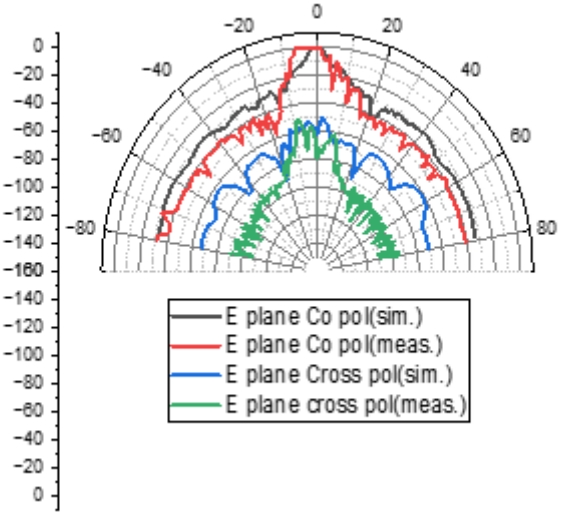

Fig. 5.10 Comparison of simulated and measured electric fields co-polarization and cross-polarization of a reflector antenna with 4×4 H-pol end-fire antenna array.

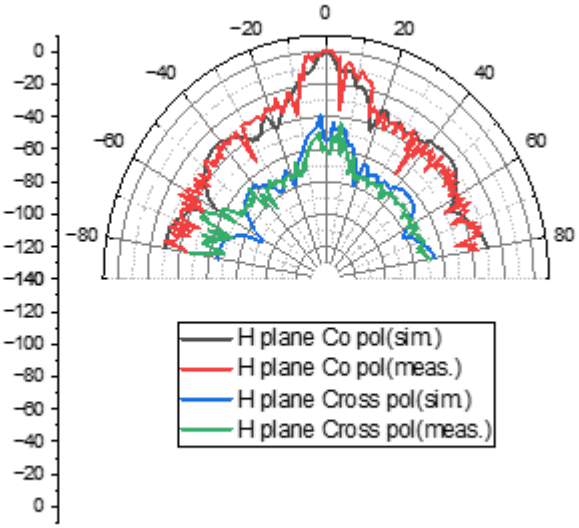

Fig. 5.11 Comparison of simulated and measured magnetic fields co-polarization and cross-polarization of a reflector antenna with 4×4 H-pol end-fire antenna array.

doi:10.6342/NTU202404478

The radiation pattern is measured at a single frequency, specifically at the antenna's center frequency of 300 GHz. Although the measured radiation pattern exhibits some degree of symmetry similar to the simulated pattern, there are minor discrepancies between the measured and simulated results. These deviations can be attributed to several factors:

- Firstly, the phase information used in the simulations might not align with the real-time phase measurements obtained during experiments.
- Additionally, simulations typically exclude certain real-world losses, while the measured patterns include these practical losses.
- Furthermore, the measurement process introduces additional losses, which become more significant at higher frequencies, contributing to the observed discrepancies.

doi:10.6342/NTU202404478

Chapter 6 Conclusion

In this thesis, we proposed an offset reflector antenna with feed as a 4×4 H-pol End-fire antenna array designed for operation at Sub-THz frequencies, specifically at 300 GHz. Compared to traditional reflector antennas, offset reflector antennas provides wide advantages in terms of feed blockage, sidelobe levels, and gain.

The primary objective was to enhance the gain of a 4×4 end-fire antenna array by integrating this reflector. By optimizing the overall antenna system, significant improvements in performance, particularly in gain, were achieved.

The design process involved the examination of various parameters, including geometrical configurations, material properties, and optimization techniques. Through detailed parametric studies and simulations, we demonstrated that precise adjustments to these parameters can achieve accurate gain at these high frequencies.

This thesis also demonstrated that undesired offset angles and incorrect focal lengths can significantly impact the performance of the offset reflector antenna. Specifically, it was shown that deviations from optimal values lead to asymmetric radiation patterns and increased side lobe levels. These findings underscore the importance of precise calibration and careful design in achieving the desired antenna performance. By addressing these issues through optimization, the research highlights strategies for mitigating such effects and improving overall antenna efficiency. This design effectively maximizes gain, minimizes sidelobe levels, and addresses the key challenges associated with Sub-THz frequency antennas.

The antenna was fabricated using CNC machining, chosen for its precision and suitability for the design requirements. Weighing approximately 23 grams, the fabricated antenna successfully meets the design specifications and demonstrates the potential for high-performance operation in the Sub-THz range. Its compact and lightweight nature makes it versatile for integration with other systems and applications.

doi:10.6342/NTU202404478

This thesis includes a thorough validation of the measured and simulated results for the offset reflector antenna system operating at Sub-THz frequencies. The validation process revealed slight deviations between the simulated and measured performance, primarily due to the losses introduced by the waveguide feeding the antenna array. At such high frequencies, waveguides experience significant attenuation and other losses, which are more pronounced compared to lower frequencies. These losses occur due to factors such as signal attenuation, scattering, and mode mismatches within the waveguide. Consequently, the practical performance of the antenna system is impacted, leading to reduced gain, increased sidelobe levels, and overall decreased efficiency compared to the idealized simulations.

The simulated results, which assume ideal conditions with negligible losses, differ from the actual measured performance where these real-world factors are present. This discrepancy highlights the importance of considering practical losses in the design and optimization of high-frequency antenna systems. The findings emphasize the need for future research to address waveguide losses, potentially through improved waveguide design or alternative feeding methods, to better align practical performance with simulated expectations and enhance the overall antenna system efficiency.

doi:10.6342/NTU202404478

REFERENCE

[1] N. P. Lawrence, B. W.. -H. Ng, H. J. Hansen and D. Abbott, "5G Terrestrial Networks: Mobility and Coverage—Solution in Three Dimensions," in IEEE Access, vol. 5, pp. 8064-8093, 2017, doi: 10.1109/ACCESS.2017.2693375.

[2] L. Boccia and O. Breinbjerg, "Antenna Basics," 2012.

[3] Y. Huang and K. Boyle, Antennas: From Theory to Practice. Wiley, 2008, pp. 107-127, doi: 10.1002/9780470772911.ch4.

[4] A. Kosogor and Y. Tikhov, "A 220-300 GHz Offset Dual-Reflector Antenna for Point-to-Point Radio," 2020 14th European Conference on Antennas and Propagation (EuCAP), Copenhagen, Denmark, 2020, pp. 1-3, doi: 10.23919/EuCAP48036.2020.9135974.

[5] C. Shu, S. Hu, Y. Yao and X. Chen, "A High-gain Antenna with Polarization-Division Multiplexing for Terahertz Wireless Communications," *2018 43rd International Conference on Infrared, Millimeter, and Terahertz Waves (IRMMW-THz)*, Nagoya, Japan, 2018, pp. 1-2, doi: 10.1109/IRMMW-THz.2018.8510118.

[6] A. Martínez, I. Maestrojuan, D. Valcazar, and J. Teniente, "High gain antenna for sub-millimeter wave communications," 2016 46th European Microwave Conference (EuMC), London, UK, 2016, pp. 37-40, doi: 10.1109/EuMC.2016.7824271.

[7] T. S. Bird, "Reflector Antennas," in Handbook of Antenna Technologies, Z. Chen, Ed. Singapore: Springer, 2015, doi: 10.1007/978-981-4560-75-7_30-1.

[8] H.T.Chou, Y.-M. Chen and C.-Y. Lee, " Novel Antenna -in Package Design based on End-Fire Radiation Subarray Decompostion to Format Broadside Array at Sub-THz Frequencies," under review, IEEE Transactions on Antennas and Propagation

doi:10.6342/NTU202404478

[9] A. Foudazi, A. R. Mallahzadeh and M. M. S. Taheri, "Pattern synthesis for multi-feed reflector antenna using IWO algorithm," *2012 6th European Conference on Antennas and Propagation (EUCAP)*, Prague, Czech Republic, 2012, pp. 1-5, doi: 10.1109/EuCAP.2012.6206381.

[10] S.-W. Lee and Y. Rahmat-Samii, "Simple formulas for designing an offset multibeam parabolic reflector," IEEE Transactions on Antennas and Propagation, vol. 29, no. 3, pp. 472-478, May 1981, doi: 10.1109/TAP.1981.1142611.

[11] J. Shinohara, N. Michishita, Y. Yamada, M. T. Islam, and N. Misran, "Measured electrical characteristics of an array feed offset parabolic reflector antenna," *2012 International Symposium on Antennas and Propagation (ISAP)*, Nagoya, Japan, 2012, pp. 1104-1107.

[12] A. Telsang, S. B. V. and S. Vedargarbham, "A Study on Reflector Antennas and Design of Reflector Antenna for 5GHz Band," 2017 International Research Journal of Engineering and Technology (IRJET), vol. 4, no. 7, July 2017.

[13] ANSYS, Inc. An Introduction to HFSS, 2017.

[14] K. Zhao and L. E. R. Petersson, "Overview of Hybrid Solver in HFSS," *2018 IEEE International Symposium on Antennas and Propagation & USNC/URSI National Radio Science Meeting*, Boston, MA, USA, 2018, pp. 411-412, doi: 10.1109/APUSNCURSINRSM.2018.8608281.

[15] W. Croswell, "Antenna theory, analysis, and design," in *IEEE Antennas and Propagation Society Newsletter*, vol. 24, no. 6, pp. 28-29, December 1982, doi: 10.1109/MAP.1982.27654

[16] K. B. Kong, H. S. Kim, R. S. Aziz, and S. O. Park, ‘‘Design of offset dual reflector antennas for improving isolation level between transmitter and receiver antennas,’’ Prog. Electromagn. Res. C, vol. 57, pp. 193–203, 2015.

doi:10.6342/NTU202404478

[17] J. Zhang, X. Kong, C. Zhang, Y. Gao, and Q. He, "Electrical performance compensation of reflector antenna based on sub-reflector array," Electronics, vol. 12, no. 23, p. 4771, 2023, doi: 10.3390/electronics12234771.

[18] R. Bhattacharjee and K. Debbarma, "Analysis of offset reflector performance fed by 2×2 microstrip antenna array using GO technique," *2018 3rd International Conference on Microwave and Photonics (ICMAP)*, Dhanbad, India, 2018, pp. 1-2, doi: 10.1109/ICMAP.2018.8354629.

doi:10.6342/NTU202404478